

T.C.
AYDIN ADNAN MENDERES UNIVERSITY
GRADUATE SCHOOL OF NATURAL AND APPLIED SCIENCES
MECHANICAL ENGINEERING
2022-DR-014



**DESIGNING OF AN ORGANIC RANKINE CYCLE POWER
PLANT BY USING LOW ENTHALPY GEOTHERMAL
RESOURCES**

Murat KARADAŞ
DOCTORATE THESIS

SUPERVISOR
Prof. Dr. Yunus ÇERÇİ

AYDIN-2022

ACKNOWLEDGEMENTS

I would like to thank to my supervisor, Prof. Dr. Yunus ÇERÇİ for his guidance and encouragement during my thesis. He did not spare his support at every stage of my doctoral education and and showed me endless patience.

I would like to express special gratitude to Prof. Dr. Yunus ÇENGEL who was my first advisor before his retirement.

I also would like to thank to my colleagues at GMK Energy Company for their kind assistance during the thesis modelling study.

Finally, I want to express my sincere gratitude to my wife Gülcan YAVUZ KARADAŞ for her endless love and support all the time. I would not have been able to complete this thesis without the support of my dear wife.

TABLE OF CONTENTS

ACCEPTANCE AND APPROVAL	i
ACKNOWLEDGEMENTS.....	ii
TABLE OF CONTENTS.....	iii
LIST OF FIGURES	v
LIST OF TABLES	vii
LIST OF SYMBOLS AND ABBREVIATIONS.....	viii
ÖZET.....	xiv
ABSTRACT	xv
1. INTRODUCTION.....	1
2. LITERATURE REVIEW.....	3
3. MATERIAL.....	9
3.1 Heat Exchangers.....	9
3.1.1 Thermal Design Considerations	10
3.2 Air Cooled Condenser.....	15
3.2.1 Arrangement & Mechanical Design.....	15
3.2.2 Header Design	19
3.2.3 Warm Air Recirculation	20
3.2.4 Condensing Discussion	23
4. METHOD.....	27
4.1 Heat Exchangers Calculation	27
4.1.1 Nucleate Pool Boiling Correlations.....	41
4.2 Air Cooled Condenser Equations	48
5. ORC DESIGNER PROGRAM DEVELOPMENT AND CALCULATIONS	67
5.1 Calculations for a Loop as an Example.....	67
5.1.1 Evaporator Calculations	67
5.1.2 Preheater Calculations.....	76

5.1.3	Air Cooled Condenser Calculations	90
5.1.4	Pump and Turbine Calculations	115
5.2	ORC Designer with MATLAB Program.....	117
6.	RESULTS.....	123
7.	DISCUSSION	144
8.	CONCLUSION AND RECOMMENDATION.....	151
	REFERENCES.....	154
	APPENDIX	161
	SCIENTIFIC STATEMENT.....	165
	CIRRICULUM VITAE	166

LIST OF FIGURES

Figure 3.1 Several types of heat exchangers (Kakac, 1992)	9
Figure 3.2 Part names of shell and tube heat exchanger (TEMA type AES WERMAC, 2022)	10
Figure 3.3 Flooded type shell and tube heat exchanger (TEMA X Shell WERMAC, 2022)	10
Figure 3.4 Heat exchanger tube-layouts (utilized from Kakac, S. (1992))	12
Figure 3.5 Different type of heat exchanger baffles (utilized from NPTEL (2015))	13
Figure 3.6 Typical Side Elevations of Air-Cooled Condensers (utilized from Tulsa (1998))	15
Figure 3.7 Typical Plan Views of Air-Cooled Condensers (API STANDARD 661 API (1997))	16
Figure 3.8 Typical Construction of Tube Section with Plug Headers (WERMAC, 2022)	20
Figure 3.9 Internal Recirculation Design (Tulsa, 1998).....	21
Figure 3.10 External Recirculation Design (Tulsa, 1998).....	22
Figure 3.11 Stratified flow with film condensation around the top internal perimeter of the tube (Wolverine Tube Inc., pp. 8.1-8.27, 2006).....	23
Figure 3.12 Typical flow patterns for condensation inside horizontal tubes (Wolverine Tube Inc., pp. 8.1- 8.27, 2006)	24
Figure 3.13 Simplified two-phase flow structures assumed for annular, stratified-wavy and stratified flow regimes (Wolverine Tube Inc., pp. 8.1-8.27, 2006)	25
Figure 4.1 LMTD correction factor F for a shell-tube heat exchanger. Two-shell passes and four or multiples of four tube passes. (From Standards of Tubular Exchanger Manufacturers Association (1988), New York.).....	29
Figure 4.2 Square and triangular pitch-tube layouts (utilized from Kakac (1992))	32
Figure 4.3 Air Film Coefficient (Tulsa, 1998)	52
Figure 4.4 ACC Phase Diagram	64
Figure 5.1 ORC Designer Program	118

Figure 5.2 ORC Designer Program Evaporator Screen.....	119
Figure 5.3 ORC Designer Program Preheater Screen	119
Figure 5.4 ORC Designer Program ACC Screen	120
Figure 5.5 ORC Designer Program Pump Screen	120
Figure 5.6 ORC Designer Program Steam Side Screen	121
Figure 5.7 ORC Designer Matlab Program Layout Screen.....	121
Figure 5.8 ORC Designer MATLAB Program Info Screen.....	122
Figure 6.1 Iteration System	125
Figure 6.2 MATLAB flow chart for calculation of ORC.....	127
Figure 6.3 ORC with Recuperator.....	128
Figure 6.4 ORC without Recuperator.....	128
Figure 6.5 ORC Panel with inputs and outputs	129
Figure 6.6 MATLAB flow chart for calculation of Preheater and Evaporator	132
Figure 6.7 MATLAB flow chart of calculation for ACC.....	133
Figure 6.8 Comparison of efficiencies of the different working fluids	137
Figure 6.9 Comparison of power productions of the different working fluids.....	137
Figure 6.10 Comparison of net power vs ACC and total heat exchanger area for the different working fluids.....	138
Figure 6.11 T-Q diagram output for n-pentane of ORC Designer Program.....	139
Figure 6.12 P-h diagram output for n-pentane of ORC Designer Program.....	141
Figure 6.13 T-s diagram output for n-pentane of ORC Designer Program.....	141
Figure 7.1 Net efficiency vs. Temperature Graph by using Geothermal Investment Tool (GMK Energy “Geothermal Investment Tool Application”, 2022)	149

LIST OF TABLES

Table 3.1 Common tube layouts (utilized from Kakac, S. (1992))	12
Table 3.2 Typical values of fouling coefficients and resistances (utilized from NPTEL (2015)).....	14
Table 3.3 Fin tube data for 25.4 mm OD tubes (utilized from Tulsa (1998))	19
Table 4.1 Correction Factor for Fluid Viscosity Within the Tubes (Tulsa, 1998)	51
Table 6.1 ORC with recuperator.....	130
Table 6.2 ORC without recuperator	130
Table 6.3 ORC Designer MATLAB Program Results under the same conditions	136
Table 6.4 Thermophysical properties of n-pentane, brine and air at each point of cycle.....	140
Table 6.5 Data sheet of Evaporator and Preheater	142
Table 6.6 Data sheet of ACC.....	143
Table 7.1 Geometrical comparison between the present results and Ref (Fu et al., 2015).....	147
Table 7.2 Thermodynamical and heat transfer comparison between the present results and Ref. Fu et al. (2015)	148

LIST OF SYMBOLS AND ABBREVIATIONS

Symbols:

A	area, m ²
ACMS	actual cubic meters per second
APF	total external area/unit length of fin tube, m ² /m
APM	area of fin tube per meter of tube length, in m ² /m
APSM	fin tube area (m ²) per m ² of bundle face area
AR	area ratio of fin tube compared to the exterior area of 2.54 cm OD bare tube
c_p	specific heat, J/kg °C
C	specific heat of fluid, J/kg °C
CL	tube layout constant
CTP	tube count constant
CMTD	corrected mean temperature difference, °C
C*	heat capacity rate ratio = (mcp) _{min} /(mcp) _{max}
CSA	cross section area, m ²
D	diameter, mm
D_s	shell inside diameter, mm
D_h	hydraulic diameter, (4rh), m
Δ	difference
E	dimensionless factor
EMTD	effective mean temperature difference

ε	thermal effectiveness
η	efficiency
η_{motor}	motor efficiency
η_{pump}	pump efficiency
η_{drive}	drive efficiency
η_{gross}	gross efficiency
η_{net}	net efficiency
F	1.correction factor 2.dimensionless factor
Fr_h	fraction of total fluid flowing within the limits of tube bundle
F_p	air pressure drop factor, Pa
f	friction factor
Fr	Froude number
FF	fouling resistance, W/m ² ·°C
G	mass velocity, kg/m ² ·s
Ga	galileo number, m/s ²
g_c	acceleration due to gravity or proportionality constant 9.81 m/s ² = 1
H	1.pump head, m 2.dimensionless factor
h	1. heat transfer coefficient, W/m ² ·°C 2. enthalpy, kJ/kg 3. fin height, mm

j	Colburn factor
Ja	Jacob number
k	thermal conductivity, $W/m \cdot ^\circ C$
L	length, m
Lb	baffle spacing, m
LH	latent heat, kJ/kg
LMTD	log mean temperature difference, $^\circ C$
λ	coefficient
m	mass flow rate, kg/s
μ	dynamic viscosity, $kg/(m \cdot s)$
NTA	naked tube area, m^2
N_r	number of tube rows
N_t	number of tubes
NTU	number of transfer units
Nu	Nusselt number
p_t	tube pitch, mm
Pr	Prandtl number
PR	tube pitch ratio
Q	heat load, W
q	heat flux, W/m^2
Re	Reynolds number
ρ	density, kg/m^3
S	distance, m

SFA	single fin area, m ²
σ	surface tension
T	Temperature, °C
θ_b	shell side angle, °
θ_{ct}	shell side baffle cut angle, °
TFA	total fin area, m ²
P	1. pressure, Pa 2. power, W
ϕ	multiplier between the two phases
U	overall heat transfer coefficient, W/m ² · °C
V	1. velocity, m/s 2. volume flow rate, m ³ /s
ν	kinematic viscosity, m ² /s
We	weber number,
W	1. width, m 2. air flow rate, kg/s
X_t	Transverse tube pitch, mm
X_l	Longitudinal tube pitch, mm
X_{tt}	MARTINELLI parameter

Subscripts:

a	air
b	baffle

bl boiling heat load

bp bypass

c 1.central

2.cold

3.crossflow

4. baffle cut

ctl central tube limit

DD diagonal diameter

eff efficiency

f fan

g gas

id ideal

in 1.inside

2. inlet

io inlet-outlet

h 1.hot

l liquid

ls superficial liquid

max maximum

min minimum

o 1.overall

2.outlet

3.outside

oh	overheating heat load
otl	outer tube limit
o_pp	tube side area per pass
pr	preheating heat load
pt	per tube
s	shell
sb	shell-to-baffle
strat	stratified
t	tube
tpp	number of passes between tubes
w	1.window 2.wall
WF	working fluid
z1	zone one
z2	zone two
z3	zone three

ÖZET

DÜŞÜK ENTALPİLİ JEOTERMAL KAYNAKLARI KULLANARAK ORGANİK RANKİNE ÇEVİRİMİ ELEKTRİK SANTRALİ TASARIMI

Karadaş M. Aydın Adnan Menderes Üniversitesi, Fen Bilimleri Enstitüsü, Makine Mühendisliği Doktora Programı, Doktora Tezi, Aydın, 2022.

Bu tez, Türkiye'de kullanılmayan düşük entalpili ve düşük debili jeotermal akışkanın elektrik üretiminde kullanılması için bir ORC sistemi geliştirmeyi amaçlamaktadır. 150 ton/saat debide ve 90 °C sıcaklıkta olan düşük sıcaklıklı jeotermal kaynaklardan yararlanarak Organik Rankine Çevrimine (ORC) dayalı bir santralin performansının ve ana ekipmanlarının (ön ısıtıcı, buharlaştırıcı ve hava soğutmalı kondenser) detay tasarımlarının hesaplanması için ORC Designer isimli detaylı bir MATLAB programı geliştirilmiştir. ORC Designer programının MATLAB algoritması farklı çalışma koşulları için ORC'nin tüm ana ekipmanlarına uygulanmış; ekipmanların geometrileri ve santral performansı üzerinde optimizasyonlar yapmaya imkan tanımıştır. Öncelikle, ORC sistemi yeterli sayıda ön ısıtıcı, bir adet buharlaştırıcı, bir adet hava soğutmalı condenser, bir adet türbin, bir adet pompa ve bir adet rekuperatörden oluşmaktadır. ORC sisteminde yapılan modellemede tüm çevrim içi akışkanlar için rekuperatörsüz sistemin daha yüksek brüt güç vermesinden dolayı rekuperatör ORC'den çıkarılmıştır. Sistem dokuz farklı organik çevrim içi akışkan ile değerlendirilmiştir. Çevrim içi akışkanların en yüksek net güç üretimine göre sıralaması, R218, n-pentan, izo-pentan, R245FA, R123, n-bütan, R236FA, izo-bütan, R134A, olup sırasıyla 197kWe, 189 kWe, 186kWe, 182 kWe, 181 kWe, 180 kWe, 177 kWe ve 166 kWe net enerji üretmektedirler. En yüksek verim ve net güç üretimi açısından optimum çevrim içi akışkan n-pentan bulunmuştur. N-pentanın toplam debisi ORC sirkülasyonunda 39.791 ton/saat'tir. N-pentanlı ORC, ortam hava sıcaklığı 18 °C iken 90 °C'de 150 ton/saat jeotermal su kullanarak %5.6 brüt ve %4.32 net verimlilikle 245 kWe brüt ve 189 kWe net elektrik üretmektedir.

Anahtar kelimeler: ORC, Eşanjör Tasarım, Düşük Entalpili Jeotermal Kaynak, Verim, N-pentan.

ABSTRACT

DESIGNING OF AN ORGANIC RANKINE CYCLE POWER PLANT BY USING LOW ENTHALPY GEOTHERMAL RESOURCES

Karadaş M. Aydın Adnan Menderes University, Graduate School of Natural and Applied Sciences, Mechanical Engineering Doctoral Program, Doctorate Thesis, Aydın, 2022.

This thesis aims to develop an ORC system to utilize the low enthalpy, low flow rate geothermal fluid, which is unused in Turkey, for power generation. A detailed MATLAB program which is named as ORC Designer is developed to evaluate the performance of an Organic Rankine Cycle (ORC) and detailed main-component (preheater, evaporator, and air-cooled condenser) design on low-temperature geothermal resources such as 150 tons/hour flow at 90 °C temperature. MATLAB algorithm of ORC Designer Program has implemented for all equipment of ORC for different working conditions, and it is developed to make optimization for performance and geometrical conditions of the equipment. First, ORC system is modelled with enough preheater, an evaporator, an air-cooled condenser, a turbine, a pump, and a recuperator. The recuperator was removed from the system because the gross energy production of ORC system without recuperator calculated higher than ORC system with recuperator system for all working fluids. The system was evaluated nine dry organic working fluids: the ranking of working fluids from highest to lowest net power generation are R218, n-pentane, iso-pentane, R245FA, R123, n-butane, R236FA, iso-butane, R134A with net power productions of 197kWe, 189 kWe, 186kWe, 182 kWe, 181 kWe, 180 kWe, 177 kWe and 166 kWe, respectively. N-pentane is found as the optimum working fluid in terms of the highest efficiency and net power generation. The total flow rate of n-pentane is 39.791 tons/hour at circulation. ORC with n-pentane generates 245 kWe gross and 189 kWe net electricity with 5.6% gross and 4.32% net efficiency by using 150 tons/hour geothermal brine at 90 °C while ambient air temperature is 18 °C.

Keywords: ORC design, Heat exchanger design, Low enthalpy geothermal, Efficiency, N-pentane.

1. INTRODUCTION

The Organic Rankine Cycle (ORC) is basically similar to the steam cycle in terms of its operating principle. The ORC cycle uses higher molecular weight liquids that can boil at lower temperatures than water, the working fluid. These cycles, which are similar to the Rankine cycle due to the use of high molecular weight fluids, are called Organic Rankine cycles. The working fluid used in ORCs is important for applications where the source temperature is below 400°C.

The ORC system was first developed and presented to the United Nations in 1961 by Israeli solar energy researchers Harry Zvi Tabor and Lucien Bronicki (2013) for electricity generation using a solar powered 3 kW system ORC. Later, this development led the way for the creation of the Ormat Company. Since the 1980s, geothermal energy has increased the share of ORC in electricity generation and the geothermal ORC installed worldwide has reached 2 GWE today. ORC Ormat's global market share is 48% for biomass, 31% for geothermal, 20% for thermal and 1% for solar. If we look closely at these ratios, we find that the share of geothermal and especially solar energy ORCs is small. For this reason, it is believed that the future of renewable energy ORC will be promising (Bronicki, 2013). A typical ORC cycle consists of four basic elements: the pump, the evaporator, the turbine, and the condenser. The organic liquid used in the cycle is directed to the evaporator by increasing the pressure with the pump. The element used as the evaporator is a heat exchanger that transfers the heat it receives from a heat source to the organic stream. As a result of this heat transfer, the organic liquid becomes hot vapour with high temperature and pressure. Under these conditions, the liquid entering the turbine expands and generates mechanical work. Usually, a preheater is used before the evaporator to increase the efficiency of the ORC cycles.

Since heat transfer is not effective at low temperatures, the choice of working fluid is important in ORC systems operating at these temperatures. The thermodynamic properties and working conditions of the fluid are some of the most important factors in selecting the working fluid. To extract heat from sources at low temperatures, the boiling temperature of the working fluid at atmospheric pressure must be lower than that of water. The working fluid must have the following properties: 1) The working fluid must have a high enthalpy of vaporization and a high density. The working fluid with a high enthalpy of vaporization can absorb more heat for the evaporator and

therefore requires a lower flow rate. As a result, the system size and pump capacity are reduced. 2) The impact of the working fluid on the environment should be minimal. It should have low ozone depletion potential (ODP) and global warming potential (GWP). 3) The working fluid should not be irritant, flammable, or toxic. The ASHRAE classification can be used for the hazard level of the fluid. 4) Organic fluids are usually subject to chemical decomposition and degradation at high temperatures. The maximum temperature of the heat source is limited by the chemical stability of the working fluid. Therefore, the freezing point should be the lowest temperature in the cycle.

The ORC has several significant advantages over conventional vapour cycles and is preferred in many applications due to its unique characteristics. 1) Conventional steam cycles run the risk of turbine damage, especially from foreign matter in the geothermal fluid that may come into contact with the steam turbine, especially in flash applications. Foreign matter in the geothermal fluid can lead to wear of the turbine blades, resulting in high maintenance costs. On the other hand, the working fluid used in ORCs can operate for up to 20 years without maintenance because the steam evaporates at a lower temperature than the turbine and is cleaner. 2) The molecular weight of the organic working fluids is higher than that of water, so the turbine blades impact at a lower speed while the steam is passed through the turbine. For this reason, turbine maintenance costs are low for ORCs. 3) Because ORCs operate at lower temperatures and pressures, mechanical and thermal fatigue of the cycle elements is much lower than conventional steam cycles and therefore component life is longer. 4) Because ORCs operate at lower temperatures, they can be controlled and operated remotely without the need for an operator, resulting in a significant reduction in operating costs. 5) ORCs can operate at high efficiency with partial heat input, e.g., at 10% of heat source capacity. This low ratio is advantageous for industrial processes where the amount of heat fluctuates and for applications based on solar energy. They can operate until the early morning hours, when the intensity of solar energy is low, and until late at night. 6) While conventional steam cycles require auxiliary equipment such as water supply and water treatment, ORCs do not require additional systems because it is a completely closed loop, such as a refrigeration cycle. For this reason, the system is easy to operate and control. 7) The steam turbines in ORCs rotate at lower speeds than the turbines in the conventional steam cycle, which reduces mechanical stress. 8) Turbine efficiencies of up to 85% can be achieved in ORCs. 9) Since micro-ORCs are usually mobile units, start-stop operation is simple and can operate for 20 years without major maintenance.

2. LITERATURE REVIEW

The advantages of ORCs and the rising cost of energy have made them an attractive power generation application and have become one of the most studied topics in the literature in recent years. In the studies of ORC, work seems to be intensified on the turbine, one of the most important components, as well as on the working fluid and other components of the cycle. Munoz et al. and Chacartegui et al. (2011) stated in their work that the ORC system is the best power generation method for low temperature sources. Wei et al. (2008) proposed two alternative approaches for dynamic modelling in ORCs and concluded that the most important characteristic of ORCs is high reliability and flexibility. Karellas et al. (2012) studied the effect of regenerator on ORC elements on key parameters using similarity analysis. Guo et al. (2011) performed thermodynamic analysis of ORC and studied the energy losses at different temperatures. Worek et al. (2007) presented optimal cost-effective design criteria for ORCs and used the ratio of net energy production to total heat exchanger area as a key function. Optimal cycle performance was demonstrated, and comparisons were made with different working fluids such as ammonia and n-pentane. The conclusion is that ammonia is the optimal fluid for ORC under the given conditions. A similar study was conducted by Sun and Li (2011) and optimized using the ORC Rosen method. In this study, a detailed ORC operational analysis was performed for a heat recovery system using R134a as the working fluid. Mathematical models were developed to optimize and analyse the performance of the system for the expansion, evaporator, air-cooled condenser, and pump. As stated in the study by Sun and Li (2011), the relationship between the variables whose optimization results are controlled (optimum working fluid flow, optimum condenser, and fan airflow) and the uncontrollable variables (source temperature and ambient temperature) is an approximately linear function for the net power generated by the system.

Bahaa and Gerald (2007) performed a thermodynamic analysis for ORC with 32 different working fluids. The fluids were identified as alkalis, fluorinated alkalis, ethers, and fluorinated ethers. The analyses showed that the maximum heat can be transferred to the working fluid when the source temperature is 120°C. Roy et al. (2009) performed extensive parametric optimization and performance analysis for waste heat as the heat source and ORC systems using R-12, R-123, and

R-134a as the working fluid. Cycles were compared for cases where the exhaust gas temperature was 140°C and the exhaust gas flow was 312 kg/s, and the best case was found with R-123 as the working fluid. Yamada et al. (2012) performed an energy analysis for a new ORC system using HFO-123yf as the working fluid. Li et al. (2011) studied the effects of dry fluid on the thermal efficiency and net power generation of ORC.

Gang et al. (2011) built and tested an experimental ORC model. The turbine shaft power is about 1 kWe and the ORC thermal efficiency is 6.8%. Schuster et al. (2010) worked with a supercritical ORC instead of a simple ORC system and showed that the heat losses were significantly reduced.

In recent years, work on ORC systems has focused on those systems that include the ejector. Jia et al. (2011) studied the behaviour of the ejector in terms of heat absorption and power generation potential of the ORC. Hem and Xu (2011) studied the ORC system with ejector and investigated the effects of the ORC on thermal efficiency. Zhao et al. (2012) used an ejector on a separate feed line in the ORC system and showed that the power system increased heat removal. Various studies on the ejector ORC system can be found in the reference list (Khaliq et al., 2012; Li and Zhang, 2012).

In ORC systems, the expander or turbine is one of the most important components that affect cost, system size, and efficiency. Gonzalez et al. (2015) identified and improved the detailed design method for ORC radial turbo-turbines. The results show that lowering the power reduces the isentropic efficiency and that the rotor and nozzle paths are the main loss points. Capata and Hernandez (2014) studied the basic designs of a turbo-turbine to meet the requirements of a variety of systems and presented a detailed design of the radial turbine. The thermomechanical performance study confirmed the structural loading and possible location.

Quoilin et al. (2010) showed that spiral turbines have potential for small expansion devices due to their low speed, high pressure ratio, and ease of replacement. Lemort et al. (2009) have studied how an air compressor can be integrated as a turbine in an ORC system. The results show that the isentropic efficiency can reach 68% and that the thermal parameters of the ORC system can be accurately calculated.

Yamada et al. (2010) developed an ORC system with a rotating blade turbine. Experimental results have shown that the turbine power can be about 1 kW under various conditions. B.R.Singh (2012)

and O.A.Singh (2012) set up a test setup for a prototype turbine with a rotating blade and investigated its performance. It has been shown that the yield values reach 95% at 3000 rpm.

Pei et al. (2011) set up an ORC system with a radial turbine in which the working fluid is R-123. Experimental measurements have shown that the isentropic turbine efficiency is 62.5%. Kang (2016) developed a two-stage radial turbine to increase the cycle efficiency by increasing the pressure ratio. The maximum electric power, cycle efficiency, and turbine efficiency were reported to be 39 kW, 9.8%, and 58.4%, respectively.

Li et al. (2018) study involves single and dual-pressure evaporation in Organic Rankine Cycle using nine different pure fluids. Evaporation pressures are optimized, and outlet temperatures are obtained. System performance is analysed and compared for temperatures between 100-200 °C. A quantitative criterion is provided to assess the optimal cycle type. Mondejar et al. (2018) studied nanofluids as potential working fluids for Organic Rankine Cycle. The impact of nanoparticle type and concentration on the heat exchangers size is analysed. Different from the traditional numerical calculation method (TNM) of ORC, a new thermodynamic cycle separating method (TCSM) is introduced in the study of (Wang et al., 2018). Braimakis and Karellas (2018) work focuses on the exergetic optimization of double stage Organic Rankine Cycle (DS ORC) for waste heat recovery. A model of a DS ORC, consisting of a high temperature (HT) stage serially connected to a low temperature (LT) stage is developed, while different combinations of working fluids with variable critical temperatures are considered in each stage.

Du et al. (2018) compares off-design performances of the basic organic Rankine cycle (ORC) and the parallel dual-pressure organic Rankine cycle (PDORC) for low temperature hot water. The particle swarm optimization (PSO) algorithm is applied to obtain optimal operating parameters. A statistical method for ORC performances analysis and comparison is introduced at (Landelle et al., 2017). An open-access database of ORC experiments is presented and released. A selection of simplified ORC thermodynamic performance criteria is proposed. Shao et al. (2017) is developed a new micro radial inflow turbine for a mini organic Rankine cycle (ORC) system in this study. With R123 as the working fluid, the turbine operational characteristics and performance are investigated by experiments. Eyerer et al. (2016) analysed R1233zd-E as a replacement for R245fa as working fluid for Organic Rankine Cycle for low temperature heat sources.

Molés et. al. (2016) analysed HCFO-1233zd-E as a replacement for HFC-245fa as working fluid for Organic Rankine Cycle for low temperature heat sources. Yuping Wang et al. (2016) made an experimental study on the practical performance of organic Rankine cycle (ORC) system using zeotropic mixture (R601a/R600a) is performed by using a small-scale ORC power generation experimental setup. In Han et al. (2014) study, a 200 kW Organic Rankine Cycle system was designed for waste heat recovery application using R245fa as a working fluid. S.Y.Cho (2015) and C.H.Cho (2015), in order to efficiently utilize such fluctuating thermal energy, an experimental study was conducted while adjusting the mass flowrate and the temperature of the working fluid.

Baral et al. (2015) introduces the concept of installing a small-scale organic Rankine cycle system for the generation of electricity in remote areas of developing countries. Hu et al. (2015) study conducts a detailed design and off-design performance analysis based on the preliminary design of turbines and heat exchangers. The radial inflow turbine and plate heat exchanger is selected in this paper. Lee et al. (2015) This paper deals with the design, fabrication, and test results of the ORC power generator. The ORC system was designed the maximum electric power output of 100kW utilizing geothermal hot water. Fu et al. (2015) involved designing and constructing a 250-kW organic Rankine cycle system, consisting of a pump, preheater, evaporator, turbine, generator, condenser, as well as hot and cooling water circulation systems. Refrigerant R245fa was used as a working fluid. The experimental tests also were performed, and the results of tests are compared with this existing study.

A practical method for designing Organic Rankine Cycle (ORC) power generation system was proposed at (Dong et al., 2015). The design method was aimed to optimize the cost performance of ORC system and based on experiments and theoretically modelling. The influences of various evaporators on the system responses of a 50 kW ORC system using R-245fa are investigated in (Lee et al., 2014).

Ata et al. (2019) evaluated the thermal efficiency of an Organic Rankine Cycle with n-pentane for medium enthalpy geothermal resource with 120 °C. Two different model has been built by using 9 different working conditions to determine thermal efficiencies in that study. In the first model, evaporation pressures change between 250-400 kPA while turbine inlet superheating temperatures are assumed constant. The turbine inlet superheating temperature varies between 0 and 20 while evaporation pressures are assumed constant in the second model. A thermodynamical energy

analysis model is developed by using Engineering Equation Solver (EES) program and it is not focused on performance and analysis of main equipment such as heat exchangers, condensers, pump and turbine. Only the thermal efficiency of the overall system has been calculated by changing of evaporation temperature and superheating temperature.

Hu et al. (2021) made an optimization of an Organic Rankine Power generation system for low enthalpy geothermal fluid with 100 °C temperature. They made a thermodynamical energy model in EES and they basically calculated the net power per unit mass flow rate of geothermal water, heat exchanger area required per kW net power and system thermal efficiency under different the narrow (pinch) point temperature difference from 0 to 16 Kelvin. They found that the best narrow point temperature difference is 5-7 K for the optimum ORC power generation and heat exchanger area. Song et al. (2020) made a comparative thermo-economic optimization study by using high-medium enthalpy geothermal resource with 180 °C. In this study, they calculated payback period of ORC by considering heat exchanger area and exergy efficiency for 6 different working fluids such as iso-pentane, R1233zd, R245fa, isobutane, R134a, R1234yf. They modelled two type ORCs with recuperated and non-recuperated cycles, but all cycle uses water cooled condenser.

Shengjun et al. (2011) studied an economical optimization and performance comparison of ORC for low temperature geothermal resource at 90 °C with 1 kg/s mass flow rate for different 16 subcritical and trans-critical working fluids. During this study, main energy and exergy balance calculated then total heat transfer area of heat exchangers evaluated for economical modelling. They calculate the heat transfer coefficients for heating, evaporating, and condensing by employing some correlations. However other geometric parameters which are studied within the scope of this thesis are not calculated except heat transfer area. The maximum theoretical net power output obtained 9.3 kW with R41 working fluid. This capacity can be applicable for only experimental studies, not industrial.

The most of studies in literature only focus on thermodynamical analysis or modelling and economical or performance optimization by using main thermodynamical and heat transfer formulas and correlations. Generally, the condensing part of ORC is selecting for water cooled system since heat transfer calculations are more simple and less complex than the air-cooled condenser. In literature who try to calculate the heat transfer coefficient by making detailed heat transfer calculations do not consider to evaluation of the fouling heat transfer coefficient. Except

only heat transfer area calculations of heat exchanger, the number of publications that focus on the geometric scaling of the main equipment of ORC is quite low.

The most important differences that distinguish this thesis from the most of studies are directly focus on detailed design of main components of Organic Rankine Cycle such as preheater, evaporator, and condenser. All geometrical properties are calculated by developed ORC Designer Program. In addition, air cooled condenser is used in the ORC because its widespread use in the geothermal industry due to scarcity of water resources. However, the water-cooled condenser is used in general literature because it is more efficient and easier to calculate. Furthermore, the heat transfer coefficient evaluation in air-cooled condensers is difficult while the detailed design and geometrical scaling calculations are very complex. Moreover, pressure drop calculations are performed in the modelling for pre-heater, evaporator and air-cooled condenser, although it has been ignored in most other studies. Heat transfer coefficient for clean and dirty (fouling) surface are calculated for all components of Organic Rankine Cycle.

The aim of this thesis is to design and prepare production data sheets of main components for an ORC unit with a gross power generation capacity of 250 kWe from a geothermal source of 90 °C, 150 tons/hour and 3 bar; and then achieve domestic manufacturing of almost 100% in future. There are many geothermal sources exploration below 100°C in geothermal fields that remain unused for electricity generation in the world. In the lowest temperature area that has been developed in Turkey, there is a geothermal power plant that generates 2.5 MWe of electricity, with a flow of about 900 tons per hour and a geothermal area of 103°C. There are some companies such as Exergy, Turboden, Electrathem, Climeon, Orcan, Rank etc. that are commercially producing low power in the world ORC. However, maximum capacities of them 100 kWe power plant over 100 ° C temperature for small scale projects. In this project the thermodynamic modelling and the main components design of the ORC plant with a capacity to produce 250 kWe of electricity from a geothermal source of 90 °C in accordance with the geothermal resources, economic and climatic conditions of our country.

3. MATERIAL

3.1 Heat Exchangers

A heat exchanger is a device for transferring heat from one fluid to another. There are three main categories: Recuperative, in which the two fluids are at all times separated by a solid wall; Regenerative, in which each fluid transfers heat to or from a matrix of material; Evaporative (direct contact), in which the enthalpy of vaporization of one of the fluids is used to provide a cooling effect (Kakac, 1992).

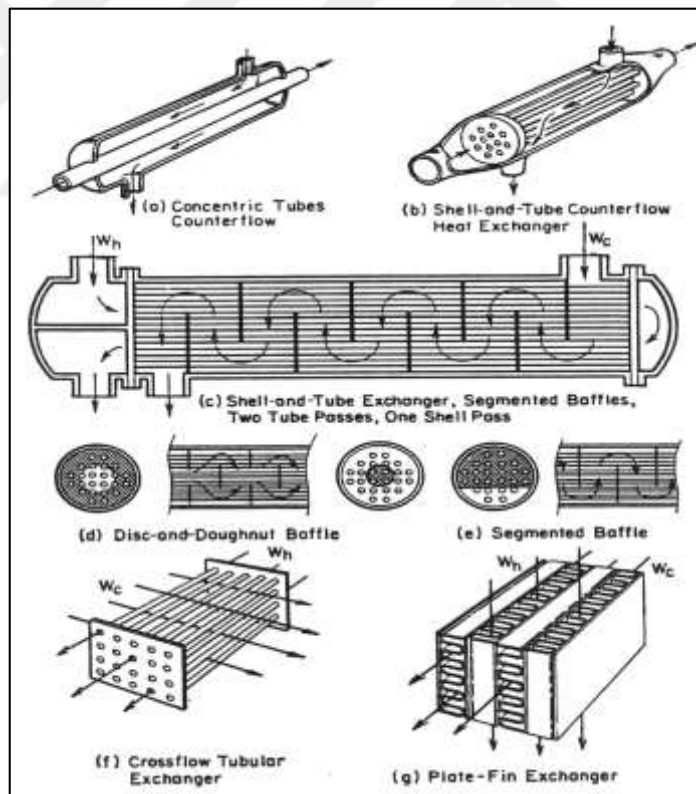


Figure 3.1 Several types of heat exchangers (Kakac, 1992)

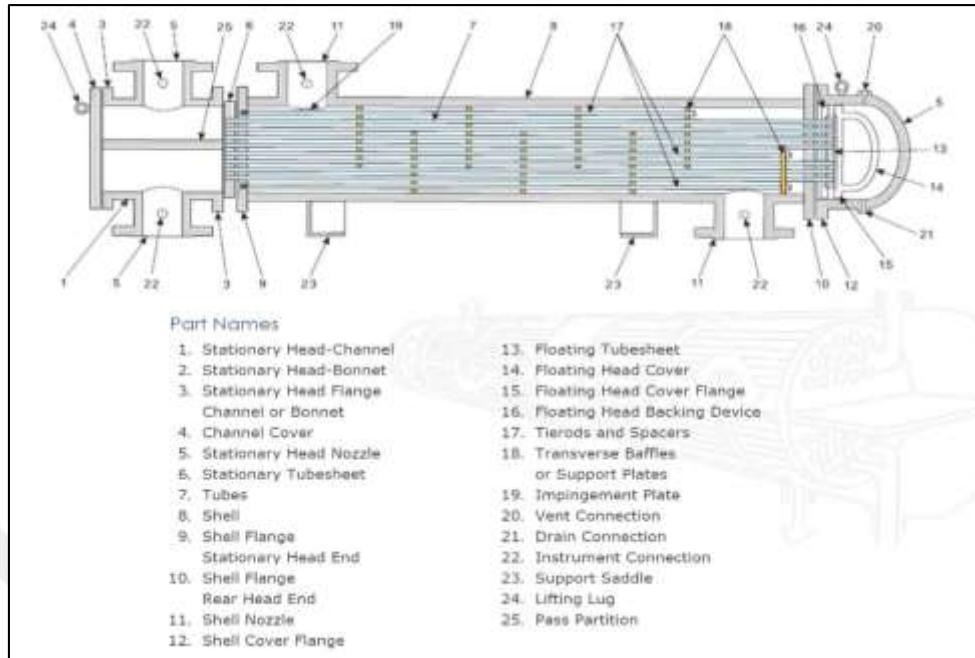


Figure 3.2 Part names of shell and tube heat exchanger (TEMA type AES WERMAC, 2022)

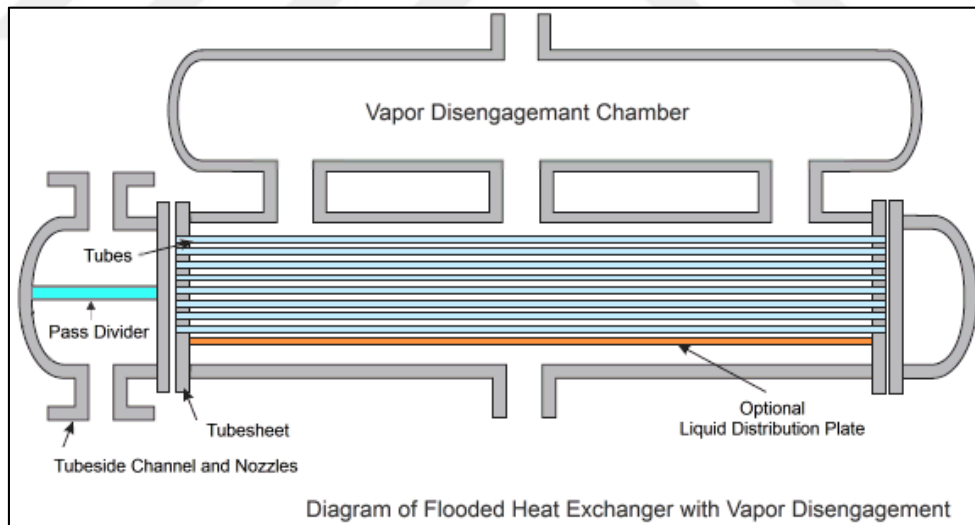


Figure 3.3 Flooded type shell and tube heat exchanger (TEMA X Shell WERMAC, 2022)

3.1.1 Thermal Design Considerations

The flow rates of both hot and cold streams, their terminal temperatures and fluid properties are the primary inputs of thermal design of heat exchangers.

Thermal design of a shell and tube heat exchanger typically includes the determination of heat transfer area, number of tubes, tube length and diameter, tube layout, number of shell and tube passes, type of heat exchanger (fixed tube sheet, removable tube bundle etc), tube pitch, number of baffles, its type and size, shell and tube side pressure drop etc (Ranjeet et al., 2020).

3.1.1.1 Shell

Shell is the container for the shell fluid and the tube bundle is placed inside the shell. Shell diameter should be selected in such a way to give a close fit of the tube bundle. The clearance between the tube bundle and inner shell wall depends on the type of exchanger. Shells are usually fabricated from standard steel pipe with satisfactory corrosion allowance. The shell thickness of 3/8 inch for the shell ID of 12-24 inch can be satisfactorily used up to 300 psi of operating pressure (Ranjeet et al., 2020).

3.1.1.2 Tube

Tube OD of $\frac{3}{4}$ and 1" are very common to design a compact heat exchanger. The most efficient condition for heat transfer is to have the maximum number of tubes in the shell to increase turbulence. The tube thickness should be enough to withstand the internal pressure along with the adequate corrosion allowance. The tube thickness is expressed in terms of BWG (Birmingham Wire Gauge) and true outside diameter (OD). The tube length of 6, 8, 12, 16, 20 and 24 ft are preferably used. Longer tube reduces shell diameter at the expense of higher shell pressure drop. Finned tubes are also used when fluid with low heat transfer coefficient flows in the shell side. Stainless steel, admiralty brass, copper, bronze, and alloys of copper-nickel are the commonly used tube materials:

3.1.1.3 Tube pitch, tube-layout, and tube-count

Tube pitch is the shortest centre to centre distance between the adjacent tubes. The widely used tube layouts are illustrated in Table 3.1. The number of tubes that can be accommodated in a given shell ID is called tube count. The tube count depends on the factors like shell ID, OD of tube, tube pitch, tube layout, number of tube passes, type of heat exchanger and design pressure.

3.1.1.4 Tube passes

The number of passes is chosen to get the required tube side fluid velocity to obtain greater heat transfer co-efficient and to reduce scale formation. The tube passes vary from 1 to 16. The tube passes of 1, 2 and 4 are common in application. The partition built into exchanger head known as partition plate (also called pass partition) is used to direct the tube side flow (Ranjeet et al., 2020).

Table 3.1 Common tube layouts (utilized from Kakac, S. (1992))

Tube OD, in	Pitch type	Tube pitch, in
3/4	Square	1
1		1/4
3/4	Triangular	15/16
3/4		1

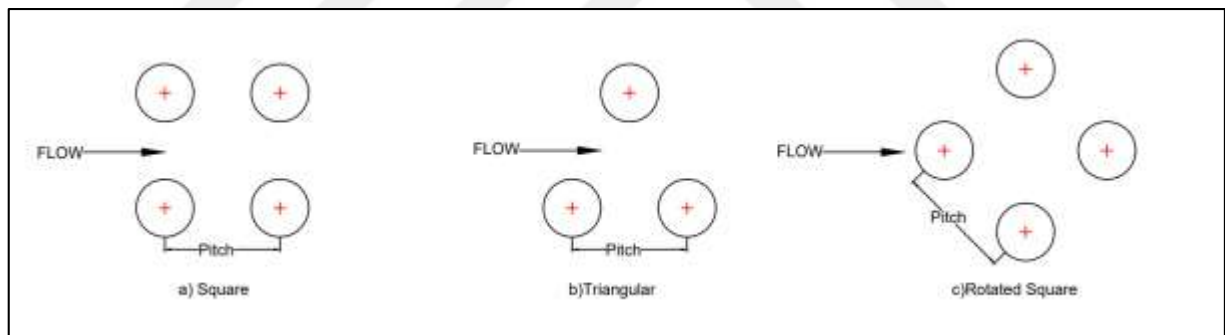


Figure 3.4 Heat exchanger tube-layouts (utilized from Kakac, S. (1992))

3.1.1.5 Baffles

Baffles are used to increase the fluid velocity by diverting the flow across the tube bundle to obtain higher transfer co-efficient. The distance between adjacent baffles is called baffle spacing. The baffle spacing of 0.2 to 1 times of the inside shell diameter is commonly used. Baffles are held in position by means of baffle spacers. Closer baffle spacing gives greater transfer co-efficient by inducing higher turbulence. The pressure drop is more with closer baffle spacing. The various types of baffles are shown in Figure 3.5. In case of cut-segmental baffle, a segment (called baffle cut) is removed to form the baffle expressed as a percentage of the baffle diameter. Baffle cuts from 15 to

45% are normally used. A baffle cut of 20 to 25% provide a good heat-transfer with the reasonable pressure drop. The % cut for segmental baffle refers to the cut away height from its diameter. Figure 3.5 also shows two other types of baffles (NPTEL, 2015).

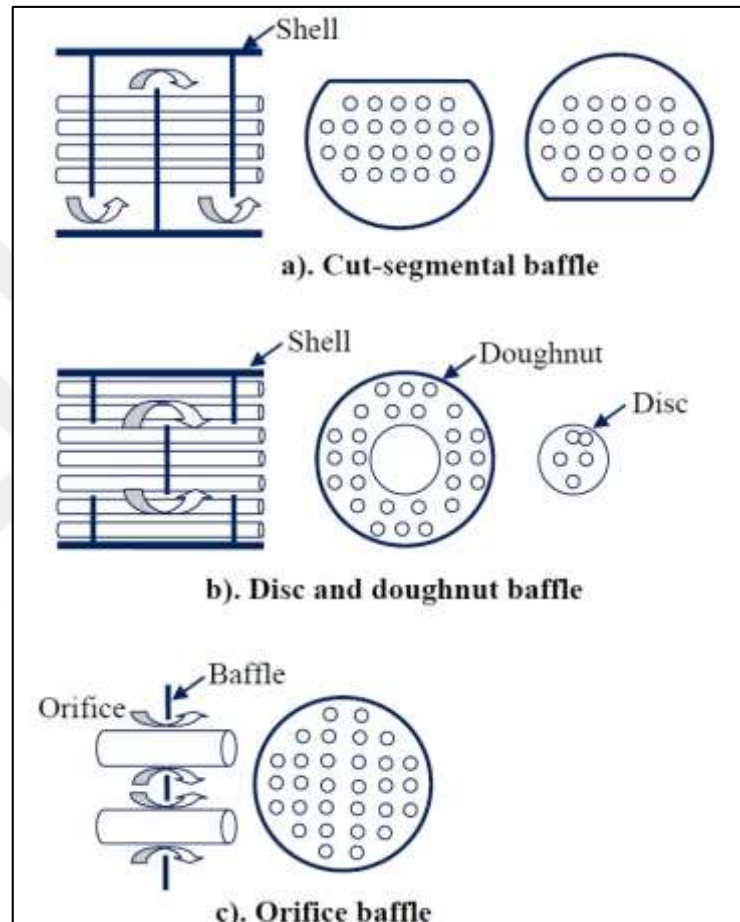


Figure 3.5 Different type of heat exchanger baffles (utilized from NPTEL (2015))

3.1.1.6 Fouling Considerations

Most of the process fluids in the exchanger foul the heat transfer surface. The material deposited reduces the effective heat transfer rate due to relatively low thermal conductivity. Therefore, net heat transfer with clean surface should be higher to compensate the reduction in performance during operation. Fouling of exchanger increases the cost of (i) construction due to oversizing, (ii) additional energy due to poor exchanger performance and (iii) cleaning to remove deposited

materials. A spare exchanger may be considered in design for uninterrupted services to allow cleaning of exchanger (Kazi, 2011).

The effect of fouling is considered in heat exchanger design by including the tube side and shell side fouling resistances. Typical values for the fouling coefficients and resistances are summarized in Table 3.2.

Table 3.2 Typical values of fouling coefficients and resistances (utilized from NPTEL (2015))

Fluid	Coefficient ($W.m^2.^{\circ}C^{-1}$)	Resistance ($m^2.^{\circ}C. W^{-1}$)
River water	3000-12,000	0.0003-0.0001
Sea water	1000-3000	0.001-0.0003
Cooling water (towers)	3000-6000	0.0003-0.00017
Towns water (soft)	3000-5000	0.0003-0.0002
Towns water (hard)	1000-2000	0.001-0.0005
Steam condensate	1500-5000	0.00067-0.0002
Steam (oil free)	4000-10,000	0.0025-0.0001
Steam (oil traces)	2000-5000	0.0005-0.0002
Refrigerated brine	3000-5000	0.0003-0.0002
Air and industrial gases	5000-10,000	0.0002-0.0001
Flue gases	2000-5000	0.0005-0.0002
Organic vapors	5000	0.0002
Organic liquids	5000	0.0002
Light hydrocarbons	5000	0.0002
Heavy hydrocarbons	2000	0.0005
Boiling organics	2500	0.0004
Condensing organics	5000	0.0002
Heat transfer fluids	5000	0.0002
Aqueous salt solutions	3000-5000	0.0003-0.0002

3.2 Air Cooled Condenser

An air-cooled heat exchanger is used to cool liquids with ambient air. Several articles have been published detailing its application and economic analysis. This section describes the general design of air-cooled heat exchangers and presents a method for approximate sizing.

3.2.1 Arrangement & Mechanical Design

Figures 3.6 show typical top and bottom views of horizontal air-cooled heat exchangers as commonly used. The basic components are one or more pipe sections served by one or more axial fans, fan drives, velocity reducers, and a shroud and support structure.

Air-cooled heat exchangers are referred to as fan heat exchangers when the tube section is on the discharge side of the fan, and suction heat exchangers when the tube section is on the suction side of the fan (Admiraal and Bullard, 1993).

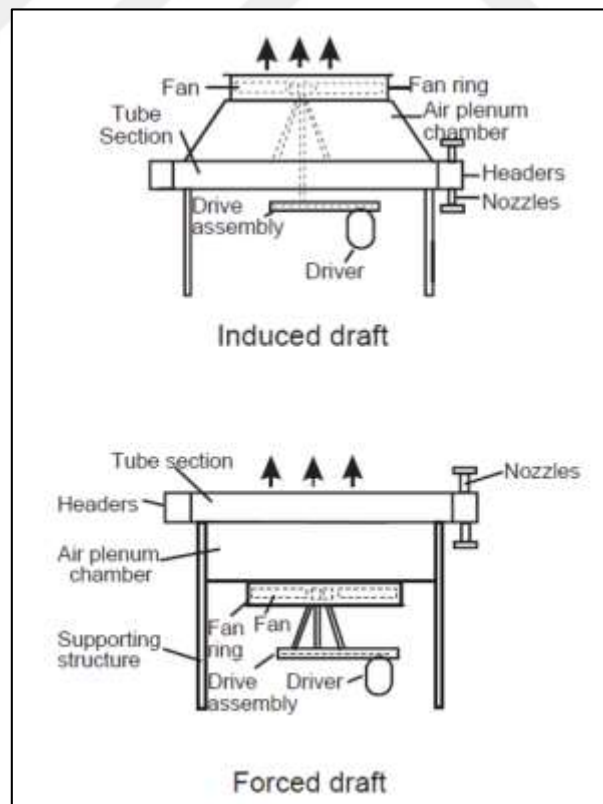


Figure 3.6 Typical Side Elevations of Air-Cooled Condensers (utilized from Tulsa (1998))

The advantages of induced draft are:

- Better distribution of air over the section.
- Less possibility of hot exhaust air flowing back to the section inlet. Hot air is expelled upward at about 2.5 times the intake velocity, or about 450 m/min.
- Less exposure to sun, rain, and hail, as 60% of the front surface of the section is covered.
- Higher capacity in case of fan failure since the natural chimney effect is much greater with the induced draft.

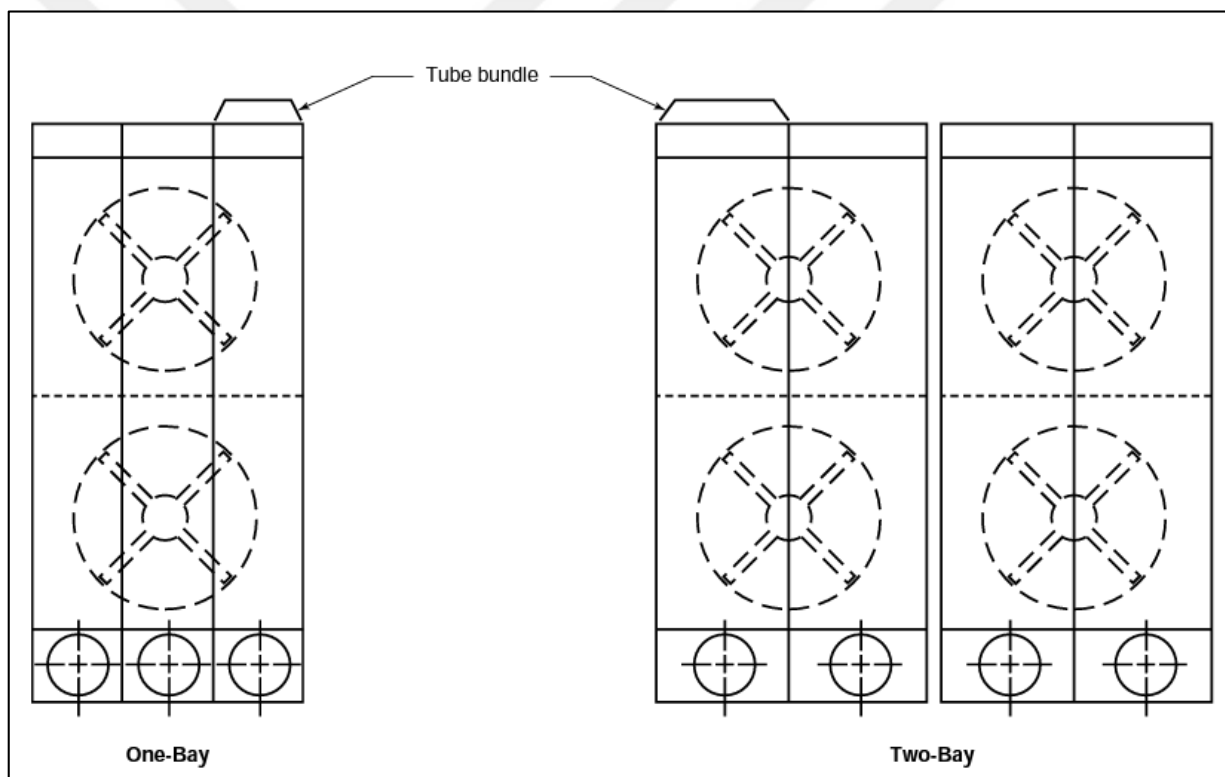


Figure 3.7 Typical Plan Views of Air-Cooled Condensers (API STANDARD 661 API (1997))

The disadvantages of the induced draft are:

- Higher power because the fan is in the hot air.
- Exhaust air temperature should be limited to 95°C to avoid possible damage to fan blades, bearings, V-belts, or other mechanical components in the hot air stream.

- Fan drive components are less accessible for maintenance and may need to be serviced in the hot air generated by natural convection.
- A blower system should be used for process fluids above 175°C, otherwise fan blades and bearings could be exposed to excessive temperatures in the event of fan failure (Michael et al., 1996).

The advantages of the forced draft are:

- Slightly lower horsepower because the fan is in cold air. (Horsepower varies directly with absolute temperature).
- Better accessibility to mechanical components for maintenance.
- Easily adaptable for warm air return in cold climates.

The disadvantages of forced draft are:

- Poor distribution of air across the section.
- Greatly increased possibility of warm air recirculation due to low discharge velocity from sections and lack of chimney.
- Low natural draft in case of fan failure due to low stack effect.
- Pipes are fully exposed to sun, rain, and hail.

The horizontal section is the most used air-cooled section and generally the most economical. For a liquid with freezing potential, the pipes should slope at least 10 mm per meter toward the outlet header. Since there is no problem with freezing in most cases and it is more costly to design an inclined unit, most chillers are designed with level sections (Tulsa, 1998).

Vertical sections are sometimes used when maximum drainage and head are required, such as in condensing units. Angle sections are used like vertical sections for condensing units and provide positive drainage. Angle sections are often inclined thirty degrees (30°) from horizontal.

The size of the fans ranges from 0.9 m to 8.5 m in diameter. However, the largest diameter normally used is 4.3 m to 4.9 m. The fans can be driven by electric motors, steam turbines, hydraulic motors,

or gasoline engines. A reduction gear, such as a V-belt drive or a reduction gear, is required to match the output speed of the drive to the relatively slow speed of the axial fan. The peak speed of the fan is typically 3650 m/min or less. V-belt drives are usually used up to a power of about 22 kW, and gear drives are used at higher powers. The size of individual drives is usually limited to 37 kW (Tulsa, 1998).

Dual fan shafts are very popular as this provides a level of security against fan or driver failure and a method of control through fan stepping. Fan coverage is the ratio between the projected area of the fan and the area served by the fan. It has been found to be best to keep this ratio above 0.40 whenever possible, as a higher ratio improves air distribution over the area of the pipe section. The face area is the footprint of the heat transfer area available to the airflow at the face of the section.

The heat transfer device is the tube section, an assembly of side frames, tube supports, headers, and finned tubes. Typically, aluminium fins are added to the tubes to provide greater surface area on the air side to compensate for the relatively low heat transfer coefficient of the air to the tube. There are several types of fins, which are tension wound, embedded, extruded, and welded (Tulsa, 1998).

For economic reasons, tension-wrapped tubing is probably the most used fin type. Tension-wrapped tubing is common for continuous service at temperatures below 200°C. Extruded fins are a mechanical connection between an inner tube, which is exposed to the process, and an outer tube or sleeve (usually aluminium), which is extruded to form a tall fin.

Embedded fins are aluminium or steel fins that are notched into the base pipe. Embedded fins are used in cyclic and high temperature applications. Other types of fin tubes available include brazed, edge-wrapped, and serrated, stress-wrapped. Coolers are regularly manufactured in tube lengths ranging from 1.8 m to 15 m and field widths from 1.2 m to 9.1 m. The use of longer tubes usually results in a more cost-effective design compared to the use of shorter tubes.

Base tubes range in diameter from 16 mm to 38 mm OD and are provided with 12.7 mm to 25.4 mm high fins spaced at 276 to 433 per meter, providing an extended fin surface that is 12 to 25 times the outer surface of the base tube. The tubes are typically arranged in a triangular grid with the fin tips of adjacent tubes touching or spaced 1.6 mm to 6.4 mm apart.

Matching the tube section to the fan system and heat transfer requirements usually results in the section having a depth of 3 to 8 rows of finned tubes, with 4 rows being most typical. A 25.4 mm OD tube is the most common diameter, and the most common fins are 12.7 mm or 15.9 mm high.

The data shown in Table 3.3 is for 25.4 mm OD tubes with 12.7 mm high fins, 354 fins/m and 15.9 mm high fins, 394 fins/m.

Table 3.3 Fin tube data for 25.4 mm OD tubes (utilized from Tulsa (1998))

Fin height by Fins/meter	12,7 mm by 354		15,9 mm by 394	
APM, m ² /m	1.16		1.70	
AR, m ² / m ²	14.5		21.4	
Tube Pitch	51 mm	57 mm	57 mm	64 mm
APSM (3 rows)	68.4	60.6	89.1	80.4
APSM (4 rows)	91.2	80.8	118.8	107.2
APSM (5 rows)	114.0	101.0	148.5	134.0
APSM (6 rows)	136.8	121.2	178.2	160.8

Note: APM is the area of fin tube per meter of tube length in m²/m. AR is the area ratio of fin tube compared to the exterior area of 25.2 mm OD bare tube which has 0.0798 m²/m. APSM is the fin tube area (m²) per m² of bundle face area.

Common materials for headers are furnace grade carbon steel, ASTM SA -515-70, SA -516-70. Tubes are generally ASTM SA -214 (ERW), SA -179 (SMLS), carbon steel. Blades are generally carbon steel or aluminium, with carbon steel being the most common and economical design. Blades are usually aluminium. Both stainless steel and brass alloys have their applications but are more expensive than carbon steel.

3.2.2 Header Design

In the construction of plug collectors, a welded box is used that allows partial access to the pipes by means of shoulder plugs opposite the pipes (Admiraal and Bullard, 1993). This construction is usually used because it is cheaper than the alternative construction with cover plates. The construction with cover plates allows full access to the tubes and the tube sheet. This design is used when fouling is high, and pressure is low. Figure 3.8 shows typical designs for both plug and cover headers (Tulsa, 1998).

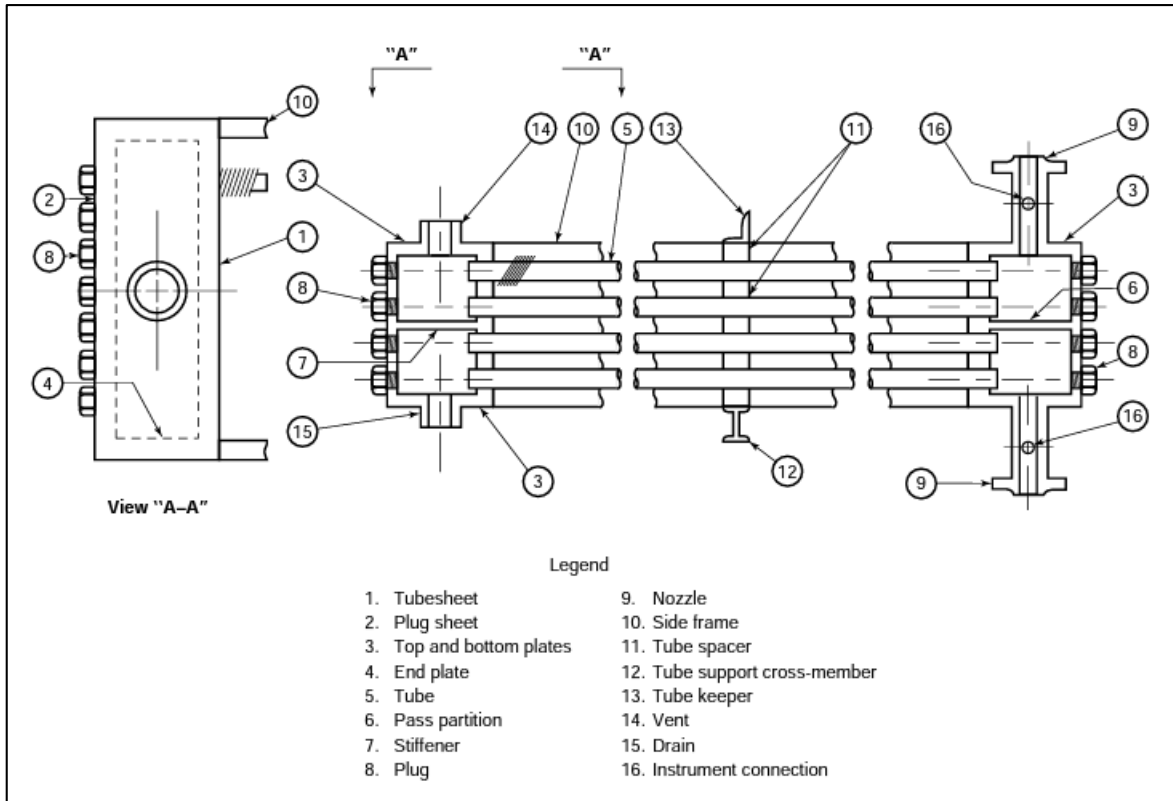


Figure 3.8 Typical Construction of Tube Section with Plug Headers (WERMAC, 2022)

3.2.3 Warm Air Recirculation

Air-cooled heat exchangers are made to operate at warm (summer) air temperatures. Seasonal variations in air temperature can cause overcooling, which may be undesirable. One way to control cooling capacity is to vary the amount of air flowing through the tube section. This can be accomplished by using various motors, 2-stage drives, variable speed motors, louvers on the front of the tube section, or variable pitch fans (Shao et al. 2017).

Extreme forms in air temperature, such as those found in northern climates, may require special air recirculation devices. These are needed to control process stream temperatures and prevent freezing of liquid streams. Hot air recirculation areas from a standard chiller with a reversible fan to a fully enclosed system with automatic louvers and fans. These two commonly used systems are referred to as "internal recirculation" and "external recirculation".

A typical layout for middle circulation is shown in Figure 3.9. When the ambient temperature is low, the manual fan continues to push air through the inlet half of the section. The automatic fan

operates in opposite mode, drawing hot air from the upper recirculation chamber down through the outlet end of the section (Russel et al. 2008). Through the lower recirculation apron, the manual fan mixes some of the hot air delivered downward by the automatically controlled fan with cold outside air and the process reruns. The upper exhaust dampers are automatically adjusted by a temperature controller that measures the flow of the process fluid. When the temperature of the liquid increases, the louvers are opened. Under normal ambient conditions, the louvers are fully open and both fans operate in ordinary forced draft mode.

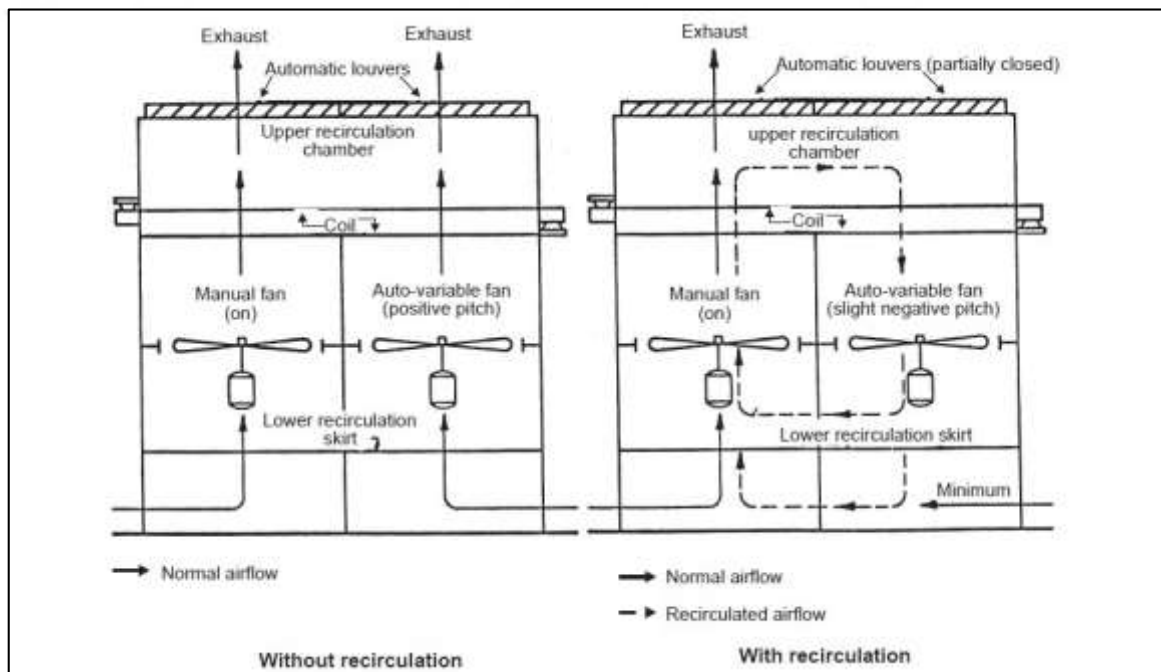


Figure 3.9 Internal Recirculation Design (Tulsa, 1998)

An internal circulation chiller is a compromise between no circulation and fully controlled external circulation. It is cheaper than full external circulation and has a lower static pressure drop at maximum ambient temperature. An internal circulation chiller is easier to erect and requires less floor space than an external circulation design. However, the latter is more expensive than a cooler without recirculation and cannot provide complete freeze protection. Since there is no control over the air supply and the fans alone cannot fully mix the air, stratified cold air can come into contact with the area. When the fans are off, high wind speed in low ambient conditions can cause too much cold air to enter the area (Tulsa, 1998).

A typical layout for external circulation is shown in Figure 3.10. For low ambient temperatures, low-speed two-stage motors or low-pitch self-regulating fans are typically used. In that design, the sides of the chiller are closed with manual louvers. At each end, a recirculation chamber projects above the section columns and provides a duct for mixing cold outside air with warm recirculated air. As with internal recirculation, the upper exhaust dampers are controlled by the temperature of the process fluid. However, this design allows control of the inlet air temperature. When the supply air damper closes, an internal damper in the end duct opens. These adjustments are determined by a controller that measures the air temperature at the fan. Once the system reaches equilibrium, it automatically regulates the process temperature and prevents excessive cooling. In warm weather, the side manual louvers are opened while the exhaust louvers nearby are modified (Tulsa, 1998).

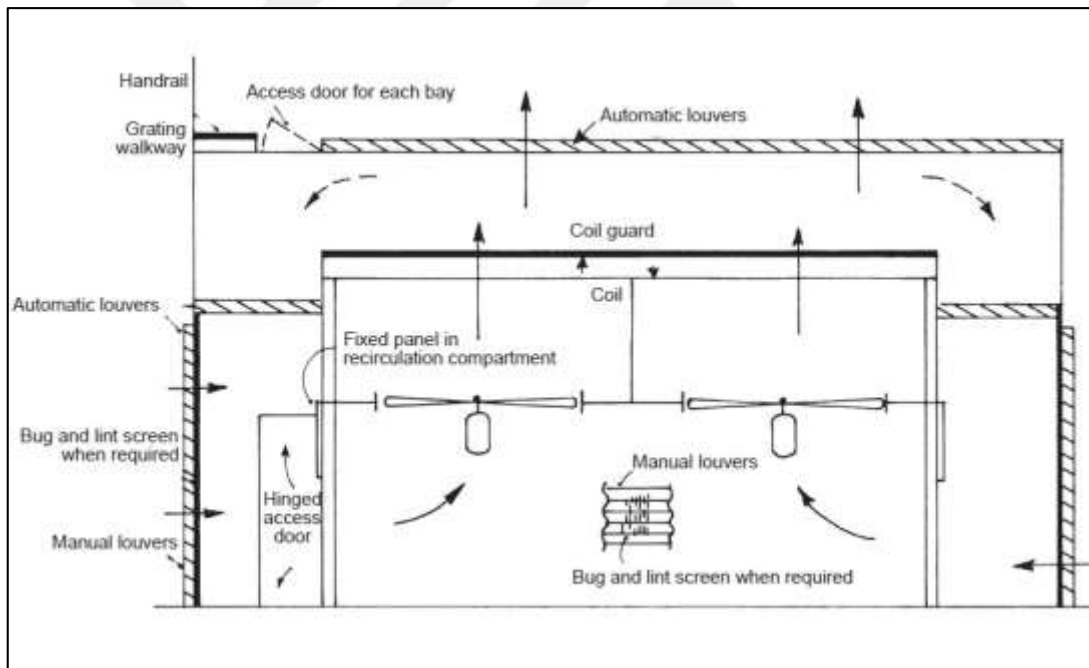


Figure 3.10 External Recirculation Design (Tulsa, 1998)

External circulation is preferred for critical control and prevention of freezing. Once in operation, it requires little attention. In the event of a loss of power or air supply, the system automatically closes to prevent freezing. It can be designed to automatically reduce motor energy consumption when excess cooling is provided. The major disadvantage of this type of system is its high cost. Multiple actuators and control devices are required, as well as more steel and fins. The system is usually too large to be shop mounted and requires more field assembly than an internal system.

Because the air supply must be throttled, this design increases static pressure, resulting in higher energy consumption and 20-25% larger motors than a standard chiller. When designing an external recirculating chiller, the depth of the plenum and piping must be considered to allow air mixing and avoid excessive static pressure drop. The air inlet area should be large enough to keep the airflow below 152 m/min at maximum design conditions (Kakac and Paykoc, 1988).

3.2.4 Condensing Discussion

Condensation in horizontal pipes may involve partial or complete condensation of the steam. Depending on the application, the entering steam may be superheated, equal to 1.0, or less than 1.0. Therefore, the condensation process may start with a dry wall flash zone, followed by a wet wall flash zone, then a saturated condensation zone, and finally a liquid sub cooling zone (Wolverine Tube Inc., pp. 8.1-8.27, 2006). The condensing heat transfer coefficient is a strong function of local vapour quality and increases with increasing vapour quality. The condensing heat transfer coefficient is also a strong function of mass velocity, increasing with increasing mass velocity. Unlike external condensation, condensation within the tube is independent of wall temperature difference ($T_{sat}-T_w$) for most operating conditions, except at low mass flow rates.

Figure 3.11-3.12 illustrate the two-phase flow patterns typical of condensation in horizontal tubes. In the upper diagram, at high mass flow rates, the flow takes the form of an annular flow with the liquid film at the periphery of the wall, the vapour in the central core, and some liquid entrained into the vapour from the tips of the waves at the interface of the film (Coker, 2015).

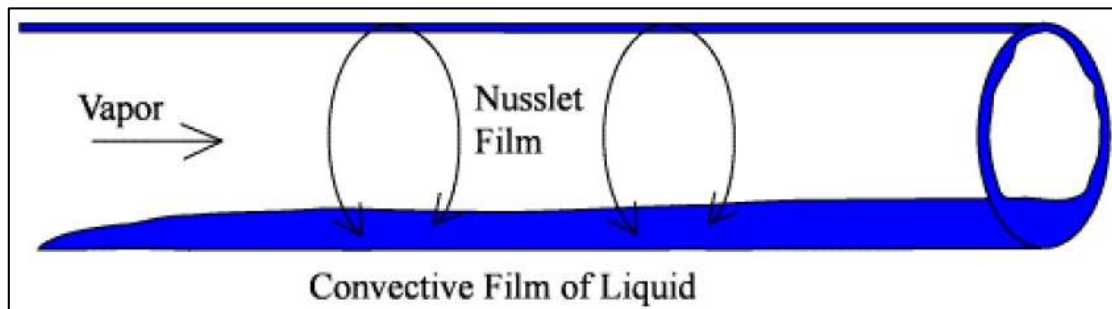


Figure 3.11 Stratified flow with film condensation around the top internal perimeter of the tube (Wolverine Tube Inc., pp. 8.1-8.27, 2006)

A film of condensate is formed which flows downward from above under the influence of gravity. The film flows laminarily and mainly downward when the velocity of the vapour core is low.

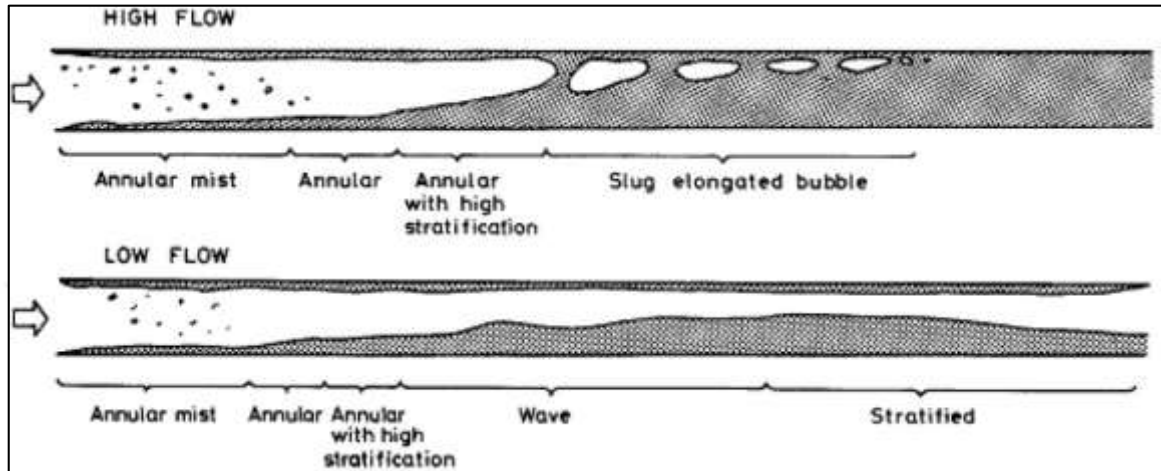


Figure 3.12 Typical flow patterns for condensation inside horizontal tubes (Wolverine Tube Inc., pp. 8.1-8.27, 2006)

When the vapour shear is sufficient and the onset of turbulence has been exceeded, a turbulent film is formed whose predominant flow direction is axial (Coker, 2015).

For condensation on the air-cooled condenser, the following equations are used as shown in Figure 3.13.

- Aker,
- Shah,
- Dobson & Chato Annular,
- Dobson & Chato Stratified Wavy,
- Dobson & Chato Stratified,
- Thome-El Hajal-Cavallini Intermittent Mist,
- Thome-El Hajal-Cavallini Stratified,

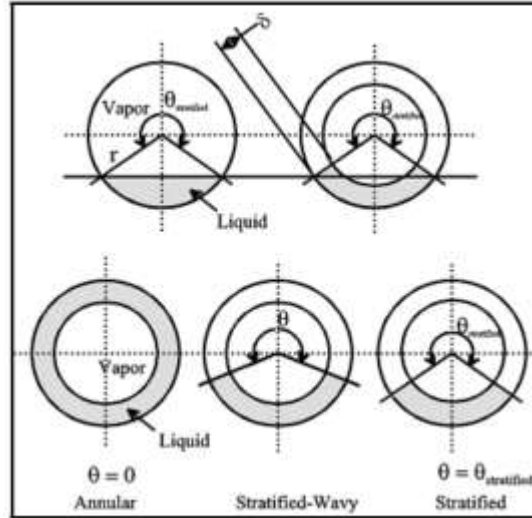


Figure 3.13 Simplified two-phase flow structures assumed for annular, stratified-wavy and stratified flow regimes (Wolverine Tube Inc., pp. 8.1-8.27, 2006)

The example given is for cooling problems and would work with straight condensation problems that have the approximate range between the dew point and bubble point of the liquid. In cases where superheating or sub cooling or disproportionate condensation occurs at certain temperatures, as with steam and non-condensable, calculations for air coolers should be done by "zone". A heat rejection curve developed from enthalpy data shows the amount of heat that must be removed between different temperatures. The zones to be calculated should be straight-line zones, i.e., from the inlet temperature of a zone to its outlet, the heat load per degree of temperature is the same (Admiraal and Bullard, 1993).

Once the zones have been determined, an approximate rate must be determined for each zone. To do this, take the rates of vapour cooling, condensation, and liquid cooling, and then average them based on the percentage of heat load for that phase within the zone. Next, calculate the LMTD of each zone. Start with the discharge zone, using the final design discharge temperature and the inlet temperature for that zone. Continue to calculate the zone as if it were a chiller, except that only one pass and one or two rows should be assumed, depending on the percentage of heat load in that zone. When calculating the pressure drop, average conditions can be used for estimation.

If the calculations for zone one (or later a subsequent zone) result in a large number of short tubes with one passage, as is the case with steam and no condensable, recalculate the zone with multiple rows (usually four) and short tubes with one passage that uses only a percentage of the total

allowable pressure drop. The total chiller is calculated as if each zone were a chiller connected in series with the next, except that only the pressure drops of the tubes for the middle zones should be calculated. Thus, each zone must have the same number of tubes, and the actual environment must be used in the LMTD calculation. Only the length of the pipes may vary, with odd lengths acceptable for a zone as long as the total length is rounded to a standard pipe length.

If the calculations for zone one (and succeeding zones) fit well into a longer tube length, the LMTD must be weighted. After the outlet zone has been calculated, calculate zone two using the inlet temperature for it and its outlet temperature, which is the inlet temperature of zone one. The “ambient” used to find the zone two LMTD will be the design ambient plus the air rise from zone one. Continue in this manner, always using the previous zone’s outlet air temperature in calculating the current zone’s LMTD. After the cooler size and configuration have been determined, the fan and motor calculations will be made in the normal manner (Admiraal and Bullard, 1993).

The final pressure drop is the sum of the drops for each zone, or approximately the sum of the drops for each phase, using the pipe length and diffuser arrangement for each phase. An estimated total pipe-side coefficient can be calculated by estimating the coefficient for each phase. Then form a weighted average based on the percentage of heat load for each phase. The total LMTD must be the weighted average of the calculated zone LMTDs (Russel et al., 2008).

4. METHOD

In this chapter, the design and modelling techniques and equations of shell-and-tube heat exchangers and air condensers and their solution methods are presented. First, a general description of the system is given. Second, the analytical and numerical modelling equations for shell and tube heat exchangers and the solution methods are examined. Finally, the modelling equations for air condensers are presented.

4.1 Heat Exchangers Calculation

HEX designers usually use two well-known methods for calculating the heat transfer rate between fluid streams-the UA-LMTD and the effectiveness-NTU (number of heat transfer units) methods. Both methods can be equally employed for designing HEXs. However, the ε -NTU method is preferred for rating problems where at least one exit temperature is unknown. If all inlet and outlet temperatures are known, the UA-LMTD method does not require an iterative procedure and is the preferred method.

The most used type of heat exchanger is the recuperative heat exchanger (Kakac, 1992). In this type the two fluids can flow in counter-flow, in parallel-flow, or in a combination of these, and crossflow. In modelling a shell and tube heat exchanger, a design problem is considered where the inlet and outlet conditions of the PTSC side (shell side of the heat exchanger) and the inlet conditions of the ORC side (tube side of the heat exchanger) are known. Using the model developed, the overall heat transfer coefficient, the heat transfer surface area and the pressure drop across the heat exchanger are found (Erdogan et al., 2017).

The ε -NTU Method:

- Capacity rate ratio:

$$C^* = \frac{C_{min}}{C_{max}} \quad (1)$$

- Heat transfer area number:

$$NTU = \frac{AU}{C_{min}} \quad (2)$$

- Exchanger heat transfer effectiveness (for 1-2 shell and tube heat):

$$\varepsilon = \frac{2}{1 + C^* + (1 + C^{*2})^{1/2}} \frac{1 + \exp[-NTU(1 + C^{*2})^{1/2}]}{1 - \exp[-NTU(1 + C^{*2})^{1/2}]} \quad (3)$$

In this study, we will use UA-LMTD method because of all inlet and outlet temperatures are known

UA-LMTD method:

The heat capacity rates for the shell fluid(iso-butane) and the tube fluid(brine) are calculated by equation (4) and (5).

$$C_h = (\dot{m}c_p)_h = \dot{m}_{brine} * c_{p,brine} \quad (4)$$

$$C_c = (\dot{m}c_p)_c = \dot{m}_{btane} * c_{p,butane} \quad (5)$$

We need to calculate Log mean temperature difference from the four-given inlet-outlet temperatures (Kakac and Liu, 1998):

$$\Delta T_1 = T_{h2} - T_{c1} = T_{brine,out} - T_{butane,in} \quad (6)$$

$$\Delta T_2 = T_{h1} - T_{c2} = T_{brine,in} - T_{butane,out} \quad (7)$$

$$\Delta T_{lm,butane} = \frac{\Delta T_2 - \Delta T_1}{\ln(\Delta T_2 / \Delta T_1)} \quad (8)$$

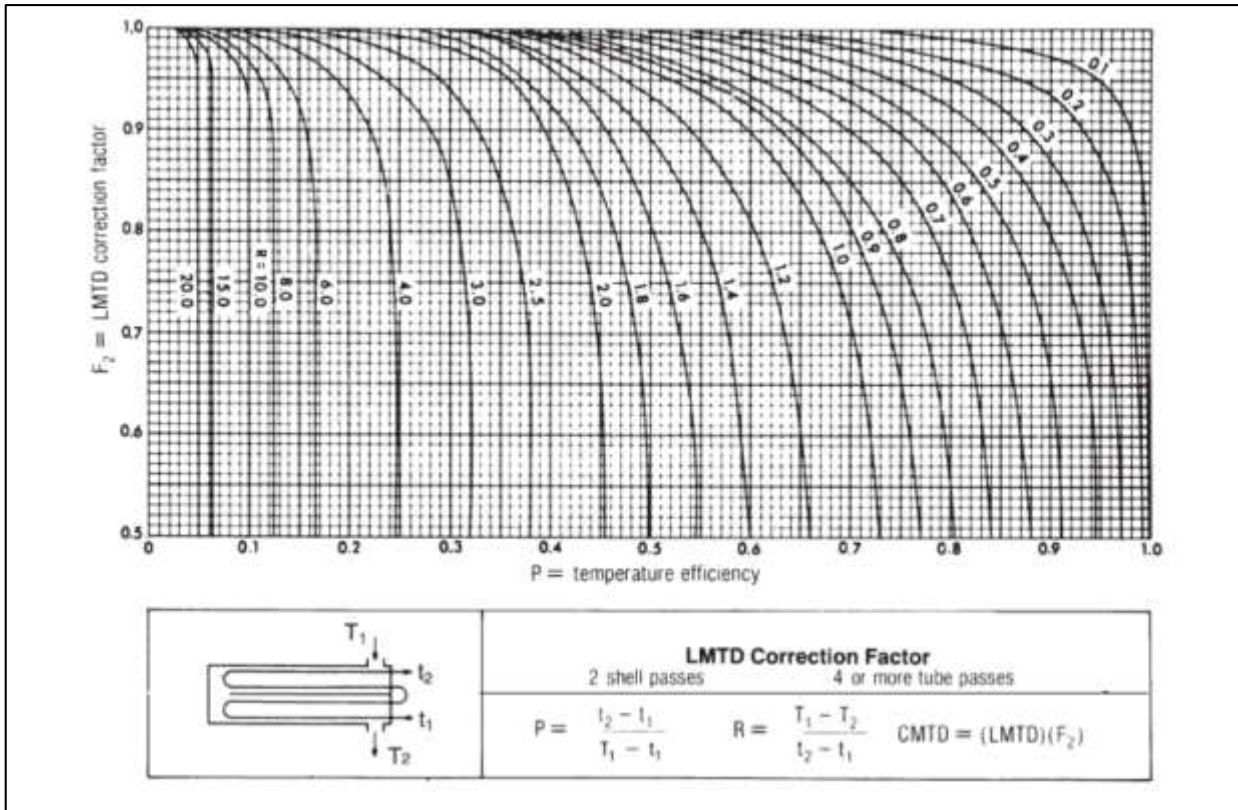


Figure 14 LMTD correction factor F for a shell-tube heat exchanger. Two-shell passes and four or multiples of four tube passes. (From Standards of Tubular Exchanger Manufacturers Association (1988), New York.)

$$P = \frac{T_{c2} - T_{c1}}{T_{h1} - T_{c1}} = \frac{\Delta T_c}{\Delta T_{max}} \quad (9)$$

$$R = \frac{C_c}{C_h} = \frac{T_{h1} - T_{h2}}{T_{c2} - T_{c1}} \quad (10)$$

P is a measure of the ratio of the heat transferred to the cold fluid to the heat which would be transferred if the same fluid were to be raised to the hot fluid inlet temperature, therefore P is the temperature effectiveness of the heat exchanger on the cold fluid side. R is heat capacity ratio (Kakac and Paycoc, 1988).

F is LMTD correction factor which is nondimensional and depends on P and R.

$$F = \frac{\sqrt{R^2 + 1} \cdot \ln[(1 - P)/(1 - PR)]}{(R - 1) \ln[(2 - P\{(R + 1 - \sqrt{R^2 + 1})\})/(2 - P\{(R + 1) + \sqrt{R^2 + 1}\})]} \quad (11)$$

We may write the total heat transfer rate between the hot and cold fluids:

$$Q_c = (\dot{m}c_p)_c (\Delta T_c) \quad (12)$$

$$Q_h = (\dot{m}c_p)_h (\Delta T_h) \quad (13)$$

$$Q_{total} = Q_f + Q_c + Q_h \quad (14)$$

Calculation of latent heat,

$$LH = h_{vapsat} - h_{liqsat} \quad (15)$$

h_{vapsat} : Saturation of vapour enthalpy

h_{liqsat} : Saturation of liquid enthalpy

The maximum heat load calculation is shown in the equation (16),

$$Q_{duty} = Q_{total} * (1 + Q_{loss}) \quad (16)$$

Heat flux calculation:

$$q = \frac{Q_{duty}}{A_{out}} \quad (17)$$

We can find the mean temperature:

$$\Delta T_m = F \cdot \Delta T_{lm, butane} \quad (18)$$

The initial size (surface area) of a heat exchanger can be estimated from:

$$A_{ex} = \frac{Q}{U \cdot \Delta T_m} \quad (19)$$

The Length of Heat Exchanger can be found by:

$$L = \frac{A_{ex}}{\pi \cdot D_{t0} N_t} \quad (20)$$

d_o : The tubes of diameter

N_t : The number of tubes

L: Tube length.

Shell Diameter:

Shell diameter in terms of main constructional diameters can be found as (Kakac and Liu, 1998):

$$D_s = 0.637 \cdot \sqrt{\frac{CL}{CTP} \left(\frac{A_{ex} \cdot (PR)^2 \cdot D_{to}}{L} \right)^{\frac{1}{2}}} \quad (21)$$

Tube layout is characterized by the included angle between tubes. Two standard types of tube layouts are the square and the equilateral triangle. Triangular pitch (30° layout) is better for heat transfer and surface area per unit length (greatest tube density.) Square pitch (45° & 90° layouts) is needed for mechanical cleaning (Lee, 2010).

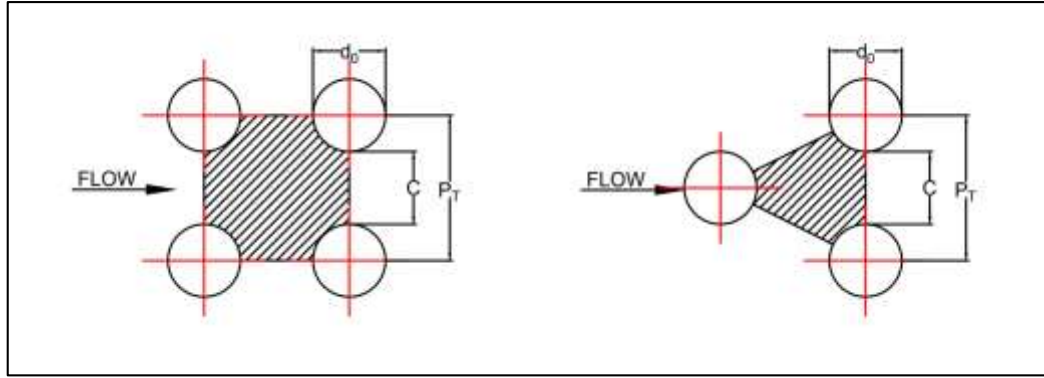


Figure 15 Square and triangular pitch-tube layouts (utilized from Kakac (1992))

For the identical tube pitch and flow rates, the tube layouts in decreasing order of shell-side heat transfer coefficient and pressure drop are: 30°, 45°, 60°, 90°.

CTP is the tube count constant which accounts for the incomplete coverage of the shell diameter by the tubes due to necessary clearances between the shell and the outer tube circle (Lee, 2010).

CL: Tube layout constant (CL=1.0 for 90° and 45° & CL=0.87 for 30° and 60°)

CTP: The tube count calculation constant (CTP=0.93 for one-tube pass & CTP=0.9 for two tube pass)

PR: Tube pitch ratio

P_t : Pitch size

$$PR = \frac{P_t}{d_o} \quad (1.25 < PR < 1.5) \quad (22)$$

The heat exchanger consists of tube and shell parts. Separate mathematical equations for both sides are available for tube and shell section sizing. In this study, each section was analysed and calculated separately. The formulas of the tube side are as follows.

Tube-Side Calculations:

The total number of tubes can be predicted as a function of the shell diameter by taking the shell circle D_s and dividing it by the projected area of the tube layout pertaining to a single tube A :

$$N_t = 0.785 \left(\frac{CTP}{CL} \right) \frac{D_s^2}{PR^2 \cdot D_{to}^2} \quad (23)$$

N_t : Number of tube passes

Diameter of outer tube limit calculation,

$$D_{otl} = \frac{\left(D_o * \left(\frac{N_t}{0.156} \right)^{\frac{1}{2.291}} \right)}{1000} \quad (24)$$

After finding number of tubes and the length of the zone using iterative solutions, the heat transfer surface area of each zone is calculated using Eq. (25) (Lee, 2010).

$$A_t = \left(\frac{\pi}{4} \right) \cdot D_{ti}^2 N_t \quad (25)$$

The flow velocity in the tube is calculated according to the following equation:

$$V_t = \left(\frac{m_t}{\rho A_t} \right) \quad (26)$$

Tube side heat transfer coefficient calculation:

$$Re_t = \left(\frac{\rho V D_{ti}}{\mu} \right) \quad (27)$$

$$Pr_t = \left(\frac{C_p \mu}{k} \right) \quad (28)$$

$$Nu = 0.024 Re_s^{0.8} \cdot Pr_s^{0.4} \quad (29)$$

μ_t : Viscosity of shell-side fluid at $T_{tube,in}$

k: Thermal conductivity

Heat transfer coefficient can be calculated by Dittus-Beelter equation:

$$h_t = Nu \left(\frac{k}{D_{ti}} \right) \quad (30)$$

Tube-Side Pressure Drop is calculated Equation (31):

$$\Delta P_t = \left(f \frac{L}{D_{ti}} \right) \frac{\rho_t \cdot V_t^2}{2} \quad (31)$$

f: Friction factor for tube-side

V_t : Mean velocity in the tube-side

D_{ti} : Inner diameter of tubes

ρ_t : Density of tube side fluid at $T_{tube,in}$

We may find the friction factor by Approximate Karman-Nikuradse Correlation:

$$4 \times 10^3 < Re < 3 \times 10^6 \Rightarrow f = (1.58 \ln Re - 3.28)^{-2} \quad (32)$$

$$3 \times 10^4 < Re < 10^6 \Rightarrow f = 0.046 Re^{-0.2} \quad (33)$$

Shell Side Calculations:

Calculation of the number of tubes inside the shell of the heat exchanger:

$$N_{tc} = \frac{D_s}{L_p} \quad (34)$$

Cross flow area equation calculated by shell diameter:

$$A_c = (D_s - N_t \cdot D_t) L_b \quad (35)$$

Calculation of shell side inside diameter,

$$D_s = D_{otl} + p_t * \frac{2}{1000} \quad (36)$$

Transverse and longitudinal tube pitch calculation for layout=45,

$$X_t = \sqrt{2} * p_t \quad (37)$$

Calculation of central baffle spacing,

$$Lb_c = D_s * ratio_{cbs} \quad (38)$$

$ratio_{cbs}$ - central baffle spacing ratio

Inlet and outlet baffle spacing calculations,

$$Lb_i = Lb_c * iobsr \quad (39)$$

$$Lb_o = Lb_c * iobsr \quad (40)$$

iobsr - inlet-outlet baffle spacing ratio

Calculation of baffle cut,

$$l_c = D_s * bafflec_p \quad (41)$$

bafflec_p – baffle cut percent

Width of bypass lane calculation,

$$w_p = 2 * D_o \quad (42)$$

On the shell side, the angle calculation is specified in the following equation,

$$\theta_b = 2 * \text{acos} \left(1 - 2 * \frac{l_c}{D_s} \right) * \frac{180}{\pi} \quad (43)$$

Gross window area calculation,

$$Afr_w = \frac{D_s^2}{4} * \left(\frac{\text{deg2rad}(\theta_b)}{2} - \left(1 - 2 * \frac{l_c}{D_s} \right) * \sin \left(\text{deg2rad} \left(\frac{\theta_b}{2} \right) \right) \right) \quad (44)$$

Calculation of diameter central tube limit,

$$D_{ctl} = D_{otl} - \frac{D_o}{1000} \quad (45)$$

Shell side baffle cut angle calculation is shown in equation (46).

$$\theta_{ctl} = 2 * \text{acos} \left(\frac{D_s - 2 * l_c}{D_{ctl}} \right) * \frac{180}{\pi} \quad (46)$$

In the equation below, the calculation of the ratio of the total tubes in the window is given,

$$F_w = \frac{\text{deg2rad}(\theta_{ctl}) - \sin(\text{deg2rad}(\theta_{ctl}))}{2 * \pi} \quad (47)$$

Equation of shell side hydraulic diameter of window

$$Dh_w = 4 * \frac{Ao_w}{\pi * \frac{D_o}{1000} * Nt_w + \pi * D_s * \left(\frac{\text{deg2rad}(\theta_b)}{2 * \pi} \right)} \quad (48)$$

Net flow area in one window equation shown in below

Flow velocity at shell:

$$V_s = \left(\frac{m_s}{\rho A_c} \right) \quad (49)$$

Shell side heat transfer coefficient calculations

$$Re_s = \left(\frac{\rho V D_{to}}{\mu} \right) \quad (50)$$

$$Pr_s = \left(\frac{C_p \mu}{k} \right) \quad (51)$$

$$Nu = 0.2 Re_s^{0.6} \cdot Pr_s^{0.4} \quad (52)$$

Colburn j factor equations

$$J_{idealFactor} = a_1 * \left(\frac{1.33}{\frac{p_t}{D_o}} \right)^a * (Re_s)^{a_2} \quad (53)$$

$$a = \frac{a_3}{1 + 0.14 * (Re_s)^{a_4}} \quad (54)$$

Baffle cut and spacing effect correction factor equation is shown below,

$$J_c = 0,55 + 0,72 * F_c \quad (55)$$

Shell-to-baffle leakage effect equation is shown below,

$$J_l = 0.44 * (1 - r_s) + (1 - 0.44 * (1 - r_s)) * e^{(-2.2 * r_{lm})} \quad (56)$$

Bundle bypassing effects correction factor calculation

$$J_b = e^{\left(-C * r_b * \left(1 - (2 * N_{ssplus})^{\frac{1}{3}} \right) \right)} \quad (57)$$

Inlet and outlet variable baffle spacing correction factor equation,

$$J_s = \frac{N_b - 1 + (iobsr)^{1-nn} + (iobsr)^{1-nn}}{N_b - 1 + iobsr + iobsr} \quad (58)$$

Shell side actual heat transfer coefficient equation,

$$h_s = h_{id} * J_c * J_l * J_b * J_s * J_r \quad (59)$$

Heat transfer coefficient can be calculated by:

$$h_s = Nu \left(\frac{k}{D_{to}} \right) \quad (60)$$

The shell-side ideal pressure drop depends on the number of tubes the fluid passes through in the tube bundle between the baffles as well as the length of each crossing.

$$\Delta P_{ideal} = f \frac{\rho \cdot V_c^2}{2} N_{rc} + K_w \frac{\rho \cdot V_c^2}{2} N_b \quad (61)$$

$$N_{rc} = N_{rc1} (N_b + 1) \quad (62)$$

$$N_b = \frac{L}{L_b} - 1 \quad (63)$$

$$N_{rc1} = \frac{0.75 D_s}{0.867 L_p} \quad (64)$$

Shell side friction factor was calculated by Equation (65).

$$f = \exp(0.576 - 0.19 \ln Re_s) \quad (65)$$

where;

$$400 < Re_s = \frac{G_s \cdot D_e}{\mu_b} < 1 \times 10^6 \quad (66)$$

Ideal friction factor equations,

$$f_{id} = 3.5 * \left(\left(1.33 * \frac{D_o}{p_t} \right)^b \right) * (Re_s^{-0.476}) \quad (67)$$

$$b = \frac{6.59}{1 + 0.14 * Re_s^{0.52}} \quad (68)$$

λ_b , λ_l and λ_s coefficient equations

$$\lambda_b = e^{\left(-D * r_b * \left(1 - (2 * N_{ssplus})^{\frac{1}{3}} \right) \right)} \quad (69)$$

$$\lambda_l = e^{(-1.33 * (1 + r_s) * r_{lm}^p)} \quad (70)$$

$$\lambda_s = \left(\frac{Lb_c}{Lb_o} \right)^{2-nprime} + \left(\frac{Lb_c}{Lb_i} \right)^{2-nprime} \quad (71)$$

Pressure drop equations,

$$\Delta P_{cr} = \Delta P_{bid} * (N_b - 1) * \lambda_b * \lambda_l \quad (72)$$

$$\Delta P_w = N_b * (2 + 0.6 * Nr_{cw}) * \frac{G_w^2}{2 * g_c * \rho_{cold}} * \lambda_l \quad (73)$$

$$\Delta P_{io} = 2 * \Delta P_{bid} * \left(1 + \frac{Nr_{cw}}{Nr_{cc}} \right) * \lambda_b * \lambda_s \quad (74)$$

Shell side pressure loss equation is shown below,

$$\Delta P_{shell} = \Delta P_{cr} + \Delta P_w + \Delta P_{io} \quad (75)$$

The overall heat transfer coefficient U based on the outside diameter of tubes can be estimated from:

$$U_c = \frac{1}{\frac{1}{h_s} + \frac{1}{h_t} \frac{D_{t0}}{D_{ti}}} \quad U_f = \frac{1}{\frac{1}{U_c} + R_{fi} \frac{D_{t0}}{D_{ti}}} \quad (76)$$

Heat load of a heat exchanger can be estimated from heat balance:

$$Q_f = U_f A \Delta T_m \quad (77)$$

Calculation of safety factor for fouling in heat exchangers:

$$F_f = \frac{U_c}{U_f} < 1.35 \quad (78)$$

Safety factor for heat transfer:

$$F_s = \frac{Q_f}{Q} \cong 1 \quad (79)$$

4.1.1 Nucleate Pool Boiling Correlations

Experimental results for heat flux q and wall superheat ΔT are usually fitted to an exponential equation with one of the following forms: $q \propto \Delta T^n$, $\alpha n b \propto \Delta T^n$, or $\alpha n b \propto q^n$, where n is on the

order of 3, 2, and 0.7, respectively. The curve for nucleate boiling is not linear at low heat fluxes or when approaching DNB (departure from nucleate boiling), but these zones are often excluded (or not measured) when fitting a curve to experimental data. The correlations for nucleate pool boiling can be formulated in any of the above forms, but those represented as $q_{nb} \propto q^n$ are the easiest to apply. Below we present some nucleate pool boiling correlations that are empirical representations of experimental data (Wolverine Tube Inc., pp. 9.1-9.38, 2006).

1. Rohsenow correlation

In 1952 Rohsenow recognized the influence of the combination of liquid and solid on heat transfer during boiling and developed a more general correlation (Tarrad, 2011):

$$\frac{c_{pL}\Delta T}{h_{fg}} = C_{sf} \left[\frac{q}{\mu_L * h_{fg}} \sqrt{\frac{\sigma_L}{g * (\rho_L - \rho_v)}} \right]^n * Pr^{m+1} \quad (80)$$

The heat transfer coefficient is obtained from the definition of the heat transfer coefficient $h_{nb} = (q/DT)$. The values of the exponents are $m = 0.7$ and $n = 0.33$ for all liquids except water, for which Rohsenow recommended $m = 0$. The values of the surface fluid factor (C_{sf}) for different surface-fluid combinations are suggested by Rohsenow with an accuracy of $\pm 20\%$ for the above correlation. This parameter apparently considers the contact angle, surface micro-roughness and their interaction in determining the nucleation density (Tarrad, 2011).

2. Kruzhlin correlation

In 1947, Kruzhlin proposed the following correlation, in which no special effort was made to explain surface properties:

$$\frac{h_{nb} * d}{k} = 0.082 \left(\frac{h_{fg} * q}{g * T_s * k} \right)^{0.7} \left(\frac{T_s * c_{pL} * \sigma_L * \rho_L}{h_{fg}^2 * \rho_v^2 * d} \right)^{0.33} * Pr^{-0.45} \quad (81)$$

3. Kutateladze correlation

Kutateladze simplified Kruzhilin's relation at the expense of its accuracy and developed an expression for the Nusselt number in the case of boiling:

$$h_{nb} = \sqrt[3]{3.37 * 10^{-9} * \frac{k}{d} * \left(\frac{h_{fg}}{c_{pL} * q}\right)^{-2} * \frac{\left(\frac{P}{\rho_v}\right)^2}{\frac{\sigma_L * g}{\rho_L - \rho_v}}} \quad (82)$$

4. Labuntsov correlation

Labuntsov derived the correlation that does not require an input of latent heat of vaporization (Tarrad, 2011):

$$h_{nb} = 0.075 \left[1 + 10 * \left(\frac{\rho_v}{\rho_L - \rho_v}\right)^{0,67} \right] * \left(\frac{k^2}{v * \sigma * (T_s + 273,15)}\right)^{0,33} * q^{0,7} \quad (83)$$

5. Foster-Zuber correlation

Foster, used bubble radius and the bubble growth velocity and obtained the following correlation:

$$q = 0.00122 * \frac{k^{0,79} * c_{pL}^{0,45} * \rho_L^{0,49}}{\sigma^{0,5} * \mu_L^{0,29} * h_{fg}^{0,24} * \rho_v^{0,24}} * \Delta T^{1,24} * \Delta P_{sat}^{0,75} \quad (84)$$

6. Mostinski correlation

Mostinski neglected the surface effects and applied the principle of corresponding states to the heat transfer data of the boiling process of nuclear pools and related the data as a function of the reduced pressure of the liquid and its critical pressure (Tarrad, 2011):

$$h_{nb} = 0.00417 * q^{0.7} * P_c^{0.69} * F_{PF} \quad (85)$$

7. Stephan-Abdelsalam correlation

Stephan proposed four specific correlations that apply a multiple statistical regression technique to water, refrigerants, organics, and cryogenics. These correlations use the physical properties of the fluid evaluated at the saturation temperature and are therefore referred to as physical property-based correlations. They proposed the following correlation for refrigerants, whose mean deviation was 10.6% in the reduced pressure range of 0.003-0.78 (Tarrad, 2011):

$$\frac{h_{nb} * d}{k} = 207 * \left(\frac{q * d_b}{k * T_s} \right)^{0.745} * \left(\frac{\rho_v}{\rho_L} \right)^{0.581} * Pr^{0.533} \quad (86)$$

8. Piro correlation

Piro modified Rohsenow correlation:

$$\frac{h_{nb} * d}{k} = C_{sf} * \sqrt[3]{\left\{ \frac{q}{\rho_v^{0.5} * h_{fg} * [\sigma_L * g(\rho_L - \rho_v)]^{0.25}} \right\}^2} \quad (87)$$

Tube side equations:

Calculation tube inner diameter in heat exchanger:

$$D_{in} = D_o - 2 * t \quad (88)$$

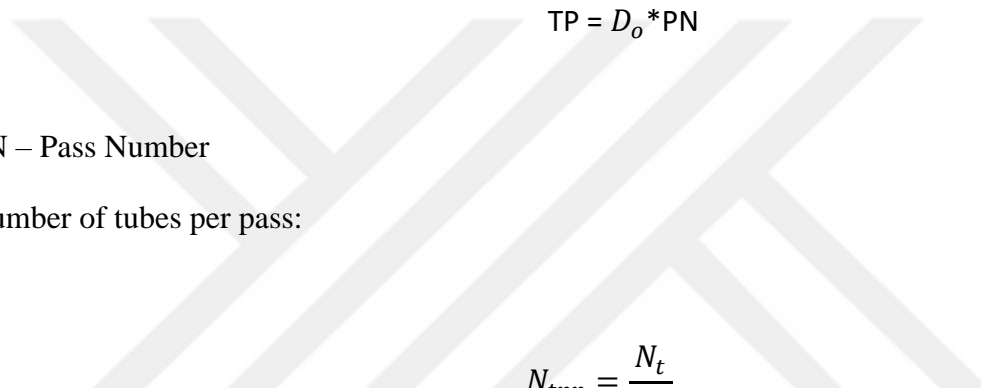
Number of tubes calculation:

$$N_t = \frac{A_{out}}{D_o * \pi * L_t} \quad (89)$$

A_{out} – Area (outside) required

L_t – Tube length

Tube pitch calculated by equation (90):



$$TP = D_o * PN \quad (90)$$

PN – Pass Number

Number of tubes per pass:

$$N_{tpp} = \frac{N_t}{PN} \quad (91)$$

Tube-side flow area per pass

$$A_{o_pp} = D_{in}^2 * \pi * N_{tpp} \quad (92)$$

Calculation of the velocity of the fluid passing through the tube:

$$V_{tube} = \frac{m}{\rho * A_{o_pp}} \quad (93)$$

Tube-side Reynolds number calculated by equation (94):

$$Re_{tube} = \frac{m * D_{in}}{A_{o_pp} * \mu} \quad (94)$$

The tube side Nusselt number calculation is as follows:

$$Nu_{tube} = 0.024 * Re_{tube}^{0,8} * Pr_{hot}^{0,4} \quad (95)$$

Tube side heat transfer coefficient calculated by equation (96)

$$h_{tube} = (Nu_{tube} * k_{hot}) / D_{in} \quad (96)$$

We chose the Labuntsov correlation, which is more convenient to calculate as the total heat transfer coefficient.

$$h_{nb} = h_{Labuntsov} \quad (97)$$

$$U_{dirty} = \frac{1}{\frac{1}{h_{Labuntsov}} + \frac{1}{FC_{cold}} + D_o * \frac{\log \frac{D_o}{D_{in}}}{2 * k_{tube}} + \frac{D_o}{D_{in}} * \left(\frac{1}{FC_{hot}} + \frac{1}{h_{tube}} \right)} \quad (98)$$

FC_{cold} – Cold side fouling coefficient

FC_{hot} – Hot side fouling coefficient

k_{tube} – Tube conductivity

$$U_{clean} = \frac{1}{\frac{1}{h_{Labuntsov}} + D_o * \frac{\log \frac{D_o}{D_{in}}}{2 * k_{tube}} + \frac{D_o}{D_{in}} * \frac{1}{h_{tube}}} \quad (99)$$

Calculation of tubes bundle diameter with equation (100).

$$D_{bundle} = 0.637 \cdot \sqrt{\frac{CL}{CTP}} (\pi * N_t * TP^2)^{\frac{1}{2}} \quad (100)$$

N_t - number of tubes

TP – tube pitch

CL – tube layout constant

CTP – tube count constant

Shell diameter calculation for heat exchanger:

$$D_{shell} = D_{bundle} * d_{ratio} \quad (101)$$

Liquid level calculation

$$L_{liquid} = D_{bundle} * d_{liq.ratio} \quad (102)$$

$d_{liq.ratio}$ – liquid level to bundle diameter of ratio

Width liquid level equation

$$W_l = 2 * \sqrt{L_{liquid} * \frac{D_{shell}}{1000 - L_{liquid}^2}} \quad (103)$$

Surface area of liquid

$$A_{liquid} = L_{tube} * W_l \quad (104)$$

Equation for calculating the vapour velocity at the surface

$$V_{vapour} = \frac{m_{cold}}{\rho * A_{liquid}} \quad (105)$$

Calculated the friction factor to find the pressure loss inside the tube

$$f_{tube} = (1.58 * \log(Re_{tube}) - 3.28)^{-2} \quad (106)$$

Tube side pressure loss calculated by equation (107):

$$\Delta P = 4 * \left(\frac{f * L_i}{d_i} + 1 \right) * N_p * \frac{1}{2} * \rho * v^2 \quad (107)$$

4.2 Air Cooled Condenser Equations

The basic equation for heat transfer for ACC:

$$Q = UA * CMTD \quad (108)$$

Normally Q is known, U and CMTD are calculated, and the equation is solved for A. The ambient temperature to be used is either known from available plant data or can be selected from summer dry bulb temperature data. The design ambient air temperature is usually considered to be the dry-bulb temperature that is exceeded less than 5 percent of the time in the area where the system is required (Tulsa, 1998). The heat load is calculated by:

$$q = m * \Delta h \quad (109)$$

When calculating LMTD, a complication arises because the air volume is a variable and therefore the air outlet temperature is not known. The procedure described here begins with a step to approximate the rise in air temperature. After the air outlet temperature is determined, the corrected LMTD is calculated in the same manner as described in the tubes and shells section, except that LMTD correction factors of 1.0 must be used for four or more passes if the passes are above and below each other (Tulsa, 1998). A correction factor of 1.0 can be used as an approximation for three passes, although in some cases the factor will be slightly lower than 1.0.

The procedure for thermal design of an air cooler is to assume a selection and then prove that it is correct. Typical total heat transfer coefficients are used to estimate the required heat transfer area. The heat transfer area is converted to a bundle area using Table 3.1, which lists the available expanded surface area per square foot of bundle area for two specific finned tubes with two different tube pitches for 3, 4, 5, and 6 rows. After you assume a tube length, Table 3.1 is also used to determine the number of tubes. Both tube-side and air-side mass velocities can now be determined (Tulsa, 1998).

LMTD can be calculated by:

$$LMTD = \Delta T_{im} = \frac{\Delta T_I - \Delta T_{II}}{\ln\left(\frac{\Delta T_I}{\Delta T_{II}}\right)} \quad (110)$$

$$\Delta T_I = T_{h,i} - T_{c,o} \quad \Delta T_{II} = T_{h,o} - T_{c,i} \quad (111)$$

Overall Heat Transfer Coefficient is calculated with:

$$\frac{1}{U_x} = \left(\frac{1}{h_t}\right) * \left(\frac{A_x}{A_i}\right) + r_{dt} * \left(\frac{A_x}{A_i}\right) + r_{mx} + \frac{1}{h_a} \quad (112)$$

Air temperature rise is estimated with:

$$\Delta t_a = \left(\frac{U_x}{60} + 0,1 \right) * \left(\frac{T_1 + T_2}{2} - t_1 \right) \quad (113)$$

Required surface area is calculated with:

$$A_x = \frac{Q}{(U_x * CMTD)} \quad (114)$$

Face area is calculated with Fin parameters from Table 3.3:

$$F_a = \frac{A_x}{APSM} \quad (115)$$

With assumed width of ACC, tube length is calculated (3 values assumed for length of all ACC)

$$Width = \frac{F_a}{L} \quad (116)$$

Number of tubes can be found by APM factor from Table 3.3:

$$N_t = \frac{A_x}{(APM) * (L)} \quad (117)$$

Tube side mass velocity is calculated with:

$$G_t = \left(\frac{W_t * N_p}{N_t * A_t} \right) \quad (118)$$

Tube side Reynolds number calculated with:

$$N_R = \frac{D_i * G_t}{\mu} \quad (119)$$

Tube side pressure drop can be calculated by the following equations:

$$\Delta P_t = \frac{f * Y * L * N_p}{\phi} + B * N_p \quad (120)$$

Table 4.1 Correction Factor for Fluid Viscosity Within the Tubes (Tulsa, 1998)

<i>Correction factor*when $\phi = \left(\frac{\mu}{\mu_w}\right)^{0.14}$</i>	Correction Factor, ϕ
Hydrocarbon vapour; steam; water	1
Hydrocarbon liquids (18 to 48 API), MEA/DEA solutions	0,96
Water/glycol solutions; heat transfer fluids	0,92
Lube oils; heavy petroleum fractions (10 to 18 API)	0.85

* When $N_r < 2100$, $\phi = \left(\frac{\mu}{\mu_w}\right)^{0.14}$ A Reynolds number of less than 2100 is only likely for lube oils or heavy petroleum fractions. The minimum recommended value of ϕ to use in Step 10 is 0.80, even though the calculated value may be lower.

Tube side film coefficient using J factor from

$$h_t = \frac{J * k * \left(\frac{C_p * \mu}{k}\right)^{\frac{1}{3}} * \phi}{D_i} \quad (121)$$

Air flow rate can be calculated by:

$$W_a = \frac{Q}{C_{pa} * \Delta t_a} \quad (122)$$

Air face mass velocity can be calculated by:

$$G_a = \frac{W_a}{F_a} \quad (123)$$

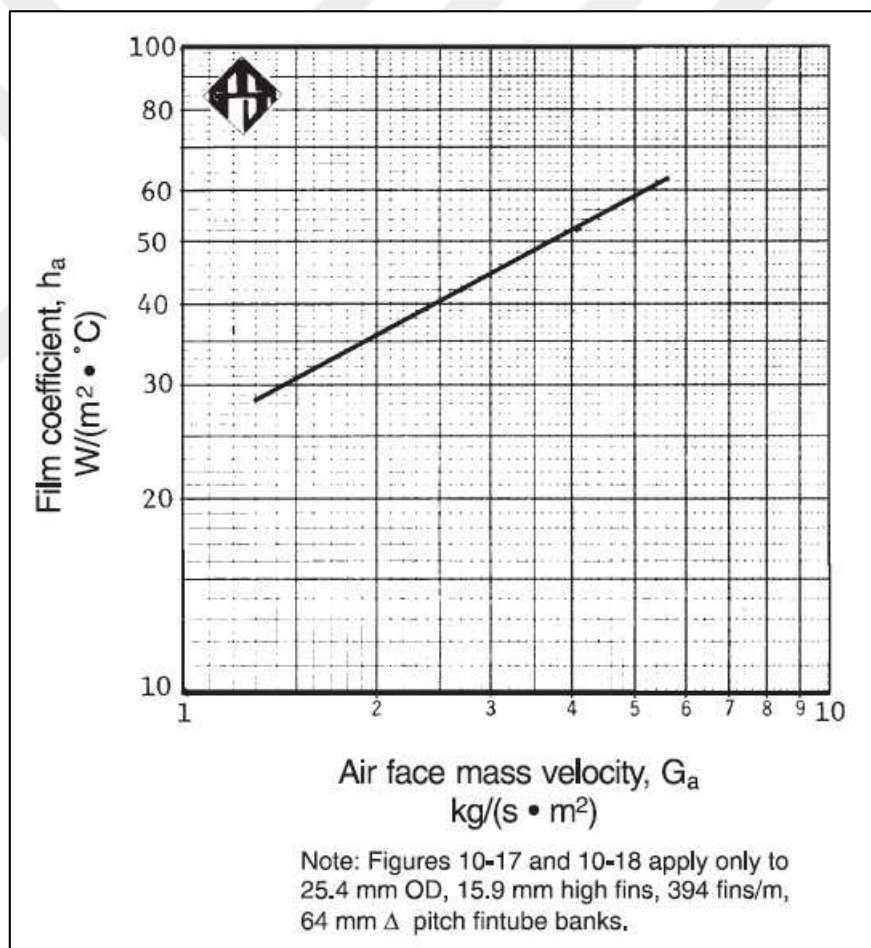


Figure 16 Air Film Coefficient (Tulsa, 1998)

Annular flow condensation correlation is calculated by equation (124):

$$Nu(x) = 0,023 * Re_{ls}^{0,8} * Pr_L^{0,4} \left[1 + \frac{2,22}{X_{tt}^{0,89}} \right] \quad (124)$$

The stratified-wavy heat transfer coefficient:

$$Nu(x) = \frac{0,23 * Re_{Go}^{0,12}}{1 + 1,11 * X_{tt}^{0,58}} * \left[\frac{Ga_L * Pr_L}{Ja_L} \right]^{0,25} + (1 - \frac{\theta_{start}}{\pi}) / Nu_{start} \quad (125)$$

Forced convection condensation in the stratified liquid is correlated as:

$$Nu_{start} = 0,0195 * Re_{ls}^{0,8} * Pr_L^{0,4} \left[1,376 + \frac{c_1}{X_{tt}^2} \right]^{1/2} \quad (126)$$

Air side heat transfer coefficient is calculated 3 different formulas and lowest of them is used in design:

$$Nu = 0,1507 * Re^{0,667} * Pr^{\frac{1}{3}} * \left(\frac{S}{l_f} \right)^{0,164} * \left(\frac{S}{t_f} \right)^{0,075} \quad (127)$$

$$Nu = 0,1378 * Re^{0,718} * Pr^{\frac{1}{3}} * \left(\frac{S}{l_f} \right)^{0,296} \quad (128)$$

$$Nu = 0,134 * Re^{0,681} * Pr^{\frac{1}{3}} * \left(\frac{S}{l_f} \right)^{0,2} * \left(\frac{S}{t_f} \right)^{0,1134} \quad (129)$$

We can calculate the overall transfer coefficient by equation (131):

$$\frac{A_x}{A_i} = \frac{(AR) * (D_o)}{D_i} \quad (130)$$

$$\frac{1}{U_x} = \left(\frac{1}{h_t}\right) * \left(\frac{A_x}{A_i}\right) + r_{dt} * \left(\frac{A_x}{A_i}\right) + r_{mx} + \frac{1}{h_a} \quad (131)$$

Minimum fan area for Air Cooled Condenser calculated with equation (132):

$$FAPF = \frac{0,4 * F_a}{N_{num.of.fans}} \quad (132)$$

Static pressure drop for Air Cooled Condenser calculated by equation (133):

$$\Delta P_a = \frac{F_p * N}{D_r} \quad (133)$$

Actual air volume using DR of air at fan inlet:

$$ACMS = \frac{W_a}{D_r (1,203 \frac{kg}{m^3})} \quad (134)$$

Approximate fan total pressure drop using DR of air at fan and fan area:

$$P_f = \Delta P_a + D_r (0,975 \frac{kg}{m^3}) \quad (135)$$

Approximate brake horsepower per fan, using 70% fan efficiency

$$Fan Power = \frac{ACMS * PF}{fan efficiency} \quad (136)$$

At low vapour shear, the condensation process on the inside around the top and sides of the tube is very similar to that on the outside of a horizontal tube. Therefore, the Nusselt falling film analysis can be applied to the upper zone of the tube, which was first done by Chaddock (1957) and then by Chato (1962). The cross-sectional area of the stratified fluid layer at the bottom of the tube can be determined from the local void fraction ε . Then the angle θ_{strat} of the stratified fluid can be determined from the geometry (Wolverine Tube Inc., pp. 8.1-8.27, 2006). The local heat transfer coefficient at this vapour quality x is obtained by multiplying the respective heat transfer coefficients with respect to the fraction of the circumference they occupy as

$$\alpha(x) = \frac{\theta_{start}}{\pi} \alpha_f + \frac{\pi - \theta_{start}}{\pi} \alpha_{start} \quad (137)$$

θ_{strat} - the angle between the top of the tube

α_f - the average heat transfer coefficient for the film obtained

Assuming that θ_{strat} is negligible compared to α_f , the second term can be neglected while α_f is determined as follows:

$$\alpha_f = \Omega \left[\frac{\rho_L * (\rho_L - \rho_G) * g * k_L^3 * h_{LG}}{\mu_L * d_i * (T_{sat} - T_w)} \right]^{1/4} \quad (138)$$

Ω is a geometric function of θ_{strat} .

Their superficial liquid Reynolds number Re_{LS} is

$$Re_{LS} = \frac{m * d_i * (1 - x)}{\mu_L} \quad (139)$$

The MARTINELLI parameter for turbulent flow in both phases, X_{tt} is

$$X_{tt} = \left(\frac{1-x}{x}\right)^{0,9} * \left(\frac{\rho_G}{\rho_L}\right)^{0,5} * \left(\frac{\mu_L}{\mu_G}\right)^{0,1} \quad (140)$$

Epsilon coefficient equation is shown below,

$$\varepsilon = \frac{1}{1 + \left(\frac{1-x}{x}\right) * \left(\frac{\rho_2}{\rho_3}\right)^{\frac{2}{3}}} \quad (141)$$

The liquid Galileo number Ga_L for the tube is

$$Ga_L = \frac{g * \rho_L * (\rho_L - \rho_G) * d_i^3}{\mu_L^2} \quad (142)$$

while the vapour only Reynolds number Re_{Go} is

$$Re_{Go} = \frac{m * d_i}{\mu_G} \quad (143)$$

Forced convection condensation in the stratified liquid is correlated as

$$Nu_{start} = 0,0195 * Re_{is}^{0,8} * Pr_L^{0,4} \left[1,376 + \frac{c_1}{X_{tt}^2}\right]^{1/2} \quad (144)$$

Dobson and Chato (1998) have proposed a far-reaching improvement of Chato's (1962) method, including both a stratified-wavy flow method with film condensation from top to bottom of the tube and an annular flow correlation. Their correlation for the annular flow of condensation is as follows.

$$Nu(x) = 0,023 * Re_{ls}^{0,8} * Pr_L^{0,4} \left[1 + \frac{2,22}{X_{tt}^{0,89}} \right] \quad (145)$$

The stratified wave heat transfer coefficient is obtained by multiplying the film condensation coefficient at the upper circumference of the tube (left term) and the forced convective heat transfer coefficient at the stratified circumference (right term) as

$$Nu(x) = \frac{0,23 * Re_{Go}^{0,12}}{1 + 1,11 * X_{tt}^{0,58}} * \left[\frac{Ga_L * Pr_L}{Ja_L} \right]^{0,25} + \left(1 - \frac{\theta_{start}}{\pi} \right) / Nu_{start} \quad (146)$$

The liquid Jacob number Ja_L

$$Ja_L = \frac{c_{pl}(T_{sat} - T_w)}{h_{LG}} \quad (147)$$

Assuming that all the liquid in the bottom of the tube is stratified (neglecting the condensate that forms on the walls), the angle from the top of the tube to the stratified layer of liquid in the bottom θ_{strat} is then determined (Wolverine Tube Inc., pp. 9.1-9.38, 2006)

$$\theta_{strat} = (\pi - arccos \cdot (2 \cdot \varepsilon - 1)) \quad (148)$$

and the liquid Froude number Fr_L is

$$Fr_L = \frac{m^2}{\rho_L^2 * g * d_i} \quad (149)$$

Wall temperature equation,

$$T_{wall} = \frac{T_{saturation} + T_{air inlet}}{2} \quad (150)$$

Tube Side Heat Transfer Coefficients:

The refrigerant heat transfer coefficient for the superheated region in the condenser is calculated:

$$h_r = C_1 * G_r * C_{p,r} * Pr^{-\frac{2}{3}} * Re^{C_2} \quad (151)$$

$$C_1 = \begin{cases} 1.10647 & Re < 3500 \\ 3.5194 \times 10^{-7} & 3500 \leq Re < 6000 \\ 0.01080 & Re \geq 6000 \end{cases} \quad (152)$$

And

$$C_2 = \begin{cases} -0.78992 & Re < 3500 \\ 1.03804 & 3500 \leq Re < 6000 \\ -0.13750 & Re \geq 6000 \end{cases} \quad (153)$$

The heat transfer coefficients for the super cooled region of the condenser are calculated using the Dittus-Boelter correlation for fully developed flow, which is recommended for simulating heat exchangers in heat pump systems

$$h_r = 0,023 * G_r * C_{p,r} * Pr^{-0,70} * Re^{-0,20} \quad (154)$$

Air Side Calculations:

The most widely accepted correlations for the airside heat transfer coefficient and the airside pressure drop are those derived from the experimental work of Edwin H. Young, Dale E. Briggs, and Ken E. Robinson at the University of Michigan, Ann Arbour.

The general correlation for heat transfer through a series of finned tubes is as follows:

$$Nu = 0,134 * Re^{0,681} * Pr^{0,33} * \left(\frac{S}{h}\right)^{0,2} * \left(\frac{S}{b}\right)^{0,1134} \quad (155)$$

Nu - Nusselt number, dimensionless

Re - Reynolds number, dimensionless

Pr - Prandtl number, dimensionless

S - fin spacing, in.

h - fin height, in.

b - fin thickness, in.

Centre-to-centre distance between the fins along the flow direction.

$$S_l = D_{TP} * \frac{\sqrt{3}}{2} \quad (156)$$

D_{TP} - Tube Pitch diameter

Diagonal pitch:

$$S_D = ((D_{tp}/2)^2 + S_l^2)^{0,5} \quad (157)$$

Distance measured normal to the flow direction

$$S_{TD} = (D_{TP} + d)/2 \quad (158)$$

Air quantity calculation for air side evaluated by equation (159)

$$W_a = Q_{hl} / (c_{p_{air}} * \Delta T_{air}) \quad (159)$$

Volume flow rate

$$v = \frac{m_{air}}{D_{air}} \quad (160)$$

Velocity of air equation,

$$V_{air} = \frac{V}{A} \quad (161)$$

If $S_{TD} > S_{DD}$, the air velocity equation

$$V_{air-max} = \frac{D_{TP}}{1000} * \frac{V_{air}}{2 * \left(S_D - \frac{D_o}{1000} \right)} \quad (162)$$

Fin spacing calculation is shown in the following equation (163)

$$FIN = (1 - FPM * t_{fin}) / FPM \quad (163)$$

FPM - fin per meter

t_{fin} - FIN thickness

Calculated Reynolds number by equation (164)

$$Re_n = \frac{D * V}{\mu} \quad (164)$$

Air face mass velocity calculation is as follows:

$$G_a = \frac{W_a}{F_a} \quad (165)$$

Since all resistances must be based on the same surface area, it is necessary to multiply the reciprocal of the tube-side film coefficient and the tube-side contamination factor by the ratio of the outer surface area to the inner surface area (Russel et al., 2008). This yields a total transfer rate based on the expanded surface area, which is referred to as U_x . The equation for the total heat transfer rate is:

$$\frac{1}{U_x} = \left(\frac{1}{h_t}\right) * \left(\frac{A_x}{A_i}\right) + r_{dt} * \left(\frac{A_x}{A_i}\right) + r_{mx} + \frac{1}{h_a} \quad (166)$$

A_x – outside extended surface of tube, m^2

A_i – inside surface of tube, m^2

r_{mx} – metal resistance referred to outside extended surface

r_{dio} – fouling resistance

The tube inside film resistance calculated by equation (167):

$$r_{io} = \frac{1}{h_i} * \frac{d_b}{d_i} \quad (167)$$

The tube inside fouling resistance calculation:

$$r_{dio} = r_{di} * \frac{d_b}{d_i} \quad (168)$$

The logarithmic mean temperature difference is calculated by the following equation

$$LMTD = Q/(U_x * A_x) \quad (169)$$

Fan Calculations

Fan area calculation for ACC follow as:

$$FAPF = \frac{0,4 * F_a}{N_{num.of.fans}} \quad (170)$$

F_a – total face area of bundles, m^2

Fan diameter which is important to optimize Air flow and power consumption can be evaluated by Equation (171):

$$D_{fan} = [4 * (FAPF)/\pi]^{0,5} \quad (171)$$

Air pressure difference calculation,

$$\Delta P_{air} = \frac{F_p * N_{tube row}}{D_r} \quad (172)$$

Static air pressure drop can be calculated by the following equation (173):

$$\Delta P_a = \frac{F_p * N}{D_r} \quad (173)$$

Calculate actual air volume using DR of air at fan inlet

$$ACMS = \frac{W_a}{D_r(1,203 \frac{kg}{m^3})} \quad (174)$$

Approximate fan total pressure using DR of air at fan and fan area.

$$P_f = \Delta P_a + D_r(0,975 \frac{kg}{m^3}) \quad (175)$$

Approximate fan total pressure using DR of air at fan and fan area

$$P_{f-z1} = \Delta P_{air} + D_r * 0,975 * \left(\frac{ACMS_{z1}}{D_{fan}^2} \right)^2 \quad (176)$$

Calculation of fan power for ACC

$$Fan\ Power = \frac{ACMS * PF}{fan\ efficiency} \quad (177)$$

Pressure Drop in Tube:

Two phase calculation is enough other pressure drops are negligible

$$D_{homogenous} = \left(\frac{x}{\rho} + \frac{1-x}{\rho} \right)^{-1} \quad (178)$$

Calculation of the flow rate equation per tube according to the number of tubes is as follows

$$m_{hot.pt} = \frac{m_{hot}}{Num.of.Tubes} \quad (179)$$

Flow rate of the liquid flowing in the tube calculated by equation (180)

$$m_{liquid} = m_{hot.pt} * (1 - x) \quad (180)$$

Gas flow rate in tube

$$m_{gas} = m_{hot.pt} * x \quad (181)$$

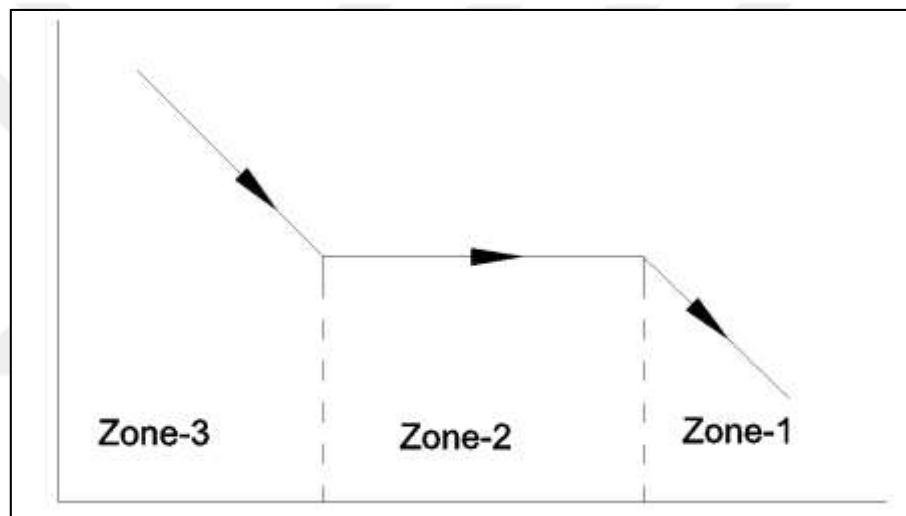


Figure 17 ACC Phase Diagram

Figure 4.4 shows the phase change diagram of working fluid inside of tubing of ACC: zone-3 (cooling)., zone-2 (condensing-phase change), zone-1 (sub-cooling). All calculations of ACC should be performed for each zone individually. The flow speed inside per tube calculated by equation (182)

$$v = m_{hot.pt} * \frac{4}{\pi * D_{in}^2} \quad (182)$$

Reynolds number for liquid in tube calculated by equation (183)

$$Re_{liquid} = \frac{v \cdot D_{in} \cdot (1 - x)}{\mu} \quad (183)$$

Reynolds number for gas in tube

$$Re_{gas} = \frac{v \cdot D_{in} \cdot x}{\mu} \quad (184)$$

Friction factor for the liquid flowing inside the tube calculated by equation (185)

$$f_{liquid} = \frac{0,079}{Re_{liquid}^{0,25}} \quad (185)$$

Friction factor for gas in tube

$$f_{gas} = \frac{0,079}{Re_{gas}^{0,25}} \quad (186)$$

The total pressure loss of the liquid in the tube is calculated by equation (187)

$$\Delta P_{liquid} = (4 * f_{liquid} * L * \rho) / (m^2 * D_{in}) \quad (187)$$

The dimensionless factors Fr_h , E, F and H are as follows:

$$Fr_h = \frac{m^2}{\rho_h^2 * g * d_i} \quad (188)$$

$$E = (1 - x)^2 + x^2 * \frac{\rho_L * f_G}{\rho_G * f_L} \quad (189)$$

$$F = x^{0,78} * (1 - x)^{0,224} \quad (190)$$

$$H = \left(\frac{\mu_G}{\mu_L}\right)^{0,19} * \left(\frac{\rho_L}{\rho_G}\right)^{0,91} * \left(1 - \frac{\mu_G}{\mu_L}\right)^{0,7} \quad (191)$$

The liquid Weber We_L is defined as:

$$We_L = \frac{m_{total}^2 * d_i}{\sigma * \rho_H} \quad (192)$$

The multiplier equation between the two phases:

$$\Phi_{fr}^2 = E + \frac{3,24 * FH}{We_L^{0,035} * Fr_H^{0,045}} \quad (193)$$

Calculation of pressure loss

$$\Delta P_{loss} = \Delta P_{liquid} * \Phi_{fr}^2 \quad (194)$$

5. ORC DESIGNER PROGRAM DEVELOPMENT AND CALCULATIONS

An ORC Designer Program have been developed under this thesis by using MATLAB software. MATLAB Program consists of three m. file editions for sub equipment: ACC design, preheater design and evaporator design which have a lot of loops and iterations. These three main equipment calculations are made with MATLAB program while main iterations, loops and ORC Designer Program for all ORC system created by APP Designer Tool Program in MATLAB.

Due to the ORC Designer program contains too many loops and conditions; the calculations of a single loop for evaporator, preheater and air-cooled condenser are presented in this section as an example. Therefore, some results of the first loop can be higher or lower than final results.

5.1 Calculations for a Loop as an Example

5.1.1 Evaporator Calculations

In evaporator calculations, input values are divided into two as hot and cold sides. Normally only hot side inputs are used for the design calculations while the working fluid (cold) side properties are evaluated by several loops and conditions. However, one loop calculations by using some assumptions of working fluid side are performed in this section to show calculation methodology. Hot side inlet and outlet temperatures $T_{hotinlet} = 90^{\circ}C$ and $T_{hotoutlet} = 68.393^{\circ}C$, pressure $P_{hot} = 3 \text{ bar}$, mass flow rate $m_{hot} = 150000 \text{ kg/h}$, hot side fouling resistance $FF_{hot} = 5.682 \times 10^3 \text{ m}^2C/W$ assumed. Cold side inlet and outlet temperatures $T_{coldinlet} = 60.393^{\circ}C$ and $T_{coldoutlet} = 63.393^{\circ}C$, pressure $P_{cold} = 2.6 \text{ bar}$, mass flow rate $m_{cold} = 39790.878 \text{ kg/h}$, hot side fouling resistance $FF_{cold} = 1.136 \times 10^4 \text{ m}^2C/W$ assumed. In the input values, the assumed pressure loss for the cold side is $APL_{cold} = 0.3 \text{ bar}$, the general heat transfer coefficient assumption is $OHTC_{int} = 1600 \text{ W/m}^2C$. Input values of the tubes inside the evaporator: tube outer diameter $D_o = 25.4 \text{ mm}$, tube wall thickness $T_{tube} = 2.1 \text{ mm}$, tube conductivity $k_{tube} = 55 \text{ W/m}^{\circ}C$, tube length $L_{tube} = 10 \text{ m}$, pitch ratio $PR = 1.5$, tube layout $TL = 45$, tube count

constant $CTP = 0.9$, tube layout constant $CL = 1$, shell diameter to bundle diameter ratio $d_{ratio} = 2$ and liquid level to bundle diameter ratio $d_{liq.ratio} = 0.9$.

LMTD & EMTD calculations:

Log mean temperature difference calculation is shown below according to the given input-output temperatures,

$$\Delta T_1 = T_{hot\ inlet} - T_{cold\ boilsat} = 90 - 62.4259 = 27.5741\ ^\circ C$$

$$\Delta T_2 = T_{hot\ outlet} - T_{cold\ boilsat} = 68.393 - 62.4259 = 5.9671\ ^\circ C$$

$$LMTD = \frac{\Delta T_2 - \Delta T_1}{\ln(\Delta T_2 / \Delta T_1)} = \frac{27.5741 - 5.9671}{\ln(\frac{27.5741}{5.9671})} = 14.1165$$

The saturation temperature at boiling ($T_{cold\ boilsat} = 62.4259\ ^\circ C$) is taken from the thermodynamic table according to the difference between the pressure on the cold side ($P_{cold} = 2.6\ bar$) and the assumed pressure loss ($APL_{cold} = 0.3\ bar$). The heat capacity and temperature efficiency ratio of the heat exchanger are calculated according to the following equations:

$$R = \frac{C_c}{C_h} = \frac{T_{h1} - T_{h2}}{T_{c2} - T_{c1}} = \frac{90 - 68.393}{63.393 - 60.393} = 7.2023 \quad ; \quad P = \frac{T_{c2} - T_{c1}}{T_{h1} - T_{c1}} = \frac{63.393 - 60.393}{90 - 60.393} = 0.1013$$

Calculation of the correction factor based on the heat capacity and the temperature efficiency of the heat exchanger:

$$F = \frac{\sqrt{R^2 + 1} \cdot \ln \left[\frac{1 - P}{1 - PR} \right]}{(R - 1) \ln \left[\frac{2 - P \{ (R + 1 - \sqrt{R^2 + 1}) \}}{2 - P \{ (R + 1) + \sqrt{R^2 + 1} \}} \right]}$$

$$= \frac{\sqrt{7.2023^2 + 1} \cdot \ln \left[\frac{1 - 0.1013}{1 - 0.1013 * 7.2023} \right]}{(7.2023 - 1) \ln \left[\frac{2 - 0.1013 * \{ (7.2023 + 1 - \sqrt{7.2023^2 + 1}) \}}{2 - 0.1013 * \{ (7.2023 + 1) + \sqrt{7.2023^2 + 1} \}} \right]} = 0.9494$$

Effective mean temperature calculation:

$$EMTD = LMTD * F = 14.1165 * 0.9494 = 13.4022$$

Thermal Calculations:

In order to calculate preheating heat load, the liquid enthalpies at the inlet and at the start of boiling are taken from the thermodynamic table according to the given cold side inlet temperature ($T_{cold\ inlet} = 60.393^{\circ}C$) and saturation temperature ($T_{cold\ boilsat} = 62.4259^{\circ}C$) at boiling.

$$Q_{pr} = (h_{cold\ boilstart} - h_{cold\ inlet}) * \frac{\dot{m}_{cold}}{3.6} = (6.4288x 10^4 - 5.9200x 10^4) * \frac{39790.878}{3.6} \\ = 56.2360 W$$

The cold side latent heat calculation equation is given below,

$$LH_{cold} = h_{coldvapsat} - h_{coldliqsat} = 3.9941 x 10^5 - 6.4288x 10^4 = 3.3512x 10^5 J/kg$$

The saturation liquid enthalpy ($h_{coldliqsat} = 6.4288x 10^4$) and saturation vapor enthalpy ($h_{coldvapsat} = 3.9941x 10^5$) used in this equation are taken from the thermodynamic table.

According to these calculations, the boiling heat load equation is shown below,

$$Q_{bl} = \frac{\dot{m}_{cold}}{3.6} * LH_{cold} = \frac{39790.878}{3.6} * 3.3512x 10^5 = 3.7041x 10^3 W$$

In order to calculate the Overheating Heat Load, the vapor outlet enthalpy ($h_{coldvapout} = 4.0095x 10^5$) for the cold side and the vapor enthalpy at the boiling end ($h_{coldboilend} = 3.9941x 10^5$) are taken from the thermodynamic table.

$$Q_{oh} = (h_{coldout} - h_{coldboilend}) * \frac{\dot{m}_{cold}}{3,6} = (4.0095x 10^5 - 3.9941x 10^5) * \frac{39790.878}{3,6}$$

$$= 17.0298 W$$

Total heat load calculation:

$$Q_{total} = Q_{oh} + Q_{bl} + Q_{pr} = 17.0298 + 3.7041x 10^3 + 56.2360 = 3.7774x 10^3 W$$

Assuming the heat loss is 0.05 (Q_{loss}), the maximum heat load calculation is shown in the equation below:

$$Q_{duty} = Q_{total} * (1 + Q_{loss}) = 3.7774x 10^3 * (1 + 0.05) = 3.9663x 10^3 W$$

Required Area calculation:

$$A_{out} = \frac{Q_{duty} * 1000}{\frac{EMTD}{OHTC_{int}}} = \frac{3.9663x 10^3 * 1000}{\frac{13.4022}{1600}} = 184.9640m^2$$

Heat flux calculation:

$$q = \frac{Q_{duty}}{A_{out}} = \frac{3.9663x 10^3}{184.9640} = 21.4434 W/m^2$$

Calculation of kinematic viscosity

$$v = \frac{h_{liquid}}{\rho_L} = \frac{1.2377 \times 10^{-4}}{581.9057} = 2.1271 \times 10^{-7} m^2/s$$

The dynamic viscosity value ($h_{liquid} = 1.2377 \times 10^{-4}$) in the equation is taken from the thermodynamic table according to the saturation temperature ($T_{cold\ boilsat} = 62.4259 \text{ }^\circ C$) at boiling.

The calculation of the Labuntsov correlation was made according to the equation given below,

$$\begin{aligned} h_{labuntsov} &= 0.075 \left[1 + 10 * \left(\frac{\rho_v}{\rho_L - \rho_v} \right)^{0.67} \right] * \left(\frac{k^2}{v * \sigma * (T_s + 273,15)} \right)^{0.33} * q^{0.7} \\ &= 0.075 * \left[1 + 10 * \left(\frac{6.4538}{581.9057 - 6.4538} \right)^{0.67} \right] \\ &\quad * \left(\frac{0.0995^2}{2.1271 \times 10^{-7} * 0.0116 * (62.4259 + 273.15)} \right)^{0.33} * 18.5856^{0.7} \\ &= 2.6709 \times 10^3 W/m^2 \text{ }^\circ C \end{aligned}$$

The vapor, liquid densities ($\rho_v = 6.4538 \text{ kg/m}^3$, $\rho_L = 581.9057 \text{ kg/m}^3$) given in the equation are taken from the thermodynamic table according to the saturation temperature ($T_{cold\ boilsat} = 62.4259 \text{ }^\circ C$) at boiling. Surface tension and liquid thermal conductivity ($\sigma=0.0116$, $k=0.0995$) in the equation are taken from the thermodynamic table according to the cold side inlet temperature ($T_{coldinlet} = 60.393^\circ C$).

Tube Side Calculations:

Tube inner diameter calculation,

$$D_{in} = D_{out} - 2 * T_{tube} = 25.4 - 2 * 2.1 = 21.2 \text{ mm}$$

Calculation number of tubes

$$N_t = 2 * \frac{A_{out}}{D_{out} * \pi * L_t} = 2 * \frac{(184.9640)}{25.4 * 3.14 * 10} = 231$$

The number of tube pitch was calculated according to the following equation,

$$TP = D_o * PR = 25.4 * 1.5 = 38.1 \text{ mm}$$

Calculation of the number of passes between tubes according to the pass number (PN=2),

$$N_{tpp} = \frac{N_t}{PN} = \frac{231}{2} = 115.5$$

Calculation of tube-side flow area per pass,

$$A_{o_pp} = \left(\frac{D_{in}}{2000}\right)^2 * \pi * N_{tpp} = \left(\frac{21.2}{2000}\right)^2 * 3.14 * 115.5 = 0.0408 \text{ m}^2$$

The velocity of the fluid passing through the tube is calculated according to the following equation,

$$V_{tube} = \frac{m_{hot}/3600}{\rho_{hot} * A_{o_pp}} = \frac{150000/3600}{972.3786 * 0.0408} = 1.0510 \text{ m/s}$$

Calculation of tube side Reynolds number,

$$Re_{tube} = \frac{m_{hot} * D_{in}}{A_{o_pp} * \mu_{hot}} = \frac{(150000/3600) * \left(\frac{21.2}{1000}\right)}{0.0408 * 3.5769 * 10^{-4}} = 6.0572 * 10^4$$

The density and viscosity values ($\rho_{hot} = 972.3786$, $\mu_{hot} = 3.5769 \times 10^{-4}$) used in the calculations are taken from the thermodynamic tables according to the mean temperature ($T_{hot_{mean}} = 79.1965 \text{ }^\circ\text{C}$) of the hot side.

The tube side Nusselt number calculation is as follows:

$$Nu_{tube} = 0.024 * Re_{tube}^{0.8} * Pr_{hot}^{0.4} = 0.024 * (6.0572 \times 10^4)^{0.8} * 2.2515^{0.4} = 222.3397$$

The Prandtl value ($Pr_{hot} = 2.2515$) is taken from the thermodynamic table according to the hot side mean ($T_{hot_{mean}} = 79.1965 \text{ }^\circ\text{C}$) temperature.

Tube side heat transfer coefficient calculation with the obtained values:

$$h_{tube} = (Nu_{tube} * k_{hot})/D_{in} = (222.3397 * 0.6666)/(21.2/1000) \\ = 6.9908 \times 10^3 \text{ W}/(m^2\text{ }^\circ\text{C})$$

Overall Heat Transfer Coefficient Calculation:

The OHTC equation is divided into two parts, dirty and clean,

$$U_{dirty} = \frac{1}{\frac{1}{h_{Labuntsov}} + \frac{1}{FF_{cold}} + D_o * \frac{\log \frac{D_{out}}{D_{in}}}{2 * k_{tube}} + \frac{D_{out}}{D_{in}} * \left(\frac{1}{FF_{hot}} + \frac{1}{h_{tube}} \right)} \\ = \frac{1}{\frac{1}{2.6709 \times 10^3} + \frac{1}{1.136 \times 10^4} + 25.4 * \frac{\log \frac{25.4}{21.2}}{2 * 55} + \frac{25.4}{21.2} * \left(\frac{1}{5.682 \times 10^3} + \frac{1}{6.9908 \times 10^3} \right)} \\ = 1.1165 \times 10^3 \text{ W}/m^2\text{ }^\circ\text{C}$$

$$\begin{aligned}
U_{clean} &= \frac{1}{\frac{1}{h_{Labuntsov}} + D_o * \frac{\log \frac{D_o}{D_{in}}}{2 * k_{tube}} + \frac{D_o}{D_{in}} * \frac{1}{h_{tube}}} \\
&= \frac{1}{\frac{1}{2.6709 \times 10^3} + 25.4 * \frac{\log \frac{25.4}{21.2}}{2 * 55} + \frac{25.4}{21.2} * \frac{1}{6.9908 \times 10^3}} \\
&= 1.6756 \times 10^3 \text{ W/m}^2\text{C}
\end{aligned}$$

Calculation of tubes bundle diameter:

$$D_{bundle} = 0.637 \cdot \sqrt{\frac{CL}{CTP} (\pi * N_t * TP^2)^{\frac{1}{2}}} = 0.637 \cdot \sqrt{\frac{1}{0.9} (3.14 * 231 * 38.1^2)^{\frac{1}{2}}} = 728 \text{ m}$$

Calculation of shell diameter for heat exchanger:

$$D_{shell} = D_{bundle} * d_{ratio} = 728 * 2 = 1456 \text{ m}$$

Calculation of liquid level in the heat exchanger,

$$L_{liquid} = D_{bundle} * d_{liq.ratio} = 728 * 0.9 = 0.6552 \text{ m}$$

Width liquid level calculation is shown below,

$$W_l = 2 * \sqrt{L_{liquid} * \frac{D_{shell}}{1000 - L_{liquid}}} = 2 * \sqrt{0.6552 * \frac{1456}{1000 - 0.6552}} = 1.4487 \text{ m}$$

Surface area of liquid calculation:

$$A_{liquid} = L_{tube} * W_l = 10 * 1.4487 = 14.4870 \text{ m}^2$$

Equation for calculating the vapour velocity at the surface,

$$V_{vapour} = \frac{m_{cold}}{\rho_v * A_{liquid}} = \frac{39790.878}{6.4538 * 15.5218} = 0.1182 \frac{m}{s}$$

To find the pressure loss in the tube, it is necessary to calculate the friction factor,

$$f_{tube} = (1.58 * \log(Re_{tube}) - 3.28)^{-2} = (1.58 * \log(6.0572x 10^4) - 3.28)^{-2} = 0.0050$$

Calculation of tube side pressure loss:

$$\begin{aligned} \Delta P &= \frac{4 * \left(\frac{f * L_{tube}}{D_{out}} + 1 \right) * N_p * \frac{1}{2} * \rho_{hot} * v_{tube}^2}{10000} \\ &= \frac{4 * \left(\frac{0.0052 * 10}{\frac{25.4}{1000}} + 1 \right) * 2 * \frac{1}{2} * 972.3786 * 1.0510^2}{10000} = 0.1278 \text{ bar} \end{aligned}$$

These results are calculated for only one loop without optimizations and iterations which were made in the preheater part MATLAB.

5.1.2 Preheater Calculations

In the preheaters, the input values are divided into two as hot and cold sides. Hot side inlet and outlet temperatures $T_{hotinlet} = 68.393^{\circ}C$ and $T_{hotoutlet} = 64.947^{\circ}C$, pressure $P_{hot} = 3 \text{ bar}$, mass flow rate $m_{hot} = 150000 \frac{kg}{h} = 41.66 \text{ kg/s}$, hot side fouling resistance $FF_{hot} = 1.760 \times 10^{-4} \text{ m}^2C/W$ are assumed while the cold side inlet and outlet temperatures $T_{coldinlet} = 38.034^{\circ}C$ and $T_{coldoutlet} = 60.393^{\circ}C$, pressure $P_{cold} = 2.62 \text{ bar}$, mass flow rate $m_{cold} = 39790.878 \text{ kg/h} = 11.05 \text{ kg/s}$, hot side fouling resistance $FF_{cold} = 8.800 \times 10^{-5} \text{ m}^2C/W$ are assumed as input at the beginning of design. Input values of the tubes inside the preheater: tube outer diameter $D_o = 25.4 \text{ mm}$, tube wall thickness $T_{tube} = 2.1 \text{ mm}$, tube conductivity $k_{tube} = 45 \text{ W/m}^{\circ}C$, tube length $L_{tube} = 10 \text{ m}$, pitch ratio $PR = 1.5$, tube layout TL=45, central baffle spacing ratio $ratio_{cbs} = 0.6$, number of tubes $N_t = 80$, inlet-outlet baffle spacing ratio $iobsr = 1.15$, baffle cut percent $baffle_{cp} = 0.25$, pass number $N_p = 2$, number of sealing strip pairs $N_{ss} = 1$, tube to baffle diameter clearance $S_{tb} = 1 \text{ mm}$, shell to baffle diameter clearance $S_{sb} = 3 \text{ mm}$ are selected. The diameter of outer tube limit can be calculated as follows:

$$D_{otl} = \frac{\left(D_o * \left(\frac{N_t}{0.156} \right)^{\frac{1}{2.291}} \right)}{1000} = \frac{\left(25.4 * \left(\frac{80}{0.156} \right)^{\frac{1}{2.291}} \right)}{1000} = 0.3870 \text{ m}$$

Tube side inside diameter calculation:

$$d_i = D_o - 2 * T_{tube} = 25.4 - 2 * 2.1 = 21.2 \text{ mm}$$

Tube pitch calculation:

$$p_t = D_o * PR = 25.4 * 1.5 = 38.1 \text{ mm}$$

Shell side inside diameter calculation:

$$D_s = D_{otl} + p_t * \frac{2}{1000} = 0.3870 + 38.1 * \frac{2}{1000} = 0.4630 \text{ m}$$

Transverse tube pitch calculation for layout=45 can be calculated:

$$X_t = \sqrt{2} * p_t = \sqrt{2} * 38.1 = 53.7401 \text{ mm}$$

Longitudinal tube pitch calculation for layout=45:

$$X_L = \sqrt{2} * p_t = \sqrt{2} * 38.1 = 53.7401 \text{ mm}$$

Central baffle spacing calculation:

$$Lb_c = D_s * ratio_{cbs} = 0.4630 * 0.6 = 0.2778 \text{ m}$$

Inlet baffle spacing calculation:

$$Lb_i = Lb_c * iobsr = 0.2778 * 1.15 = 0.3195 \text{ m}$$

Calculation of outlet baffle spacing is presented below:

$$Lb_o = Lb_c * iobsr = 0.2778 * 1.15 = 0.3195 \text{ m}$$

Calculation of baffle cut is presented below:

$$l_c = D_s * bafflec_p = 0.4630 * 0.25 = 0.1160 \text{ m}$$

Width of bypass lane can be evaluated by the following equation:

$$w_p = 2 * D_o = 2 * 25.4 = 50.8 \text{ mm}$$

The heat capacity and temperature efficiency ratio calculations are presented below:

$$R = \frac{C_c}{C_h} = \frac{T_{h1} - T_{h2}}{T_{c2} - T_{c1}} = \frac{68.393 - 64.947}{60.393 - 38.034} = 0.1541$$

$$P = \frac{T_{c2} - T_{c1}}{T_{h1} - T_{c1}} = \frac{60.393 - 38.034}{68.393 - 60.393} = 0.7365$$

Log mean temperature difference calculation is shown below according to the given input-output temperatures:

$$\Delta T_1 = T_{hot\ inlet} - T_{cold\ outlet} = 68.393 - 60.393 = 8\text{ }^\circ\text{C}$$

$$\Delta T_2 = T_{hot\ outlet} - T_{cold\ outlet} = 64.947 - 60.393 = 26.9130\text{ }^\circ\text{C}$$

$$LMTD = \frac{\Delta T_2 - \Delta T_1}{\ln(\frac{\Delta T_2}{\Delta T_1})} = \frac{26.9130 - 8}{\ln(\frac{26.9130}{8})} = 15.5898$$

The FT value is obtained by looping and iterating with the while command in the MATLAB program. The value of FT=0.9401 was accepted for sample calculation. Calculation of EMTD:

$$EMTD = LMTD * FT = 15.5898 * 0.9401 = 14.6563$$

Calculation of heat load is presented below:

$$Q = m_{hot} * Cp_{hot} * (T_{hot\ inlet} - T_{hot\ outlet}) = 41.66 * 4.1884 * (68.393 - 64.947) \\ = 601.2824\text{ }W$$

The specific heat shown in the equation is taken from the thermodynamic table according to the mean temperature value ($T_{hot,mean} = 66.67\text{ }^\circ\text{C}$) of the hot side.

Hot and cold side mean temperature can be calculated by the following formulas:

$$T_{hot_{mean}} = \frac{T_{hot\ inlet} + T_{hot\ outlet}}{2} = \frac{68.393 + 64.947}{2} = 66.67\text{ }^{\circ}\text{C}$$

$$T_{cold_{mean}} = \frac{T_{cold\ inlet} + T_{cold\ outlet}}{2} = \frac{38.034 + 60.393}{2} = 51.4905\text{ }^{\circ}\text{C}$$

Shell Side Calculations:

Shell side angle calculation:

$$\theta_b = 2 * \text{acos} \left(1 - 2 * \frac{l_c}{D_s} \right) * \frac{180}{\pi} = 2 * \text{acos} \left(1 - 2 * \frac{0.1160}{0.4630} \right) * \frac{180}{3.14} = 120.1428^{\circ}$$

Gross window area calculations:

$$\begin{aligned} Afr_w &= \frac{D_s^2}{4} * \left(\frac{\text{deg2rad}(\theta_b)}{2} - \left(1 - 2 * \frac{l_c}{D_s} \right) * \sin \left(\text{deg2rad} \left(\frac{\theta_b}{2} \right) \right) \right) \\ &= \frac{0.4630^2}{4} \\ &\quad * \left(\frac{\text{deg2rad}(120.1428^{\circ})}{2} - \left(1 - 2 * \frac{0.1160}{0.4630} \right) * \sin \left(\text{deg2rad} \left(\frac{120.1428^{\circ}}{2} \right) \right) \right) \\ &= 0.0330\text{ }m^2 \end{aligned}$$

Calculation of diameter central tube limit can be calculated as follows:

$$D_{ctl} = D_{otl} - \frac{D_o}{1000} = 0.3870 - \frac{25.4}{1000} = 0.3616\text{ }m$$

Calculation of shell side baffle cut angle,

$$\theta_{ctl} = 2 * \arccos\left(\frac{D_s - 2 * l_c}{D_{ctl}}\right) * \frac{180}{\pi} = 2 * \arccos\left(\frac{0.4630 - 2 * 0.1160}{0.3616}\right) * \frac{180}{3.14} = 100.5905^\circ$$

Fraction of total tubes in the window Calculation,

$$F_w = \frac{\text{deg2rad}(\theta_{ctl}) - \sin(\text{deg2rad}(\theta_{ctl}))}{2 * \pi}$$

$$= \frac{\text{deg2rad}(100.5905^\circ) - \sin(\text{deg2rad}(100.5905^\circ))}{2 * 3.14} = 0.1230$$

Number of tubes in window calculation,

$$N_{t_w} = F_w * N_t = 0.1230 * 80 = 9.8379$$

Calculation of area occupied by tubes in window,

$$A_{fr_t} = \frac{\pi}{4} * \left(\frac{D_o}{1000}\right)^2 * F_w * N_t = \frac{3.14}{4} * \left(\frac{25.4}{1000}\right)^2 * 0.1230 * 80 = 0.0050 \text{ m}^2$$

Net flow area in one window calculation shown in below,

$$A_{o_w} = A_{fr_w} - A_{fr_t} = 0.0330 - 0.0050 = 0.0280 \text{ m}^2$$

Calculation of shell side hydraulic diameter of window,

$$Dh_w = 4 * \frac{A_{o_w}}{\pi * \frac{D_o}{1000} * N_{t_w} + \pi * D_s * \left(\frac{\text{deg2rad}(\theta_b)}{2 * \pi}\right)}$$

$$= 4 * \frac{A_{o_w}}{3.14 * \frac{25.4}{1000} * 9.8379 + 3.14 * 0.4630 * \left(\frac{\text{deg2rad}(120.1428^\circ)}{2 * 3.14}\right)}$$

$$= 0.0883 \text{ m}$$

Number of effective tube rows in crossflow calculation,

$$Nr_{cw} = \frac{0.8}{\frac{X_l}{1000}} * (l_c - 0.5 * (D_s - D_{ctl})) = \frac{0.8}{\frac{53.7401}{1000}} * (0.1160 - 0.5 * (0.4630 - 0.3616))$$

$$= 1$$

Fraction of total number of tubes in crossflow calculation,

$$F_c = 1 - 2 * F_w = 1 - 2 * 0,1230 = 0,7541$$

Calculation of one crossflow section between baffle tips,

$$Nr_{cc} = \frac{D_s - 2 * l_c}{\frac{X_l}{1000}} = \frac{0.4630 - 2 * 0.3616}{\frac{53.7401}{1000}} = 4$$

Crossflow area with plain tubes at or near the shell centreline for one crossflow section with layout=45 calculation,

$$Ao_{cr} = Lb_c * \left(D_s - D_{otl} + 2 * \frac{D_{ctl}}{\frac{X_t}{1000}} * \frac{p_t - D_o}{1000} \right)$$

$$= 0.2778 * \left(0.4630 - 0.3870 + 2 * \frac{0.3616}{\frac{53.7401}{1000}} * \frac{38.1 - 25.4}{1000} \right) = 0.0682 \text{ m}^2$$

Calculation shell side number of baffles,

$$N_b = \frac{Tube_L - Lb_i - Lb_o}{Lb_c} + 1.0 = \frac{10 - 0.3195 - 0.3195}{0.2778} + 1.0 = 35$$

Bypass flow area calculation,

$$A_{o_{bp}} = Lb_c * \left(D_s - D_{otl} + 0.5 * N_p * \frac{w_p}{1000} \right) = 0.2778 * \left(0.4630 - 0.3870 + 0.5 * 2 * \frac{50.8}{1000} \right) \\ = 0.0352 \text{ m}^2$$

Leakage Flow Area calculation,

$$A_{o_{tb}} = \pi * \frac{D_o}{1000} * \frac{S_{tb}}{1000} * N_t * \frac{1 - F_w}{2} = 3.14 * \frac{25.4}{1000} * \frac{1}{1000} * 2 * \frac{1 - 0.1230}{2} = 0.0028 \text{ m}^2$$

Calculation of shell-to-baffle leakage area for one baffle,

$$A_{o_{sb}} = \pi * D_s * \frac{S_{sb}}{2000} * \left(1 - \frac{\text{deg2rad}(\theta_b)}{2 * \pi} \right) \\ = 3.14 * 0.4630 * \frac{3}{2000} * \left(1 - \frac{\text{deg2rad}(120.1428^\circ)}{2 * 3.14} \right) = 0.0015 \text{ m}^2$$

Shell side tube pitch efficiency calculation for layout=45,

$$p_{t_{eff}} = \frac{p_t}{\sqrt{2}} = \frac{38.1}{\sqrt{2}} = 26.8701$$

Calculation of shell side cross flow area,

$$S_m = Lb_c * \left((D_s - D_{otl}) + \left(D_{otl} - \frac{D_o}{1000} \right) * \frac{p_t - D_o}{p_{t_{eff}}} \right) \\ = 0.2778 * \left((0.4630 - 0.3870) + \left(0.3870 - \frac{25.4}{1000} \right) * \frac{38.1 - 25.4}{26.8701} \right) \\ = 0.0682 \text{ m}^2$$

Shell side mass velocity calculation,

$$G_s = \frac{m_{cold}}{Sm} = \frac{11.05}{0.0682} = 161.9814 \frac{kg}{m^2 * h}$$

Reynolds number shell side calculation,

$$Re_s = \frac{G_s * \left(\frac{D_o}{1000}\right)}{\mu_{cold}} = \frac{161.9814 * \left(\frac{25.4}{1000}\right)}{1.3822x 10^{-4}} = 2.9768x 10^4$$

The dynamic viscosity value used in the calculation is taken from the thermodynamic table according to the cold side mean temperature ($T_{cold_{mean}} = 51.4905 \text{ }^\circ\text{C}$) and pressure values ($P_{cold} = 2.62\text{bar}$). Although the pressure value given here is entered manually at first, it is then made according to iteration with a loop.

Tube wall temperature calculation,

$$T_w = \frac{T_{hot\ inlet} + T_{cold\ inlet}}{2} = \frac{68.393 + 38.034}{2} = 53.2135 \text{ }^\circ\text{C}$$

Colburn j factor calculations,

$$a = \frac{a_3}{1 + 0.14 * (Re_s)^{a_4}} = \frac{1.930}{1 + 0.14 * (2.9768x 10^4)^{0.500}} = 0.0767$$

$$J_{idealFactor} = a_1 * \left(\frac{1.33}{\frac{p_t}{D_o}}\right)^{a_2} * (Re_s)^{a_2} = 0.370 * \left(\frac{1.33}{\frac{38.1}{25.4}}\right)^{0.0767} * (2.9768x 10^4)^{-0.396}$$

$$= 0.0062$$

The values taken in Colburn calculations are taken from the table according to layout=45 and Reynolds number (a1=0.370; a2=-0.396; a3=1.930; a4=0.500;).

Calculation of ideal shell-side heat transfer coefficient,

$$\begin{aligned}
h_{id} &= C p_{cold} * \left(\frac{m_{cold}}{Sm} \right) * J_{idealFactor} * (Pr_{cold})^{-\frac{2}{3}} * \left(\frac{\mu_{cold}}{\mu_w} \right)^{0.14} \\
&= 2.4451x 10^3 * \left(\frac{11.05}{0.0682} \right) * 0.0062 * (3.2936)^{-\frac{2}{3}} * \left(\frac{1.3822x 10^{-4}}{1.3585x 10^{-4}} \right)^{0.14} \\
&= 1.1127x 10^3 \frac{W}{m^2 \cdot ^\circ C}
\end{aligned}$$

The cold side Prandtl and specific heat value shown in the calculation are taken from the thermodynamic tables according to the pressure ($P_{cold} = 2.62bar$) and mean temperature ($T_{cold_{mean}} = 51.4905 \text{ }^\circ C$).

Baffle cut and spacing effect correction factor calculations,

$$J_c = 0.55 + 0.72 * F_c = 0.55 + 0.72 * 0.7541 = 1.0929$$

$$r_s = \frac{A_{o_{sb}}}{A_{o_{sb}} + A_{o_{tb}}} = \frac{0.0015}{0.0015 + 0.0028} = 0.3418$$

$$r_{lm} = \frac{A_{o_{sb}} + A_{o_{tb}}}{A_{o_{cr}}} = \frac{0.0015 + 0.0028}{0.0682} = 0.0623$$

Shell-to-baffle leakage effect calculation,

$$\begin{aligned}
J_l &= 0.44 * (1 - r_s) + (1 - 0.44 * (1 - r_s)) * e^{(-2.2 * r_{lm})} \\
&= 0.44 * (1 - 0.3418) + (1 - 0.44 * (1 - 0.3418)) * e^{(-2.2 * 0.0623)} = 0.9090
\end{aligned}$$

$$r_b = \frac{A_{o_{bp}}}{A_{o_{cr}}} = \frac{0.0352}{0.0682} = 0.5164$$

$$N_{ssplus} = \frac{N_{ss}}{Nr_{cc}} = \frac{1}{4} = 0.250$$

Bundle bypassing effects correction factor calculation is shown below,

$$J_b = e^{\left(-C * r_b * \left(1 - (2 * N_{ssplus})^{\frac{1}{3}} \right) \right)} = e^{\left(-1.25 * 0.5164 * \left(1 - (2 * 0.250)^{\frac{1}{3}} \right) \right)} = 0.8753$$

Inlet and outlet variable baffle spacing correction factor calculation,

$$J_s = \frac{N_b - 1 + (iobsr)^{1-nn} + (iobsr)^{1-nn}}{N_b - 1 + iobsr + iobsr} = \frac{35 - 1 + (1.15)^{1-0.6} + (1.15)^{1-0.6}}{35 - 1 + 1.15 + 1.15} = 0.9949$$

If $Re_s > 100$ J_r factor equal to 1.

Calculation of actual shell side heat transfer coefficient,

$$\begin{aligned} h_s &= h_{id} * J_c * J_l * J_b * J_s * J_r = 1.1127 \times 10^3 * 0.3418 * 0.9090 * 0.8753 * 0.9949 * 1 \\ &= 962.6099 \frac{W}{m^2 \cdot ^\circ C} \end{aligned}$$

Tube Side Calculations:

Number of tubes per pass calculation,

$$N_{tp} = \frac{N_t}{n_p} = \frac{80}{2} = 40$$

Tube-side flow area per pass calculation,

$$A_{ot} = \left(\frac{D_{in}}{1000}\right)^2 * \frac{\pi}{4} * N_{tp} = \left(\frac{21.2}{1000}\right)^2 * \frac{3.14}{4} * 40 = 0.0141 \text{ m}^2$$

Tube-side Reynolds number calculation,

$$Re_t = \frac{m_{hot} * \left(\frac{D_{in}}{1000}\right)}{A_{ot} * \mu_{hot}} = \frac{41.66 * \left(\frac{21.2}{1000}\right)}{0.0141 * 4.2276 \times 10^{-4}} = 1.4796 \times 10^5$$

The hot side dynamic viscosity value used in this calculation is taken from the thermodynamic tables according to the mean temperature ($T_{hot_{mean}} = 66.67\text{ }^{\circ}\text{C}$) and pressure ($P_{hot} = 3\text{ bar}$) inputs.

The tube side Nusselt number calculation is as follows:

$$Nu_t = 0.024 * Re_t^{0.8} * Pr_{hot}^{0.4} = 0.024 * (1.4796 \times 10^5)^{0.8} * 2.6942^{0.4} = 488.0855$$

Tube side heat transfer coefficient calculation,

$$h_t = (Nu_t * k_{hot}) / (D_{in} / 1000) = (488.0855 * 0.6571) / (21.2 / 1000) = 1.5129 \times 10^4 \frac{W}{m^2 \cdot ^{\circ}C}$$

Heat transfer area for dirty and clean side calculations,

$$U_{dirty} = \left(\frac{1}{h_s} + FF_{cold} + \frac{D_o}{1000} * \frac{\log\left(\frac{D_o}{D_{in}}\right)}{2 * k_w} + FF_{hot} * \frac{D_o}{D_{in}} + \frac{1}{h_t} * \frac{D_o}{D_{in}} \right)^{-1}$$

$$= \left(\frac{1}{962.6099} + 8.800 \times 10^{-5} + \frac{25.4}{1000} * \frac{\log\left(\frac{25.4}{21.2}\right)}{2 * 45} + 1.760 \times 10^{-4} * \frac{25.4}{21.2} + \frac{1}{1.5129 \times 10^4} * \frac{25.4}{21.2} \right)^{-1} = 681.2380 \text{ W/m}^2\text{C}$$

$$U_{clean} = \left(\frac{1}{h_s} + \frac{D_o}{1000} * \frac{\log\left(\frac{D_o}{d_i}\right)}{2 * k_w} + \frac{1}{h_t} * \frac{D_o}{d_i} \right)^{-1}$$

$$= \left(\frac{1}{962.6099} + \frac{25.4}{1000} * \frac{\log\left(\frac{25.4}{21.2}\right)}{2 * 45} + \frac{1}{1.5129 \times 10^4} * \frac{25.4}{21.2} \right)^{-1}$$

$$= 855.3971 \text{ W/m}^2\text{C}$$

Calculation of heat transfer area,

$$A_a = \pi * Tube_L * \frac{D_o}{1000} * N_t = 3.14 * 10 * \frac{25.4}{1000} * 80 = 63.8372 \text{ m}^2$$

Heat duty equation to be added or subtracted from process fluids,

$$Q_a = A_a * U_{o_{dirty}} * \frac{EMTD}{1000} = 63.8372 * 681.2380 * \frac{14.6563}{1000} = 637.3769 \text{ W}$$

Shell Side Pressure Loss Calculations:

The values taken in friction factor calculations are taken from the table according to layout=45 and Reynolds number (b1=3.5; b2=0.52; b3=6.59; b4=-0.476),

$$b = \frac{6.59}{1 + 0.14 * Re_s^{0.52}} = \frac{6.59}{1 + 0.14 * (2.9768x 10^4)^{0.52}} = 0.2148$$

Ideal friction factor calculation,

$$\begin{aligned} f_{id} &= 3.5 * \left(\left(1.33 * \frac{D_o}{p_t} \right)^b \right) * (Re_s^{-0.476}) \\ &= 3.5 * \left(\left(1.33 * \frac{25.4}{38.1} \right)^{0.2148} \right) * ((2.9768x 10^4)^{-0.476}) = 0.0253 \end{aligned}$$

Shell side ideal pressure loss calculation,

$$\begin{aligned} \Delta P b_{id} &= 4 * f_{id} * G_s^2 * \frac{Nr_{cc}}{2 * g_c * \rho_{cold}} * \left(\frac{\mu_w}{\mu_{cold}} \right)^{0.25} \\ &= 4 * 0.0253 * (161.9814)^2 * \frac{4}{2 * 1 * 593.9747} * \left(\frac{1.3585x 10^{-4}}{1.3822x 10^{-4}} \right)^{0.25} \\ &= 8.9119 \text{ bar} \end{aligned}$$

The dynamic viscosity value on the wall is taken from the thermodynamic table according to the temperature of the wall ($T_w = 53.2135 \text{ }^\circ\text{C}$) and the cold side pressure ($P_{cold} = 2.62\text{bar}$) values.

λ_b coefficient calculation,

$$\lambda_b = e^{\left(-D * r_b * \left(1 - (2 * N_{ssptus})^{\frac{1}{3}}\right)\right)} = e^{\left(-3.7 * 0.5164 * \left(1 - (2 * 0.25)^{\frac{1}{3}}\right)\right)} = 0.6743$$

$$p = (-0.15 * (1 + r_s) + 0.8) = (-0.15 * (1 + 0.3418) + 0.8) = 0.5987$$

λ_l coefficient calculation,

$$\lambda_l = e^{(-1.33 * (1 + r_s) * r_{lm}^p)} = e^{(-1.33 * (1 + 0.3418) * 0.0623^{0.5987})} = 0.7126$$

Shell side window area velocity

$$G_w = \frac{m_{cold}}{(A_{ocr} * A_{ow})^{0.5}} = \frac{11.05}{(0.0682 * 0.0280)^{0.5}} = 252.6943 \frac{kg}{m^2 * s}$$

Pressure drop in crossflow calculation,

$$\Delta P_{cr} = \Delta P_{bid} * (N_b - 1) * \lambda_b * \lambda_l = 8.9119 * (35 - 1) * 0.6743 * 0.7126 = 145.5891 Pa$$

Calculation of Pressure drop in window,

$$\begin{aligned} \Delta P_w &= N_b * (2 + 0.6 * N r_{cw}) * \frac{G_w^2}{2 * g_c * \rho_{cold}} * \lambda_l \\ &= 35 * (2 + 0.6 * 1) * \frac{(252.6943)^2}{2 * 1 * 593.9747} * 0.7126 = 3.4857 * 10^3 Pa \end{aligned}$$

Calculation of λ_s coefficient,

$$\lambda_s = \left(\frac{Lb_c}{Lb_o}\right)^{2-nprime} + \left(\frac{Lb_c}{Lb_i}\right)^{2-nprime} = \left(\frac{0.2778}{0.3195}\right)^{2-0.2} + \left(\frac{0.2778}{0.3195}\right)^{2-0.2} = 1.5552$$

Calculation of Pressure drop in inlet–outlet sections,

$$\begin{aligned}\Delta P_{io} &= 2 * \Delta P_{bid} * \left(1 + \frac{Nr_{cw}}{Nr_{cc}}\right) * \lambda_b * \lambda_s = 2 * 8.9119 * \left(1 + \frac{1}{4}\right) * 0.6743 * 1.5552 \\ &= 23.3618 Pa\end{aligned}$$

Shell side pressure loss

$$\Delta P_{shell} = \frac{\Delta P_{cr} + \Delta P_w + \Delta P_{io}}{100000} = \frac{145.5891 + 3.4857 \times 10^3 + 23.3618}{100000} = 0.0365 bar$$

Tube Side Pressure Loss:

Tube side velocity calculation,

$$v_{tube} = \frac{\frac{m_{hot}}{\rho_{hot}}}{\frac{N_t}{n_p} * \pi * \left(\frac{D_o}{2000}\right)^2} = \frac{\frac{41.66}{979.7230}}{\frac{80}{2} * 3.14 * \left(\frac{25.4}{2000}\right)^2} = 2.0980 \frac{m}{s}$$

Calculation of tube side friction factor,

$$f_{tube} = (1.58 * \log(Re_t) - 3.28)^{-2} = (1.58 * \log(1.4796 \times 10^5) - 3.28)^{-2} = 0.0041$$

Tube side pressure loss calculation,

$$\begin{aligned}\Delta P_{tube} &= \frac{4 * \left(f_{tube} * \frac{Tube_L}{\frac{D_o}{1000}} + 1\right) * n_p * 0.5 * \rho_{hot} * v_{tube}^2}{100000} \\ &= \frac{4 * \left(0.0041 * \frac{10}{\frac{25.4}{1000}} + 1\right) * 2 * 0.5 * 979.7230 * (2.0980)^2}{100000} = 0.4541 bar\end{aligned}$$

5.1.3 Air Cooled Condenser Calculations

Input values of hot side in air cooled condenser system: Hot side inlet and outlet temperatures $T_{hotinlet} = 48.15^{\circ}C$ and $T_{hotoutlet} = 38^{\circ}C$, pressure $P_{hot} = 1.09 \text{ bar}$, mass flow rate $m_{hot} = 150 \text{ kg/s}$, hot side inner and outer fouling resistance $FF_{outer}=0.000352 \text{ m}^2C/W$, $FF_{inner}=0.000210 \text{ m}^2C/W$ the ayes have it. Air cooled condenser air inlet temperature $T_{air inlet}=18^{\circ}C$ and air inlet pressure $P_{air} = 1 \text{ bar}$. Input values of tube, fin and fan in air cooled condenser system: tube outer diameter $D_o = 25.4 \text{ mm}$, tube wall thickness $T_{tube} = 1.65 \text{ mm}$, tube conductivity $k_{tube} = 55 \text{ W/m}^{\circ}C$, tube row number $N_{tube row}=4$, fin height $h = 15.9 \text{ mm}$, tube pitch diameter $D_{tp} = 58.74 \text{ mm}$, fins per meter $FPM = 413.4$, fin thickness $t_{fin} = 0.4$, air cooled condenser width $Width = 20$, fan area ration $FAR = 0.4$, fan efficiency $\eta_{fan} = 0.7$, reducer efficiency $\eta_{reducer} = 0.92$. Since there are phase transitions in air-cooled condensers, calculations will be according to zone-1, zone-2, and zone-3.

Calculation of temperature difference between zones:

$$\Delta T_{z-1} = T_{hot inlet} - T_{zone-1} = 48.15 - 38.216 = 9.9340 \text{ }^{\circ}C$$

$$\Delta T_{z-2} = T_{zone-1} - T_{zone-2} = 38.2160 - 38.2160 = 0 \text{ }^{\circ}C$$

$$\Delta T_{z-3} = T_{zone-3} - T_{out inlet} = 38.2160 - 38.000 = 0.216 \text{ }^{\circ}C$$

In this calculation, T_{zone-1} value was taken from the thermodynamic table according to the hot side pressure ($P_{hot} = 1.09 \text{ bar}$).

Enthalpy, specific heat, dynamic viscosity, thermal conductivity, Prandtl, density values used in the calculations on the tube side are taken from the thermodynamic tables according to the hot side inlet-outlet temperatures ($T_{hotinlet} = 48.15^{\circ}C$, $T_{hotoutlet} = 38^{\circ}C$), zone-1 outlet temperature ($T_{zone-1} = 38.216 \text{ }^{\circ}C$) and inlet pressure ($P_{hot} = 1.09 \text{ bar}$).

Tube Side Thermal Properties:

Calculation of specific heat average between zones:

$$c_{p-z1} = \frac{c_{p-1} + c_{p-2}}{2} = \frac{1.8079x 10^3 + 1.7698x 10^3}{2} = 1.7888x 10^3 \frac{J}{kg^{\circ}C}$$

$$c_{p-z2} = \frac{c_{p-2} + c_{p-3}}{2} = \frac{1.7698x 10^3 + 2.3788x 10^3}{2} = 2.0743x 10^3 \frac{J}{kg^{\circ}C}$$

$$c_{p-z3} = \frac{c_{p-3} + c_{p-4}}{2} = \frac{2.3788x 10^3 + 2.3777x 10^3}{2} = 2.3783x 10^3 \frac{J}{kg^{\circ}C}$$

Calculation of dynamic viscosity average between zones:

$$\mu_{z1} = \frac{\mu_1 + \mu_2}{2} = \frac{7.1860x 10^{-6} + 6.9460x 10^{-6}}{2} = 7.0659x 10^{-6} \frac{kg}{m \cdot s}$$

$$\mu_{z2} = \frac{\mu_2 + \mu_3}{2} = \frac{6.9460x 10^{-6} + 0.1575x 10^{-3}}{2} = 8.2214x 10^{-5} \frac{kg}{m \cdot s}$$

$$\mu_{z3} = \frac{\mu_3 + \mu_4}{2} = \frac{0.1575x 10^{-3} + 0.1578x 10^{-3}}{2} = 1.5765x 10^{-4} \frac{kg}{m \cdot s}$$

Calculation of thermal conductivity average between zones:

$$k_{z1} = \frac{k_1 + k_2}{2} = \frac{0.0168 + 0.0158}{2} = 0.0163 \text{ W/m} \cdot ^{\circ}C$$

$$k_{z2} = \frac{k_2 + k_3}{2} = \frac{0.0158 + 0.1072}{2} = 0.0615 \text{ W/m} \cdot ^{\circ}C$$

$$k_{z3} = \frac{k_3 + k_4}{2} = \frac{0.1072 + 0.1072}{2} = 0.1072 \text{ W/m} \cdot ^{\circ}C$$

Calculation of Prandtl number average between zones:

$$Pr_{z1} = \frac{Pr_1 + Pr_2}{2} = \frac{0.7717 + 0.7768}{2} = 0.7743$$

$$Pr_{z2} = \frac{Pr_2 + Pr_3}{2} = \frac{0.7768 + 3.4958}{2} = 2.1363$$

$$Pr_{z3} = \frac{Pr_3 + Pr_4}{2} = \frac{3.4958 + 3.4993}{2} = 3.4976$$

Tube Bundle Parameters Calculation:

Tube inner diameter calculation equation:

$$D_{in} = D_o - 2 * T_{tube} = 25,4 - 2 * 1,65 = 22,1 \text{ mm}$$

Single fin area calculation equation is shown below,

$$SFA = \left(\left(\pi * \frac{\left(\frac{D_o + 2 * h}{1000} \right)^2}{4} \right) - \left(\pi * \frac{\left(\frac{D_o}{1000} \right)^2}{4} \right) \right) * 2$$

$$= \left(\left(3.14 * \frac{\left(\frac{25.4 + 2 * 15.9}{1000} \right)^2}{4} \right) - \left(3.14 * \frac{\left(\frac{25.4}{1000} \right)^2}{4} \right) \right) * 2 = 0.0041 \text{ m}^2$$

Calculation of total fin area,

$$TFA = FPM * SFA = 413.4 * 0.0041 = 1.7057$$

Naked tube area calculation equation:

$$NTA = \frac{D_o}{1000} * \pi = \frac{25.4}{1000} * 3.14 = 0.0798$$

Calculation of fin tube area is shown below:

$$APM = TFA + NTA = 1.7057 + 0.0798 = 1.7855$$

Fintube area calculation per m² of bundle face area,

$$APSM = \frac{1}{\frac{D_{tp}}{1000}} * APM * N_{row} = \frac{1}{\frac{58.74}{1000}} * 1.7855 * 4 = 121.5850 \text{ m}^2$$

$$AR = \frac{APM}{NTA} = \frac{1.7855}{0.0798} = 22.3754$$

Calculation of cross section area:

$$CSA = \frac{\pi * D_{in}^2}{4} = \frac{3.14 * 22.1^2}{4} = 383.5963 \text{ m}^2$$

Thermal Calculations:

The following calculations give the resulting values without the if loop.

The phase transitions for the heat load are calculated with the following equations,

$$Q_{z1} = m_{hot} * \frac{(h_1 - h_2)}{1000} = 150 * \frac{(378.8552 - 361.0862)}{1000} = 0.1963 \text{ W}$$

$$Q_{z2} = m_{hot} * \frac{(h_2 - h_3)}{1000} = 150 * \frac{(361.0862 - 5.1249)}{1000} = 3.9334 \text{ W}$$

$$Q_{z3} = m_{hot} * \frac{(h_3 - h_4)}{1000} = 150 * \frac{(5.1249 - 4.6112)}{1000} = 0.0057 \text{ W}$$

Total heat load calculation formula,

$$Q_{total} = Q_{z1} + Q_{z2} + Q_{z3} = 0.1963 + 3.9334 + 0.0057 = 0.0057 W$$

Total heat transfer coefficient calculation for dirty side is given below to calculate LMTD and air outlet temperature values for ACC.

$$\frac{1}{U_x} = \left(\frac{1}{h_t}\right) * \left(\frac{A_x}{A_i}\right) + r_{dt} * \left(\frac{A_x}{A_i}\right) + r_{mx} + \frac{1}{h_a}$$

$$U_{xz1-dirty} = 0.00000000003 * (P_1 * 100)^3 - 0.0000004 * (P_1 * 100)^2 + 0.0035 * (P_1 * 100) + 8.3705 = 8.7473$$

$$U_{xz2-dirty} = 27$$

$$U_{xz3-dirty} = -0.0486 * (\mu_4 * 1000)^3 + 1.0537 * (\mu_4 * 1000)^2 - 8.1266 * (\mu_4 * 1000) + 27.985 = 26.7285$$

Air outlet temperature calculations,

$$\begin{aligned} \Delta T_{air_z-1} &= \left(\frac{U_{xz1-dirty}}{41 + 0.1}\right) * \left(\frac{T_{hot\ inlet} + T_{zone-1}}{2} - T_{air\ inlet}\right) \\ &= \left(\frac{8.7473}{41 + 0.1}\right) * \left(\frac{48.15 + 38.216}{2} - 18\right) = 7.8911\ ^\circ C \end{aligned}$$

$$\begin{aligned} \Delta T_{air_z-2} &= \left(\frac{U_{xz2-dirty}}{41 + 0.1}\right) * \left(\frac{T_{zone-1} + T_{zone-2}}{2} - T_{air\ inlet}\right) \\ &= \left(\frac{27}{41 + 0.1}\right) * \left(\frac{38.216 + 38.216}{2} - 18\right) = 15.3346\ ^\circ C \end{aligned}$$

$$\begin{aligned} \Delta T_{air_z-3} &= \left(\frac{U_{xz3-dirty}}{41 + 0.1}\right) * \left(\frac{T_{zone-2} + T_{zone-3}}{2} - T_{air\ inlet}\right) \\ &= \left(\frac{26,9699}{41 + 0.1}\right) * \left(\frac{38.216 + 38.000}{2} - 18\right) = 15.1195\ ^\circ C \end{aligned}$$

$$T_{airoutlet_{z-1}} = T_{air\ inlet} + \Delta T_{air_{z-1}} = 7.8911 + 18 = 25.8911\text{ }^{\circ}\text{C}$$

$$T_{airoutlet_{z-2}} = T_{air\ inlet} + \Delta T_{air_{z-2}} = 15.3346 + 18 = 33.3346\text{ }^{\circ}\text{C}$$

$$T_{airoutlet_{z-3}} = T_{air\ inlet} + \Delta T_{air_{z-3}} = 15.1195 + 18 = 33.1195\text{ }^{\circ}\text{C}$$

$$T_{airaverage_{z-1}} = \frac{T_{air\ inlet} + T_{airoutlet_{z-1}}}{2} = \frac{18 + 25.8911}{2} = 21.9455\text{ }^{\circ}\text{C}$$

$$T_{airaverage_{z-2}} = \frac{T_{air\ inlet} + T_{airoutlet_{z-2}}}{2} = \frac{18 + 33.3346}{2} = 25.6673\text{ }^{\circ}\text{C}$$

$$T_{airaverage_{z-2}} = \frac{T_{air\ inlet} + T_{airoutlet_{z-3}}}{2} = \frac{18 + 33.1195}{2} = 25.5597\text{ }^{\circ}\text{C}$$

Logarithmic mean temperature difference calculations,

$$\Delta T_{1-z-1} = T_{zone-1} - T_{airoutlet_{z-1}} = 38.216 - 25.8911 = 22.2589\text{ }^{\circ}\text{C}$$

$$\Delta T_{1-z-2} = T_{zone-2} - T_{airoutlet_{z-2}} = 38.216 - 33.3346 = 4.8814\text{ }^{\circ}\text{C}$$

$$\Delta T_{1-z-3} = T_{zone-3} - T_{airoutlet_{z-3}} = 38.216 - 33.1195 = 5.0965\text{ }^{\circ}\text{C}$$

$$\Delta T_{2-z-1} = T_{zone-2} - T_{air\ inlet} = 38.216 - 18 = 20.2160\text{ }^{\circ}\text{C}$$

$$\Delta T_{2-z-2} = T_{zone-3} - T_{air\ inlet} = 38.216 - 18 = 20.2160\text{ }^{\circ}\text{C}$$

$$\Delta T_{2-z-3} = T_{hot\ outlet} - T_{air\ inlet} = 38 - 18 = 20\text{ }^{\circ}\text{C}$$

$$\begin{aligned} LMTD_{z-1} &= (\Delta T_{1-z-1} - \Delta T_{2-z-1}) / \log(\Delta T_{1-z-1} / \Delta T_{2-z-1}) \\ &= (22.2589 - 20.2160) / \log(22.2589 / 20.2160) = 21.2211 \end{aligned}$$

$$\begin{aligned} LMTD_{z-2} &= (\Delta T_{1-z-2} - \Delta T_{2-z-2}) / \log(\Delta T_{1-z-2} / \Delta T_{2-z-2}) \\ &= (4.8814 - 20.2160) / \log(4.8814 / 20.2160) = 10.7911 \end{aligned}$$

$$\begin{aligned} LMTD_{z-3} &= (\Delta T_{1-z-3} - \Delta T_{2-z-3}) / \log(\Delta T_{1-z-3} / \Delta T_{2-z-3}) = (5.0965 - 20) / \log(5.0965 / 20) \\ &= 10.9009 \end{aligned}$$

Calculation of heat transfer area according to the obtained values,

$$A_{z-1} = \frac{Q_{z1} * 1000000}{U_{xz1-dirty} * LMTD_{z-1}} = \frac{0.1963 * 1000000}{8.7473 * 21.2211} = 1.0578x 10^3 m^2$$

$$A_{z-2} = \frac{Q_{z2} * 1000000}{U_{xz2-dirty} * LMTD_{z-2}} = \frac{3.9334 * 1000000}{27 * 10.7911} = 1.3500x 10^4 m^2$$

$$A_{z-3} = \frac{Q_{z3} * 1000000}{U_{xz3-dirty} * LMTD_{z-3}} = \frac{0.0057 * 1000000}{26.7285 * 10.9009} = 19.4832 m^2$$

$$A_{total} = A_{z-1} + A_{z-2} + A_{z-3} = (1.0578x 10^3) + (1.3500x 10^4) + (19.4832) \\ = 1.4577x 10^4 m^2$$

Calculation of face area,

$$A_{face-z-1} = \frac{A_{z-1}}{APSM} = \frac{1.0578x 10^3}{121.5850} = 8.6997 m^2$$

$$A_{face-z-2} = \frac{A_{z-2}}{APSM} = \frac{1.3500x 10^4}{121.5850} = 111.0337 m^2$$

$$A_{face-z-3} = \frac{A_{z-3}}{APSM} = \frac{19.4832}{121.5850} = 0.1602 m^2$$

$$A_{face-all} = A_{face-z-1} + A_{face-z-2} + A_{face-z-3} = 8.6997 + 111.0337 + 0.1602 \\ = 119.8936 m^2$$

Tube Length calculation for each phase is shown below:

$$L_{z-1} = \frac{A_{face-z-1}}{Width} = \frac{8.6997}{20} = 0.4350 m$$

$$L_{z-2} = \frac{A_{face-z-2}}{Width} = \frac{111.0337}{20} = 5.5517 m$$

$$L_{z-3} = \frac{A_{face-z-3}}{Width} = \frac{0.1602}{20} = 0.0080 m$$

$$L_{z-total} = L_{z-1} + L_{z-2} + L_{z-3} = 0.4350 + 5.5517 + 0.0080 = 5.9947 m$$

Number of tubes calculation,

$$N_t = \frac{A_{z-1}}{APM * L_{z-1}} = \frac{1.0578x 10^3}{1.7855 * 0.4350} = 1362$$

Tube side mass velocity is calculated with,

$$G_t = \left(\frac{m_{hot} * N_p}{N_t * CSA} \right) * 1000000 = \left(\frac{11.05 * 1}{1362 * 383.5963} \right) * 1000000 = 21.1500 \frac{kg}{m^2 * h}$$

The Reynold number calculation for each phase is shown below:

$$Re_{z-1} = \frac{D_{in}}{1000} * \frac{G_t}{\mu_{z1}} = \frac{22.1}{1000} * \frac{21.1500}{7.0659x 10^{-6}} = 6.6151x 10^4$$

$$Re_{z-2} = \frac{D_{in}}{1000} * \frac{G_t}{\mu_{z2}} = \frac{22.1}{1000} * \frac{21.1500}{8.2214x 10^{-5}} = 5.6854x 10^3$$

$$Re_{z-3} = \frac{D_{in}}{1000} * \frac{G_t}{\mu_{z3}} = \frac{22.1}{1000} * \frac{21.1500}{1.5765x 10^{-4}} = 2.9649x 10^3$$

Liquid+gas calculations for the second zone:

The following calculations are made by selecting the appropriate a (a=1,04) and b (b=1,26) values by running the if command according to the Reynolds number.

Their superficial liquid Reynolds number Re_{LS} is,

$$Re_{LS} = \frac{G_t * (D_{in}/1000) * (1 - x)}{\mu_3} = \frac{21.1500 * 22.1 * (1 - 0.5)}{0.1575x 10^{-3}} = 1.4840x 10^3$$

The MARTINELLI parameter for turbulent flow in both phases, X_{tt} is

$$X_{tt} = \left(\frac{1-x}{x}\right)^{0.9} * \left(\frac{\rho_2}{\rho_3}\right)^{0.5} * \left(\frac{\mu_3}{\mu_2}\right)^{0.1} = \left(\frac{1-0.5}{0.5}\right)^{0.9} * \left(\frac{3.1856}{607.7525}\right)^{0.5} * \left(\frac{0.1575x 10^{-3}}{0.6946x 10^{-5}}\right)^{0.1}$$

$$= 0.0989$$

The liquid Galileo number Ga_L for the tube is

$$Ga_L = \frac{g * \rho_3 * (\rho_3 - \rho_2) * \left(\frac{D_{in}}{1000}\right)^3}{\mu_3^2} = \frac{9.81 * 607.7525 * (607.7525 - 3.1856) * \left(\frac{22.1}{1000}\right)^3}{(0.1575x 10^{-3})^2}$$

$$= 1.5688x 10^9 m/s^2$$

Epsilon number calculation,

$$\varepsilon = \frac{1}{1 + \left(\frac{1-x}{x}\right) * \left(\frac{\rho_2}{\rho_3}\right)^{\frac{2}{3}}} = \frac{1}{1 + \left(\frac{1-0.5}{0.5}\right) * \left(\frac{3.1856}{607.7525}\right)^{\frac{2}{3}}} = 0.9707$$

θ_{strat} and wall temperature number calculation,

$$\theta_{strat} = (\pi - \arccos \cdot (2 \cdot \varepsilon - 1)) = (3.14 - \arccos \cdot (2 \cdot 0.9707 - 1)) = 2.7976$$

Calculation of wall temperature,

$$T_{wall} = \frac{T_{zone-2} + T_{air inlet}}{2} = \frac{38.216 + 18}{2} = 28.1080^\circ C$$

The liquid Jacob number Ja_L ,

$$Ja_L = \frac{c_{p3}(T_2 - T_{wall})}{(h_2 - h_3)/1000} = \frac{2.3788 \times 10^3 * (38.216 - 28.1080)}{(361.0862 - 5.1249)/1000} = 0.0675$$

and the liquid Froude number Fr_L is

$$Fr_L = \frac{G_t^2}{\rho_3^2 * g * \left(\frac{D_{in}}{1000}\right)} = \frac{21.1500^2}{607.7525^2 * 9.81 * \left(\frac{22.1}{1000}\right)} = 0.0056$$

while the vapour only Reynolds number Re_{Go} is

$$Re_{Go} = \frac{Gt * D_{in}}{\mu_2} = \frac{21.1500 * 22.1}{6.9460 \times 10^{-6}} = 6.7295 \times 10^4$$

Forced convection condensation in the stratified liquid is correlated as

$$\begin{aligned} Nu_{start} &= 0,0195 * Re_{ls}^{0,8} * Pr_L^{0,4} * \left[1,376 + \frac{c_1}{X_{tt}^2}\right]^{\frac{1}{2}} \\ &= 0,0195 * (1.4840 \times 10^3)^{0,8} * 3.4958^{0,4} * \left[1,376 + \frac{4.2026}{0,0989^{1.6550}}\right]^{\frac{1}{2}} \\ &= 176.9097 \end{aligned}$$

Their correlation for the annular flow of condensation is as follows. In these calculations, circular condensate flow and layered wave calculations were made by multiplying the thermal conductivity coefficient.

$$\begin{aligned}
Nu(x) &= 0.023 * Re_{ls}^{0.8} * Pr_L^{0.4} * \left[1 + \frac{2.22}{X_{tt}^{0.89}} \right] * \frac{k_3}{\frac{D_{in}}{1000}} \\
&= 0.023 * (1.4840x 10^3)^{0.8} * 3.4958^{0.4} * \left[1 + \frac{2.22}{0.0989^{0.89}} \right] * \frac{0.1072}{\frac{22.1}{1000}} \\
&= 1.1662x 10^3
\end{aligned}$$

The stratified wave calculation,

$$\begin{aligned}
Nu(x) &= \left(\frac{0.23 * Re_{Go}^{0.12}}{1 + 1.11 * X_{tt}^{0.58}} * \left[\frac{Ga_L * Pr_L}{Ja_L} \right]^{0.25} + \frac{1 - \frac{\theta_{start}}{\pi}}{Nu_{start}} \right) * \frac{k_3}{\frac{D_{in}}{1000}} \\
&= \left(\frac{0.23 * (6.7295x 10^4)^{0.12}}{1 + 1.11 * 0.1582^{0.58}} * \left[\frac{1.5688x 10^9 * 3.4958}{0.2124} \right]^{0.25} + \frac{1 - \frac{2.7976}{3.14}}{176.9097} \right) \\
&\quad * \frac{0.1072}{\frac{22.1}{1000}} = 1.8457x 10^3
\end{aligned}$$

Stratified calculation,

$$N = Nu_{start} * \frac{k_3}{\frac{D_{in}}{1000}} = 176.9097 * \frac{0.1072}{\frac{22.1}{1000}} = 857.8233$$

Tube Side Heat Transfer Coefficients calculations:

$$\begin{aligned}
h_{z1} &= C_1 * G_t * c_{p-z1} * Pr_{z1}^{-\frac{2}{3}} * Re_{z1}^{c2} \\
&= 0.0108 * 21.1500 * 1.7888x 10^3 * 0.7743^{-\frac{2}{3}} * 6.6151x 10^4^{-0.1375} \\
&= 105.3288 \frac{W}{m^2 \cdot C}
\end{aligned}$$

$$h_{z2} = 857.8233 \frac{W}{m^2 \cdot ^\circ C}$$

$$h_{z3} = 0.023 * 21.1500 * 2.3783 \times 10^3 * 3.4976^{-0.7} * 2.9649 \times 10^3^{-0.2} = 97.3336 \frac{W}{m^2 \cdot ^\circ C}$$

ACC Air Side Calculations.

Density, specific heat, dynamic viscosity, thermal conductivity, Prandtl values used in air side thermal calculations for ACC are taken from thermodynamic tables for each phase according to air average temperature ($T_{airaverage_{z-1}} = 21.9455 \text{ }^\circ C$, $T_{airaverage_{z-2}} = 25.6673 \text{ }^\circ C$, $T_{airaverage_{z-3}} = 25.5597 \text{ }^\circ C$) and air pressure ($P_{air} = 1 \text{ bar}$) values.

Kinematic viscosity calculations for each phase transition of the air side,

$$\vartheta_{air-z1} = \frac{\mu_{air-z1}}{\rho_{air-z1}} = \frac{1.8480 \times 10^{-5}}{1.1810} = 1.5496 \times 10^{-5} \frac{m^2}{s}$$

$$\vartheta_{air-z2} = \frac{\mu_{air-z2}}{\rho_{air-z2}} = \frac{1.8480 \times 10^{-5}}{1.1662} = 1.5846 \times 10^{-5} \frac{m^2}{s}$$

$$\vartheta_{air-z3} = \frac{\mu_{air-z3}}{\rho_{air-z3}} = \frac{1.8475 \times 10^{-5}}{1.1666} = 1.5836 \times 10^{-5} \frac{m^2}{s}$$

Center-to-center distance between the fins along the flow direction calculation,

$$S_l = \left(\frac{D_{TP}}{1000} \right) * \frac{\sqrt{3}}{2} = \left(\frac{58.74}{1000} \right) * \frac{\sqrt{3}}{2} = 0.0509 \text{ m}$$

Calculation of diagonal pitch:

$$S_D = \left(\left(\frac{D_{TP}}{2000} \right)^2 + S_l^2 \right)^{0.5} = \left(\left(\frac{58.74}{2000} \right)^2 + 0.0509^2 \right)^{0.5} = 0.0587 \text{ m}$$

Distance measured normal to the flow direction

$$S_{TD} = \frac{D_{TP} + D_o}{2} = \frac{58.74 + 25.4}{2} = 42.0700 \text{ m}$$

Calculation of air flow rate,

$$W_{air-z1} = \frac{Q_{z1} * 1000000}{c_{p_{air-z1}} * \Delta T_{air-z1}} = \frac{0.1963 * 1000000}{1.0062x 10^3 * 7.8911} = 24.7294 \frac{kg}{s}$$

$$W_{air-z2} = \frac{Q_{z2} * 1000000}{c_{p_{air-z2}} * \Delta T_{air-z2}} = \frac{3.9334 * 1000000}{1.0063x 10^3 * 15.3346} = 254.8949 \frac{kg}{s}$$

$$W_{air-z3} = \frac{Q_{z3} * 1000000}{c_{p_{air-z3}} * \Delta T_{air-z3}} = \frac{0.0057 * 1000000}{1.0063x 10^3 * 15.1195} = 0.3731 \frac{kg}{s}$$

$$W_{air-total} = W_{air-z1} + W_{air-z2} + W_{air-z3} = 24.7294 + 254.8949 + 0.3731 = 279.9973 \frac{kg}{s}$$

Average air outlet temperature calculation.

$$\begin{aligned} T_{airoutlet \text{ average}} &= \frac{T_{airoutlet z-1} * W_{air-z1} + T_{airoutlet z-2} * W_{air-z2} + T_{airoutlet z-3} * W_{air-z3}}{W_{air-z1} + W_{air-z2} + W_{air-z3}} \\ &= \frac{25.8911 * 24.7294 + 33.3346 * 254.8949 + 33.1195 * 0.3731}{24.7294 + 254.8949 + 0.3731} \\ &= 32.6769 \text{ } ^\circ\text{C} \end{aligned}$$

Volume flow rate calculation,

$$V_{z1} = \frac{W_{air-z1}}{\rho_{air-z1}} = \frac{24.7294}{1.1810} = 20.9401 \frac{m^3}{s}$$

$$V_{z2} = \frac{W_{air-z2}}{\rho_{air-z2}} = \frac{254.8949}{1.1662} = 218.5670 \frac{m^3}{s}$$

$$V_{z3} = \frac{W_{air-z3}}{\rho_{air-z3}} = \frac{0.3731}{1.1666} = 218.4881 \frac{m^3}{s}$$

Velocity of air calculation,

$$V_{air-z1} = \frac{V_{z1}}{A_{face-z-1}} = \frac{20.9401}{8.6997} = 2.4070 \frac{m}{s}$$

$$V_{air-z2} = \frac{V_{z2}}{A_{face-z-2}} = \frac{218.5670}{111.0337} = 1.9685 \frac{m}{s}$$

$$V_{air-z3} = \frac{V_{z3}}{A_{face-z-3}} = \frac{218.4881}{0.1602} = 1.3635 \times 10^3 \frac{m}{s}$$

Diagonal pitch diameter:

$$S_{DD} = 2 * \left(S_D - \frac{D_o}{1000} \right) = 2 * \left(0.0587 - \frac{25.4}{1000} \right) = 0.0667 \text{ m}$$

$$S_{TD} = \frac{D_{TP} - D_o}{1000} = \frac{58.74 - 25.4}{1000} = 0.0333 \text{ m}$$

If $S_{TD} > S_{DD}$, the air velocity calculations for each phase are given below,

$$V_{air-max-z1} = \frac{D_{TP}}{1000} * \frac{V_{air-z1}}{2 * \left(S_D - \frac{D_o}{1000} \right)} = \frac{58.74}{1000} * \frac{2.4070}{2 * \left(0.0587 - \frac{25.4}{1000} \right)} = 4.2408 \frac{m}{s}$$

$$V_{air-max-z2} = \frac{D_{TP}}{1000} * \frac{V_{air-z2}}{2 * \left(S_D - \frac{D_o}{1000} \right)} = \frac{58.74}{1000} * \frac{1.9685}{2 * \left(0.0587 - \frac{25.4}{1000} \right)} = 3.4682 \frac{m}{s}$$

$$V_{air-max-z3} = \frac{D_{TP}}{1000} * \frac{V_{air-z3}}{2 * \left(S_D - \frac{D_o}{1000}\right)} = \frac{58,74}{1000} * \frac{1.3635x 10^3}{2 * \left(0.0587 - \frac{25.4}{1000}\right)} = 2.4022x 10^3 \frac{m}{s}$$

Fin spacing calculation is shown in the following equation,

$$FS = \frac{1 - FPM * t_{fin}}{FPM} = \frac{1 - 413.4 * 0.4}{413.4} = 0.0020$$

Calculations of Reynolds number,

$$Re_{D-max-z1} = \frac{\frac{D_o}{1000} * V_{air-max-z1}}{\vartheta_{air-z1}} = \frac{\frac{25.4}{1000} * 4.2408}{1.5496x 10^{-5}} = 6.9512x 10^3$$

$$Re_{D-max-z2} = \frac{\frac{D_o}{1000} * V_{air-max-z2}}{\vartheta_{air-z2}} = \frac{\frac{25.4}{1000} * 3.4682}{1.5846x 10^{-5}} = 5.5591x 10^3$$

$$Re_{D-max-z3} = \frac{\frac{D_o}{1000} * V_{air-max-z3}}{\vartheta_{air-z3}} = \frac{\frac{25.4}{1000} * 2.4022x 10^3}{1.5836x 10^{-5}} = 3.8530x 10^6$$

Air side Nusselt number is calculated 3 different formulas and lowest of them is used in design:

$$\begin{aligned} Nu_{1-z1} &= 0.134 * Re_{D-max-z1}^{0.681} * Pr_{air-z1}^{0.33} * \left(\frac{FS}{h}\right)^{0.2} * \left(\frac{FS}{t_{fin}}\right)^{0.1134} \\ &= 0.134 * (6.9512x 10^3)^{0.681} * (0.7077)^{0.33} * \left(\frac{0.0020}{\left(\frac{15.9}{1000}\right)}\right)^{0.2} * \left(\frac{0.0020}{\left(\frac{0.4}{1000}\right)}\right)^{0.1134} \\ &= 39.2617 \end{aligned}$$

$$\begin{aligned}
Nu_{1-z2} &= 0.134 * Re_{D-max-z2}^{0.681} * Pr_{air-z2}^{0.33} * \left(\frac{FS}{h}\right)^{0.2} * \left(\frac{FS}{t_{fin}}\right)^{0.1134} \\
&= 0.134 * (5.5591x 10^3)^{0.681} * (0.7072)^{0.33} * \left(\frac{0.0020}{\left(\frac{15.9}{1000}\right)}\right)^{0.2} * \left(\frac{0.0020}{\left(\frac{0.4}{1000}\right)}\right)^{0.1134} \\
&= 33.7113
\end{aligned}$$

$$\begin{aligned}
Nu_{1-z3} &= 0.134 * Re_{D-max-z3}^{0.681} * Pr_{air-z3}^{0.33} * \left(\frac{FS}{h}\right)^{0.2} * \left(\frac{FS}{t_{fin}}\right)^{0.1134} \\
&= 0.134 * (3.8530x 10^6)^{0.681} * (0.7072)^{0.33} * \left(\frac{0.0020}{\left(\frac{15.9}{1000}\right)}\right)^{0.2} * \left(\frac{0.0020}{\left(\frac{0.4}{1000}\right)}\right)^{0.1134} \\
&= 2.8997x 10^3
\end{aligned}$$

$$\begin{aligned}
Nu_{2-z1} &= 0.1378 * Re_{D-max-z1}^{0.718} * Pr_{air-z1}^{\frac{1}{3}} * \left(\frac{FS}{h}\right)^{0.296} \\
&= 0.1378 * (6.9512x 10^3)^{0.718} * (0.7077)^{\frac{1}{3}} * \left(\frac{0.0020}{\left(\frac{15.9}{1000}\right)}\right)^{0.296} = 38.2384
\end{aligned}$$

$$\begin{aligned}
Nu_{2-z2} &= 0.1378 * Re_{D-max-z2}^{0.718} * Pr_{air-z2}^{\frac{1}{3}} * \left(\frac{FS}{h}\right)^{0.296} \\
&= 0.1378 * (5.5591x 10^3)^{0.718} * (0.7072)^{\frac{1}{3}} * \left(\frac{0.0020}{\left(\frac{15.9}{1000}\right)}\right)^{0.296} = 32.5623
\end{aligned}$$

$$\begin{aligned}
Nu_{2-z3} &= 0.1378 * Re_{D-max-z3}^{0.718} * Pr_{air-z3}^{\frac{1}{3}} * \left(\frac{FS}{h}\right)^{0.296} \\
&= 0.1378 * (3.8530x 10^6)^{0.718} * (0.7072)^{\frac{1}{3}} * \left(\frac{0.0020}{\left(\frac{15.9}{1000}\right)}\right)^{0.296} = 3.5679x 10^3
\end{aligned}$$

$$\begin{aligned}
Nu_{3-z1} &= 0.1507 * Re_{D-max-z1}^{0.667} * Pr_{air-z1}^{\frac{1}{3}} * \left(\frac{FS}{h}\right)^{0.164} * \left(\frac{FS}{t_{fin}}\right)^{0.075} \\
&= 0.1507 * (6.9512x 10^3)^{0.667} * (0.7077)^{\frac{1}{3}} * \left(\frac{0.0020}{\left(\frac{15.9}{1000}\right)}\right)^{0.164} * \left(\frac{0.0020}{\left(\frac{0.4}{1000}\right)}\right)^{0.075} \\
&= 39.4872
\end{aligned}$$

$$\begin{aligned}
Nu_{3-z2} &= 0.1507 * Re_{D-max-z2}^{0.667} * Pr_{air-z2}^{\frac{1}{3}} * \left(\frac{FS}{h}\right)^{0.164} * \left(\frac{FS}{t_{fin}}\right)^{0.075} \\
&= 0.1507 * (5.5591x 10^3)^{0.667} * (0.7072)^{\frac{1}{3}} * \left(\frac{0,0020}{\left(\frac{15,9}{1000}\right)}\right)^{0.164} * \left(\frac{0,0020}{\left(\frac{0,4}{1000}\right)}\right)^{0,075} \\
&= 34.0111
\end{aligned}$$

$$\begin{aligned}
Nu_{3-z3} &= 0.1507 * Re_{D-max-z3}^{0.667} * Pr_{air-z3}^{\frac{1}{3}} * \left(\frac{FS}{h}\right)^{0.164} * \left(\frac{FS}{t_{fin}}\right)^{0.075} \\
&= 0.1507 * (3.8530x 10^6)^{0.667} * (0.7072)^{\frac{1}{3}} * \left(\frac{0.0020}{\left(\frac{15.9}{1000}\right)}\right)^{0.164} * \left(\frac{0.0020}{\left(\frac{0.4}{1000}\right)}\right)^{0.075} \\
&= 2.6695x 10^3
\end{aligned}$$

Air face mass velocity calculation is as follows,

$$G_{a-z1} = \frac{W_{air-z1}}{A_{face-z-1}} = \frac{24.7294}{8.6997} = 2.8426 \frac{kg}{m * s}$$

$$G_{a-z2} = \frac{W_{air-z2}}{A_{face-z-2}} = \frac{254.8949}{111.0337} = 2.2957 \frac{kg}{m * s}$$

$$G_{a-z3} = \frac{W_{air-z3}}{A_{face-z-3}} = \frac{0.3731}{0.1602} = 2.3284 \frac{kg}{m * s}$$

Air side heat transfer area for each zone's calculations,

$$h_{a-z1} = Nu_{2-z1} * \frac{k_{a-z1}}{\frac{D_0}{1000}} = 38.2384 * \frac{0.0260}{\frac{25.4}{1000}} = 39.1700 \frac{W}{m^2 \cdot C}$$

$$h_{a-z2} = Nu_{2-z2} * \frac{k_{a-z2}}{\frac{D_0}{1000}} = 32.5623 * \frac{0.0263}{\frac{25.4}{1000}} = 33.7111 \frac{W}{m^2 \cdot C}$$

$$h_{a-z3} = Nu_{3-z3} * \frac{k_{a-z3}}{\frac{D_0}{1000}} = 2.6695 \times 10^3 * \frac{0.0263}{\frac{25.4}{1000}} = 2.7629 \times 10^3 \frac{W}{m^2 \cdot C}$$

Calculation of heat transfer area air according to the obtained values,

$$\frac{A_x}{A_i} = AR * \frac{D_0}{D_{in}} = 22.3754 * \frac{25.4}{22.1} = 25.7165$$

The calculation of clean and dirty shares in the heat transfer coefficient separately for each phase is shown below,

$$\begin{aligned} U_{x-z1-dirty} &= \left(\frac{1}{h_{z1}} \right) * \left(\frac{A_x}{A_i} \right) + FF_{outer} * \left(\frac{A_x}{A_i} \right) + FF_{inner} + \frac{1}{h_{a-z1}} + \frac{D_0}{1000} * \frac{\log\left(\frac{D_0}{D_{in}}\right)}{(2 * k)^{-1}} \\ &= \left(\frac{1}{105.3288} \right) * 25.7165 + 0.000352 * 25.7165 + 0.000210 + \frac{1}{39.1700} \\ &\quad + \frac{25.4}{1000} * \frac{\log\left(\frac{25.4}{22.1}\right)}{(2 * 55)^{-1}} = 3.5845 \frac{W}{m^2 \cdot C} \end{aligned}$$

$$\begin{aligned} U_{x-z2-dirty} &= \left(\frac{1}{h_{z2}} \right) * \left(\frac{A_x}{A_i} \right) + FF_{outer} * \left(\frac{A_x}{A_i} \right) + FF_{inner} + \frac{1}{h_{a-z2}} + \frac{D_0}{1000} * \frac{\log\left(\frac{D_0}{D_{in}}\right)}{(2 * k)^{-1}} \\ &= \left(\frac{1}{857.8233} \right) * 25.7165 + 0.000352 * 25.7165 + 0.000210 + \frac{1}{33.7111} \\ &\quad + \frac{25.4}{1000} * \frac{\log\left(\frac{25.4}{22.1}\right)}{(2 * 55)^{-1}} = 14.5060 \frac{W}{m^2 \cdot C} \end{aligned}$$

$$\begin{aligned}
U_{x-z3-dirty} &= \left(\frac{1}{h_{z3}}\right) * \left(\frac{A_x}{A_i}\right) + FF_{outer} * \left(\frac{A_x}{A_i}\right) + FF_{inner} + \frac{1}{h_{a-z3}} + \frac{D_0}{1000} * \frac{\log\left(\frac{D_0}{D_{in}}\right)}{(2 * k)^{-1}} \\
&= \left(\frac{1}{97.3336}\right) * 25.7165 + 0.000352 * 25.7165 + 0.000210 + \frac{1}{2.7629 \times 10^3} \\
&\quad + \frac{25.4}{1000} * \frac{\log\left(\frac{25.4}{22.1}\right)}{(2 * 55)^{-1}} = 3.6514 \text{ W/m}^2\text{C}
\end{aligned}$$

$$\begin{aligned}
U_{x-z1-clean} &= \left(\frac{1}{h_{z1}}\right) * \left(\frac{A_x}{A_i}\right) + \frac{1}{h_{a-z1}} + \frac{D_0}{1000} * \frac{\log\left(\frac{D_0}{D_{in}}\right)}{(2 * k)^{-1}} \\
&= \left(\frac{1}{105.3288}\right) * 25.7165 + \frac{1}{39.1700} + \frac{25.4}{1000} * \frac{\log\left(\frac{25.4}{22.1}\right)}{(2 * 55)^{-1}} = 3.7076 \text{ W/m}^2\text{C}
\end{aligned}$$

$$\begin{aligned}
U_{x-z2-clean} &= \left(\frac{1}{h_{z2}}\right) * \left(\frac{A_x}{A_i}\right) + \frac{1}{h_{a-z2}} + \frac{D_0}{1000} * \frac{\log\left(\frac{D_0}{D_{in}}\right)}{(2 * k)^{-1}} \\
&= \left(\frac{1}{857.8233}\right) * 25.7165 + \frac{1}{33.7111} + \frac{25.4}{1000} * \frac{\log\left(\frac{25.4}{22.1}\right)}{(2 * 55)^{-1}} = 16.7575 \text{ W/m}^2\text{C}
\end{aligned}$$

$$\begin{aligned}
U_{x-z3-clean} &= \left(\frac{1}{h_{z3}}\right) * \left(\frac{A_x}{A_i}\right) + \frac{1}{h_{a-z3}} + \frac{D_0}{1000} * \frac{\log\left(\frac{D_0}{D_{in}}\right)}{(2 * k)^{-1}} \\
&= \left(\frac{1}{97.3336}\right) * 25.7165 + \frac{1}{2.7629 \times 10^3} + \frac{25.4}{1000} * \frac{\log\left(\frac{25.4}{22.1}\right)}{(2 * 55)^{-1}} = 3.7792 \text{ W/m}^2\text{C}
\end{aligned}$$

Overall heat transfer coefficient for clean and dirty sides calculation,

$$\begin{aligned}
U_{x-overall-dirty} &= \frac{U_{x-z1-dirty} * Q_{z1} + U_{x-z2-dirty} * Q_{z2} + U_{x-z3-dirty} * Q_{z3}}{Q_{z1} + Q_{z2} + Q_{z3}} \\
&= \frac{3.5845 * 0.1963 + 14.5060 * 3.9334 + 3.6514 * 0.0057}{0.1963 + 3.9334 + 0.0057} = 13.9726 \text{ W/m}^2\text{C}
\end{aligned}$$

$$U_{x\text{-overall-clean}} = \frac{U_{x-z1\text{-clean}} * Q_{z1} + U_{x-z2\text{-clean}} * Q_{z2} + U_{x-z3\text{-clean}} * Q_{z3}}{Q_{z1} + Q_{z2} + Q_{z3}}$$

$$= \frac{3.7076 * 0.1963 + 16.7575 * 3.9334 + 3.7792 * 0.0057}{0.1963 + 3.9334 + 0.0057} = 16.1201 \text{ W/m}^2\text{C}$$

$$LMTD_{total} = \frac{Q_{total} * 1000000}{U_{x\text{-overall-dirty}} * A_{total}} = \frac{4.1354 * 1000000}{13.9726 * 1.4577 * 10^4} = 20.3032$$

Fan Calculations:

Fan area calculation,

$$A_{fan-z1} = A_{face-z-1} * FAR = 8.6997 * 0.4 = 3.4799 \text{ m}^2$$

$$A_{fan-z2} = A_{face-z-2} * FAR = 111.0337 * 0.4 = 44.4135 \text{ m}^2$$

$$A_{fan-z3} = A_{face-z-3} * FAR = 0.1602 * 0.4 = 0.0641 \text{ m}^2$$

$$A_{fan-total} = A_{fan-z1} + A_{fan-z2} + A_{fan-z3} = 3.4799 + 44.4135 + 0.0641 = 47.9574 \text{ m}^2$$

Calculation of fan diameter,

$$D_{fan-z1} = \left(4 * \frac{A_{fan-z1}}{\pi}\right)^{0.5} = \left(4 * \frac{3.4799}{3.14}\right)^{0.5} = 2.1049 \text{ m}$$

$$D_{fan-z2} = \left(4 * \frac{A_{fan-z2}}{\pi}\right)^{0.5} = \left(4 * \frac{44.4135}{3.14}\right)^{0.5} = 7.5199 \text{ m}$$

$$D_{fan-z3} = \left(4 * \frac{A_{fan-z3}}{\pi}\right)^{0.5} = \left(4 * \frac{0.0641}{3.14}\right)^{0.5} = 0.2857 \text{ m}$$

$$Fp_{z1} = -0.2395 * Ga_{z1}^3 + 3.6848 * Ga_{z1}^2 - 4.5269 * Ga_{z1} + 5.4539$$

$$= -0.2395 * 2.8426^3 + 3.6848 * 2.8426^2 - 4.5269 * 2.8426 + 5.4539$$

$$= 16.8587$$

$$\begin{aligned}
 Fp_{z2} &= -0.2395 * Ga_{z2}^3 + 3.6848 * Ga_{z2}^2 - 4.5269 * Ga_{z2} + 5.4539 \\
 &= -0.2395 * 2.2957^3 + 3.6848 * 2.2957^2 - 4.5269 * 2.2957 + 5.4539 \\
 &= 11.5832
 \end{aligned}$$

$$\begin{aligned}
 Fp_{z3} &= -0.2395 * Ga_{z3}^3 + 3.6848 * Ga_{z3}^2 - 4.5269 * Ga_{z3} + 5.4539 \\
 &= -0.2395 * 2.3284^3 + 3.6848 * 2.3284^2 - 4.5269 * 2.3284 + 5.4539 \\
 &= 11.8668
 \end{aligned}$$

Air density ratio calculations,

$$\rho_{ratio-z1} = \frac{\rho_{air-z1}}{1.203} = \frac{1.1810}{1.203} = 0.9817 \text{ kg/m}^3$$

$$\rho_{ratio-z2} = \frac{\rho_{air-z2}}{1.203} = \frac{1.1662}{1.203} = 0.9694 \text{ kg/m}^3$$

$$\rho_{ratio-z3} = \frac{\rho_{air-z3}}{1.203} = \frac{1.1666}{1.203} = 0.9698 \text{ kg/m}^3$$

Air delta pressure calculation,

$$\Delta P_{air-z1} = \frac{Fp_{z1} * N_{tube \text{ row}}}{\rho_{ratio-z1}} = \frac{16.8587 * 4}{0.9817} = 68.6933 \text{ Pa}$$

$$\Delta P_{air-z2} = \frac{Fp_{z2} * N_{tube \text{ row}}}{\rho_{ratio-z2}} = \frac{11.5832 * 4}{0.9694} = 47.7944 \text{ Pa}$$

$$\Delta P_{air-z3} = \frac{Fp_{z3} * N_{tube \text{ row}}}{\rho_{ratio-z3}} = \frac{11.8668 * 4}{0.9698} = 48.9470 \text{ Pa}$$

Calculation of ACMS per fan,

$$ACMS_{z1} = \frac{W_{air-z1}}{\rho_{air-z1}} = \frac{24.7294}{1.1810} = 20.9401 \text{ m}^3/\text{s}$$

$$ACMS_{z2} = \frac{W_{air-z2}}{\rho_{air-z2}} = \frac{254.8949}{1.1662} = 218.5670 \text{ m}^3/\text{s}$$

$$ACMS_{z3} = \frac{W_{air-z3}}{\rho_{air-z3}} = \frac{0.3731}{1.1666} = 0.3198 \text{ m}^3/\text{s}$$

Approximate fan total pressure using DR of air at fan and fan area,

$$\begin{aligned} P_{f-z1} &= \Delta P_{air-z1} + \rho_{ratio-z1} * 0.975 * \left(\frac{ACMS_{z1}}{D_{fan-z1}^2} \right)^2 \\ &= 68.6933 + 0.9817 * 0.975 * \left(\frac{20.9401}{2.1049^2} \right)^2 = 90.0721 \text{ Pa} \end{aligned}$$

$$\begin{aligned} P_{f-z2} &= \Delta P_{air-z2} + \rho_{ratio-z2} * 0.975 * \left(\frac{ACMS_{z2}}{D_{fan-z2}^2} \right)^2 \\ &= 47.7944 + 0.9694 * 0.975 * \left(\frac{218.5670}{7.5199^2} \right)^2 = 61.9144 \text{ Pa} \end{aligned}$$

$$\begin{aligned} P_{f-z3} &= \Delta P_{air-z3} + \rho_{ratio-z3} * 0.975 * \left(\frac{ACMS_{z3}}{D_{fan-z3}^2} \right)^2 \\ &= 48.9470 + 0.9817 * 0.975 * \left(\frac{0.3198}{0.2857^2} \right)^2 = 63.4670 \text{ Pa} \end{aligned}$$

$$\begin{aligned} P_{f-total} &= \frac{P_{f-z1} * W_{air-z1} + P_{f-z2} * W_{air-z2} + P_{f-z3} * W_{air-z3}}{W_{air-z1} + W_{air-z2} + W_{air-z3}} \\ &= \frac{90.0721 * 24.7294 + 61.9144 * 254.8949 + 63.4670 * 0.3731}{90.0721 + 61.9144 + 63.4670} \\ &= 64.4034 \text{ Pa} \end{aligned}$$

Fan power calculation equations,

$$Fan Power_{z1} = \frac{ACMS_{z1} * P_{f-z1}}{\frac{\eta_{fan}}{\eta_{reducer}} / 1000} = \frac{20.9401 * 90.0721}{\frac{0.7}{0.92} / 1000} = 2.9288 W$$

$$Fan Power_{z2} = \frac{ACMS_{z2} * P_{f-z2}}{\frac{\eta_{fan}}{\eta_{reducer}} / 1000} = \frac{218.5670 * 61.9144}{\frac{0.7}{0.92} / 1000} = 21.0131 W$$

$$Fan Power_{z3} = \frac{ACMS_{z3} * P_{f-z3}}{\frac{\eta_{fan}}{\eta_{reducer}} / 1000} = \frac{0.3198 * 63.4670}{\frac{0.7}{0.92} / 1000} = 0.0315 W$$

$$Fan Power_{total} = Fan Power_{z1} + Fan Power_{z2} + Fan Power_{z3} \\ = 2.9288 + 21.0131 + 0.0315 = 23.9734 W$$

Pressure Drop in Tube:

$$D_{homogenous} = \left(\frac{x_{z2}}{\rho_2} + \frac{1 - x_{z2}}{\rho_3} \right)^{-1} = \left(\frac{0.5}{3.1856} + \frac{1 - 0.5}{607.7525} \right)^{-1} = 6.3379$$

Dynamic viscosity ratio calculation,

$$\mu_{ratio} = \frac{\mu_3}{\mu_2} = \frac{0.1575 \times 10^{-3}}{0.6946 \times 10^{-5}} = 22.6729$$

Calculation of the flow rate equation per tube,

$$m_{hot.pt} = \frac{m_{hot}}{N_t} = \frac{11.05}{1362} = 0.0081 \frac{kg}{s}$$

Flow rate of the liquid flowing in the tube calculation,

$$m_{liquid} = m_{hot.pt} * (1 - x_{z2}) = 0.0081 * (1 - 0.5) = 0.0041 \frac{kg}{s}$$

Calculation of gas flow rate,

$$m_{gas} = m_{hot.pt} * x_{z2} = 0.0081 * 0.5 = 0.0041 \frac{kg}{s}$$

The flow speed inside per tube calculation

$$v = m_{hot.pt} * \frac{4}{\pi * D_{in}^2} = 0.0081 * \frac{4}{3.14 * 22.1^2} = 21.1500 \frac{kg}{s * m^2}$$

Calculation of Reynolds number for liquid,

$$Re_{liquid} = \frac{v \cdot D_{in} \cdot (1 - x_{z2})}{\mu_3} = \frac{21.1500 \cdot 22.1 \cdot (1 - 0.5)}{0.1575 \times 10^{-3}} = 1.4840 \times 10^3$$

Calculation of Reynolds number for gas,

$$Re_{gas} = \frac{v \cdot D_{in} \cdot x_{z2}}{\mu_2} = \frac{21.1500 \cdot 22.1 \cdot 0.5}{0.6946 \times 10^{-5}} = 3.3647 \times 10^4$$

Calculation of Friction factor for the liquid flowing inside the tube,

$$f_{Liquid} = \frac{0.079}{Re_{liquid}^{0.25}} = \frac{0.079}{(1.4840 \times 10^3)^{0.25}} = 0.0127$$

Calculation of Friction factor for the gas flowing inside the tube

$$f_{Gas} = \frac{0.079}{Re_{gas}^{0.25}} = \frac{0.079}{(3.3647 \times 10^4)^{0.25}} = 0.0058$$

The calculation of total pressure loss of the liquid in the tube,

$$\Delta P_{liquid} = \frac{4 * f_{liquid} * L_{z-2} * \rho_3}{v^2 * D_{in}} = \frac{4 * 0.0127 * 5.5517 * 607.7525}{21.1500^2 * \left(\frac{22.1}{1000}\right)} = 4.7068 Pa$$

The dimensionless factors Fr_h , E, F and H calculations,

$$H = \left(\frac{\mu_2}{\mu_3}\right)^{0.19} * \left(\frac{\rho_3}{\rho_2}\right)^{0.91} * \left(1 - \frac{\mu_2}{\mu_3}\right)^{0.7}$$

$$= \left(\frac{0.6946 \times 10^{-5}}{0.1575 \times 10^{-3}}\right)^{0.19} * \left(\frac{607.7525}{3.1856}\right)^{0.91} * \left(1 - \frac{0.6946 \times 10^{-5}}{0.1575 \times 10^{-3}}\right)^{0.7} = 63.6841$$

$$E = (1 - x_{z2})^2 + x_{z2}^2 * \frac{\rho_3 * f_G}{\rho_2 * f_L} = (1 - 0.5)^2 + 0.5^2 * \frac{607.7525 * 0.0058}{3.1856 * 0.0127} = 22.1076$$

$$F = x_{z2}^{0.78} * (1 - x_{z2})^{0.224} = 0.5^{0.78} * (1 - 0.5)^{0.224} = 0.4986$$

$$Fr_h = \frac{v^2}{D_{homogenous}^2 * g * D_{in}} = \frac{21.1500^2}{6.3379^2 * 9.81 * \left(\frac{22.1}{1000}\right)} = 51.3648$$

The liquid Weber We_l is defined as:

$$We_L = \frac{v^2 * D_{in}}{\sigma * D_{homogenous}} = \frac{21.1500^2 * (\frac{22.1}{1000})}{0.014 * 6.3379} = 111.3675$$

The surface tension value is taken from the thermodynamic table according to the zone-1 temperature ($T_{zone-1} = 72,1051 \text{ }^\circ\text{C}$).

The multiplier equation between the two phases,

$$\Phi_{fr}^2 = E + \frac{3.24 * F * H}{We_L^{0.035} * Fr_H^{0.045}} = 22.1076 + \frac{3.24 * 0.4986 * 63.6841}{111.3675^{0.035} * (51.3648)^{0.045}} = 95.1753$$

Calculation of pressure loss,

$$\Delta P_{loss} = \frac{\Delta P_{liquid} * \Phi_{fr}^2}{10^5} = \frac{4.7068 * 95.1753}{10^5} = 0.0045 \text{ bar}$$

Since the values taken in the calculations are for a single loop, the result is not optimized. Results will be optimized by MATLAB program along with other loops and iterations.

5.1.4 Pump and Turbine Calculations

Input values given in the calculation of the pump part: variable frequency drive efficiency $\eta_{drive} = 0.95$, motor efficiency $\eta_{motor} = 0.95$, pump efficiency $\eta_{pump} = 0.80$, pump friction loss $P_{ploss} = 0.5 \text{ bar}$.

Pump head calculation,

$$H_{pump} = \frac{(P_{WF1} - P_{WF5}) * 100000}{9.8 \rho_{WF5}} + P_{ploss} = \frac{(2.62 - 1.09) * 100000}{607.74} + 0,5 = 26.18 \text{ m}$$

The density value given in this calculation is taken from the thermodynamic table according to the temperature ($T_{coldinlet} = 38^{\circ}C$) and pressure ($P_{cold} = 1.09 \text{ bar}$) obtained as a result of iterations.

Calculation of unit power pump,

$$P_{unitpower} = m_{WF5} * H_{pump} * \rho_{WF5} * \frac{9.8}{3.6 * 10^6} = \frac{65.47 * 26.18 * 607.74 * 9.8}{3.6 * 10^6 * 0.8} = 3.545 \text{ kW}$$

The specific heat value shown in the calculation is taken from the thermodynamic table according to the inlet temperature ($T_{coldinlet} = 38^{\circ}C$) and pressure ($P_{cold} = 1.09 \text{ bar}$) obtained because of iterations.

Calculation of pump consumption,

$$P_{consumption} = \frac{P_{unitpower}}{\eta_{motor} * \eta_{drive}} = \frac{3.545}{0.95 * 0.95} = 3.917 \text{ kW}$$

Pump temperature difference calculation,

$$\begin{aligned} \Delta T_{pump} &= P_{unitpower} * \frac{1 - \eta_{pump}}{\frac{c_{pWF5}}{1000} * \frac{m_{WF5}}{3600} * \rho_{WF5}} = 3.545 * \frac{1 - 0.8}{\frac{2.3777 * 10^3}{1000} * \frac{65.47}{3600} * 607.74} \\ &= 0.026 \text{ }^{\circ}C \end{aligned}$$

Turbine Calculations:

Calculation of gross power,

The enthalpy values given in the calculation are taken from the thermodynamic tables according to the pressure ($P_{WF3} = 2.3 \text{ bar}$; $P_{WF4} = 1.09 \text{ bar}$;) and temperature ($T_{WF3} = 63.39^\circ\text{C}$; $T_{WF4} = 48.15^\circ\text{C}$) obtained as a result of the iterations.

$$P_{grosspower} = m_{WF} * (h_{WF3} - h_{WF4}) * 0.99 = \frac{39.791}{3.6} * (401.17 - 378.75) * 0.99$$

$$= 245.370 \text{ kW}$$

Gross efficiency calculation,

$$\eta_{gross} = \frac{P_{grosspower}}{P_{evaporator} + P_{preheater}} = \frac{245.370}{3779.584 + 601.511} = 0.0560$$

Net power calculation,

$$P_{netpower} = P_{grosspower} - P_{ACC} - P_{pump} = 245.370 - 52.096 - 3.917 = 189.358 \text{ kW}$$

Calculation of net efficiency,

$$\eta_{net} = \frac{P_{netpower}}{P_{evaporator} + P_{preheater}} = \frac{189.358}{3779.584 + 601.511} = 0.0432$$

5.2 ORC Designer with MATLAB Program

The prepared MATLAB ORC Designer program main screens are presented in Figure-5.1. ORC Designer program is developed to make detailed ORC design, geometrical calculations of heat exchangers and performance calculations of different working fluids at different conditions. Evaporator, preheater, ACC, pump, turbine input etc. screens are presents at Figure 5.2-5.8.

This report presents a model to evaluate the performance of an Organic Rankine cycle (ORC) at low temperature geothermal resources such as 150 tons/hour flow rate at 90 °C temperature. The system was evaluated nine dry organic working fluids, R218, R134a, R245fa, R236fa, R123, iso-pentane, n-pentane, iso-butane, and n-butane.

After run program, 4 files, which are detailed power generation and efficiency results and ACC, evaporator, preheater data sheets, create in desktop for selected working fluid as notepad (see Appendix).

The data sheet files of air-cooled condenser, preheaters and evaporator include all manufacturing and heat transfer details for production.

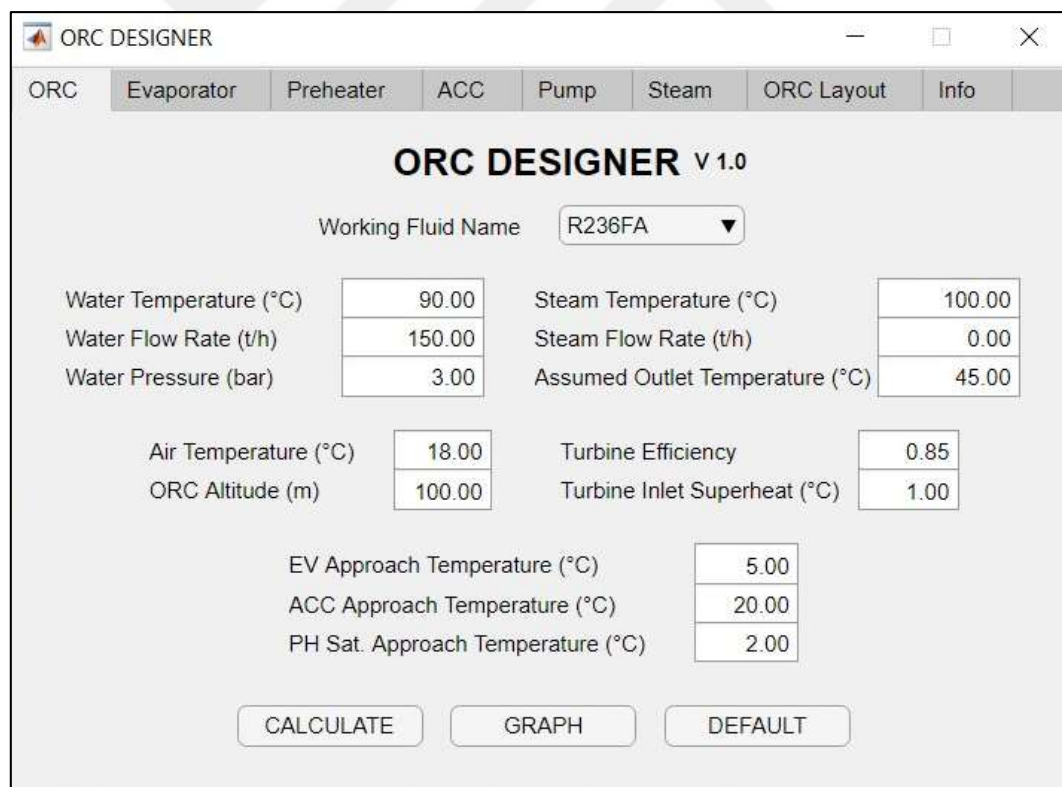


Figure 18 ORC Designer Program

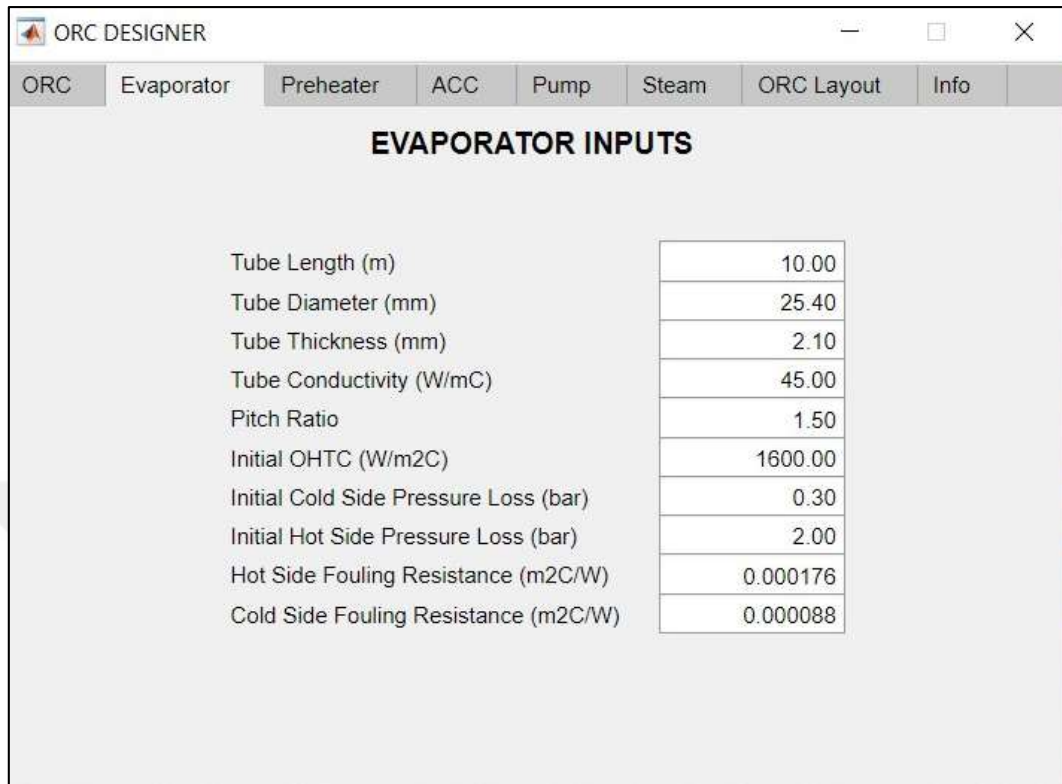


Figure 19 ORC Designer Program Evaporator Screen

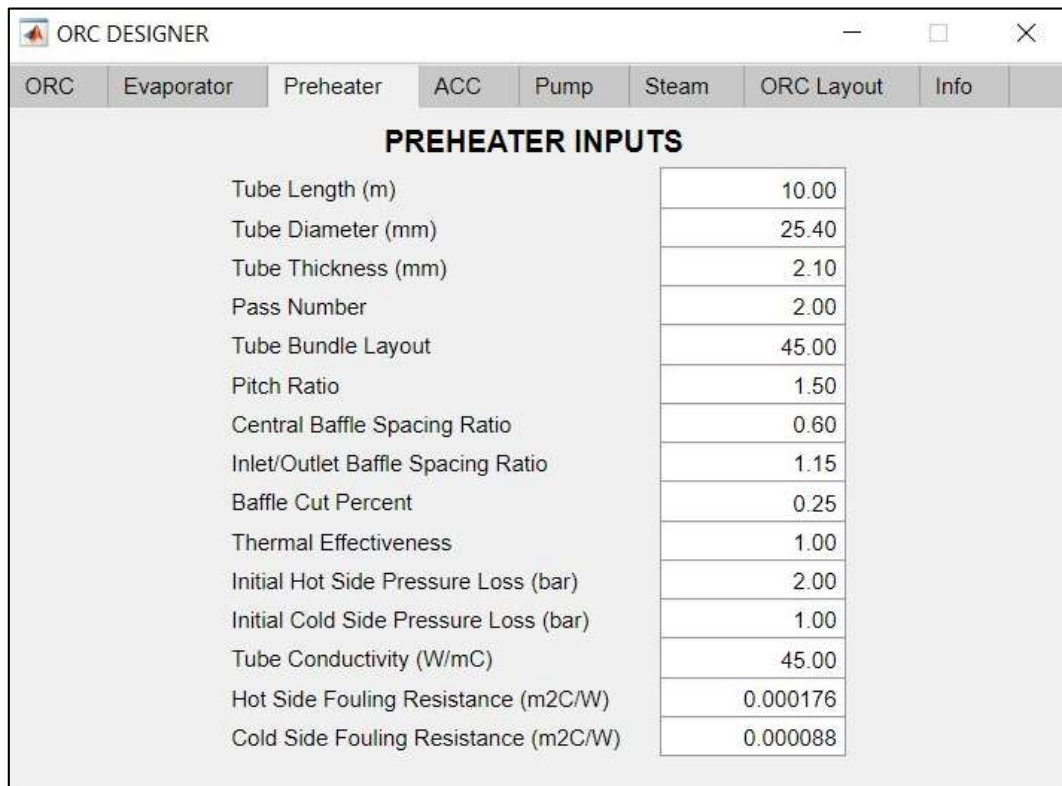


Figure 20 ORC Designer Program Preheater Screen

ORC DESIGNER

ORC | Evaporator | Preheater | ACC | Pump | Steam | ORC Layout | Info

AIR COOLED CONDENSER INPUTS

ACC Width (m)	20.00
Tube Row Number	4.00
Tube Diameter	25.40
Tube Thickness (mm)	1.65
Tube Pitch (mm)	58.74
Fin Height (mm)	15.90
Fin Thickness (mm)	0.40
Fin Per Meter	413.40
Fan Area Ratio	0.40
Fan Efficiency	0.70
Reducer Efficiency	0.92
Tube Conductivity (W/mC)	45.00
Outside Fouling Resistance (m2C/W)	0.000352
Inside Fouling Resistance (m2C/W)	0.000210

Figure 21 ORC Designer Program ACC Screen

ORC DESIGNER

ORC | Evaporator | Preheater | ACC | Pump | Steam | ORC Layout | Info

PUMP INPUTS

Variable Frequency Drive Efficiency	0.95
Motor Efficiency	0.95
Pump Efficiency	0.80
Pump Friction Loss (bar)	0.50

Figure 22 ORC Designer Program Pump Screen

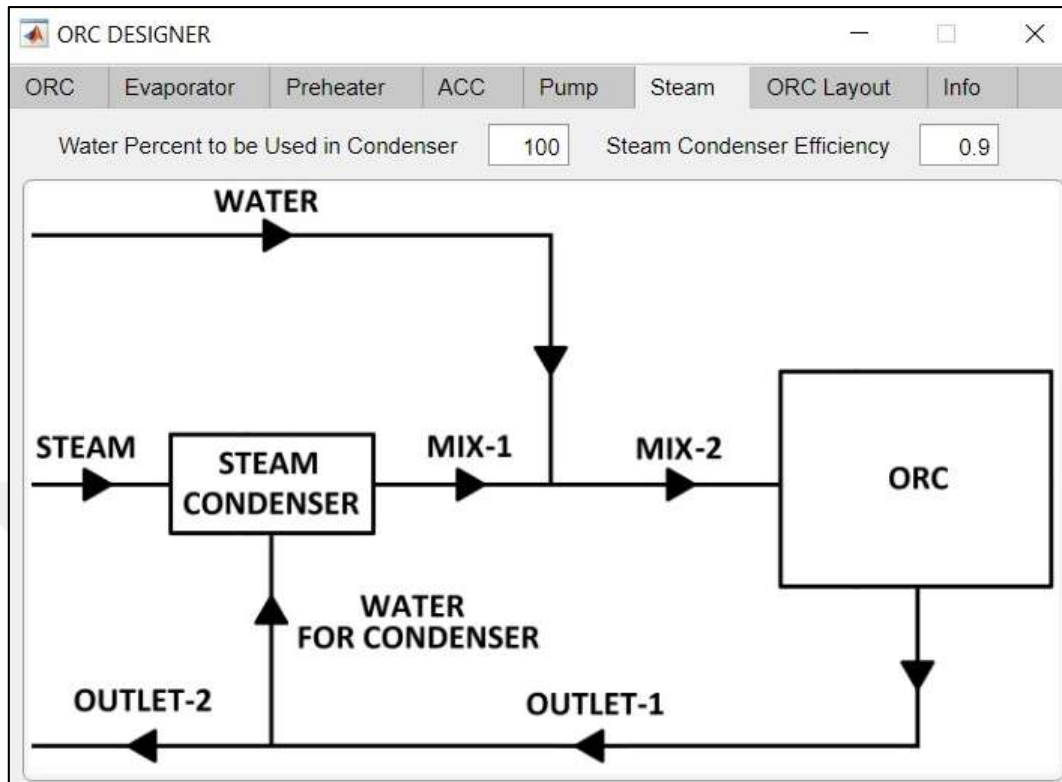


Figure 23 ORC Designer Program Steam Side Screen

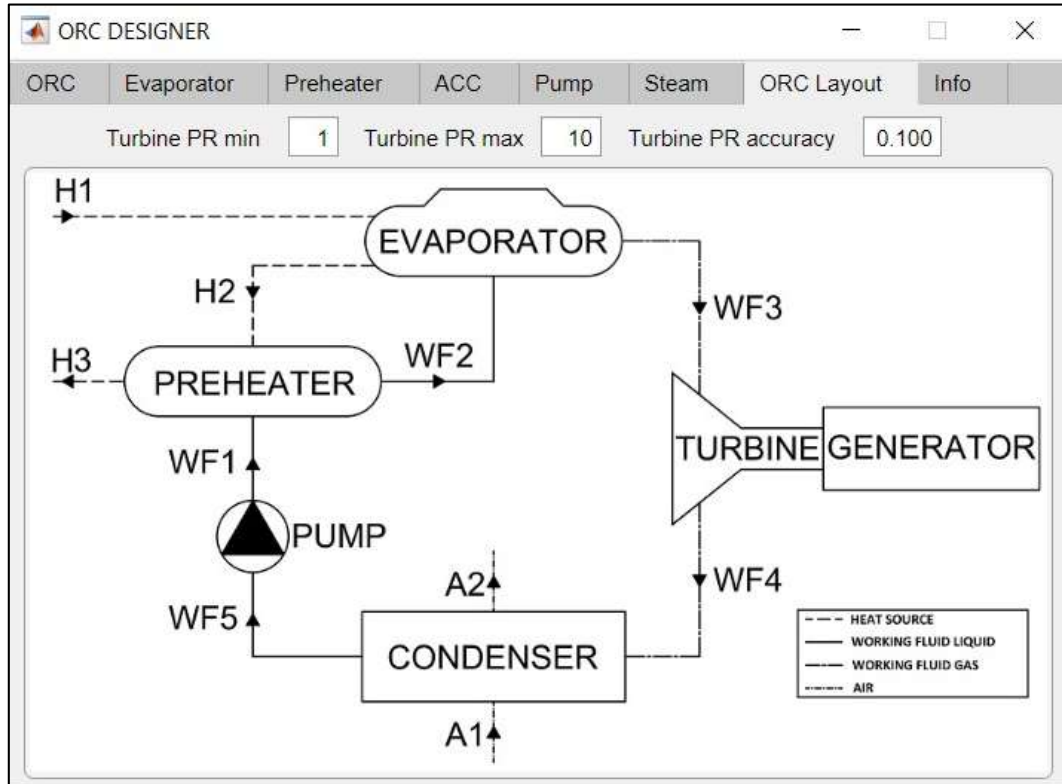


Figure 24 ORC Designer Matlab Program Layout Screen

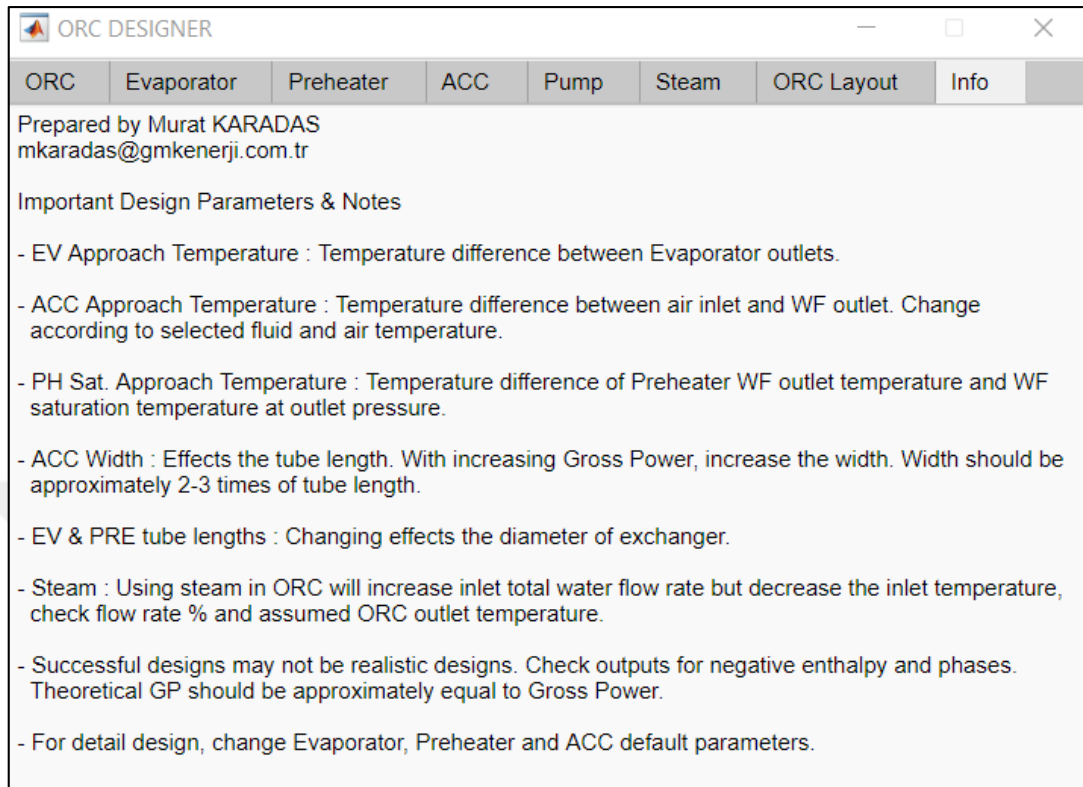


Figure 25 ORC Designer MATLAB Program Info Screen

6. RESULTS

This thesis first focuses on general ORC design to decide ORC type. The first mission is to prepare an algorithm to choose and calculate process cycle stages in the designed Organic Rankine Cycle. For this part of the thesis, R245FA is selected as a preliminary working fluid to prepare the method and algorithm for process design, which will be used throughout thesis. Various working fluids will be tried after the application of R245FA to choose best one for the given case conditions. The low enthalpy geothermal resource and the cooling resource used in the design are 95 °C geothermal brine at 3 bar and 150 tons/hour flow rate at 20 °C ambient air temperature.

MATLAB is used to create algorithm for the Organic Rankine Cycle process design as main calculation software. Process is designed for two different cases, which are with recuperator and without recuperator.

To obtain properties of fluids at every cycle and point, Coolprop addon is installed to MATLAB, as a separate function which works as follows:

```
CoolProp.PropsSI('H','T',B1.T+273.15,'P',B1.P*100000,fluid1)
```

Inputs of the Coolprop function is 'B1.T' which is the temperature in Celsius (added 273.15 to convert it to Kelvin), 'B1.P' which is pressure in bara (multiplied by 100000 to convert it to Pa) and fluid1 is the name of the fluid which for our case 'WATER' or 'R245FA'. Output is 'H' which is the enthalpy of the selected fluid.

Algorithm:

Details of parts of the MATLAB code is specified as follows:

Preliminary Inputs: These are brine values at the inlet and outlet of the system, which are temperature, pressure, flow rate. System is designed according to these values. Outlet parameters are inputs at this stage of thesis but later they will be calculated according to the heat exchangers.

Initial Assumptions:

These are assumed values that can change throughout the study depending on the design and optimization.

- **Efficiencies of Turbine and Heat Exchangers:** These parameters are selected as an average 80% for turbine and 90% for heat exchangers from similar size and capacity of Organic Rankine Cycles.
- **Pressure Drops in Cycle:** These parameters are selected from literature with similar sizes. It is assumed 0.5 bar for each heat exchanger at brine side while it is 0.5 bar for preheater and 0.1 bar for evaporator at working fluid side.
- **Approach Temperature:** This value is assumed 5 °C for this part of the study.
- **Condenser Output Temperature:** Because at this stage of the study we do not know much about the air-cooled condenser specifications, *Condenser Output Temperature* is selected such that with the given air temperature working fluid can be condensed (with the turbine output pressure).
- **Turbine Pressure Ratio:** This value is assumed increasingly up to a value for every calculation loop.
- **Evaporator Brine Outlet Temperature:** This value is assumed between maximum and minimum brine temperature for every calculation loop.
- **Working Fluid Flow Rate:** This value is assumed increasingly up to a value for every calculation loop.

Code continues with calculation and output loops.

Iteration & Calculation:

Firstly, heat exchanger duties are calculated with the assumed evaporator brine outlet temperature.

Calculation at this point can be split into two parts. First one is starting from turbine inlet and goes in reverse direction to cycle to pump outlet. Second part starts with turbine inlet and goes with the cycle direction to the inlet of the pump.

In first part, evaporator working fluid outlet temperature is calculated with the assumed approach temperature and assumed evaporator loop brine outlet temperature. Pressure of the evaporator working fluid outlet is set such that it is superheated for a set temperature (0.2°C). Then evaporator working fluid inlet temperature calculated according to heat transfer across evaporator. Then preheater working fluid inlet temperature calculated according to heat transfer across preheater. Pressures at each point calculated with the pre-assumed exchanger pressure losses.

In second part, turbine outlet parameters are calculated with the pre-assumed turbine efficiency, assumed turbine loop pressure ratio and calculated evaporator outlet parameters. Condenser outlet pressure is calculated with the assumed exchanger pressure loss. With the calculated pressure, condenser outlet temperature is calculated assuming working fluid at the outlet of condenser is at 0.5°C subcooled state. Pump outlet parameters are calculated which temperature is same with the condenser outlet, but pressure is calculated according to the pressure losses and evaporator outlet pressure.

Calculation of the cycle with the recuperator involves one more step. Working fluid at the outlet of pump cools the working fluid at the turbine outlet. With recuperator cold side inlet and outlet is known and hot side inlet known, hot side outlet is calculated.

Finally, for each iteration, power generation and gross efficiency is calculated.

All calculated data at every loop is stored in the database for further analysis. Such as;

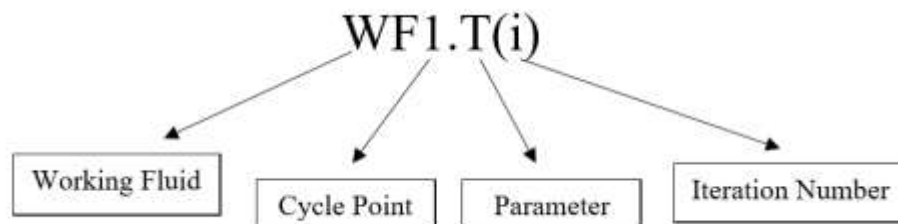


Figure 26 Iteration System

Parameters are flow rate, temperature, pressure, density, enthalpy, entropy, and phase.

Iterations of the turbine pressure ratio, evaporator brine outlet temperature and working fluid flow rates are done with a predetermined step value. This step value is chosen as minimum as zero point one (0.1) because of calculation times. Smaller step values will be chosen after algorithm is optimized further. Smaller step values will help the algorithm to come up with better gross efficiencies. But for this stage of the study zero point one (0.1) is considered sufficient.

Final Analysis (If Loop):

In this part, algorithm tries to find the iterations which satisfy following statements:

- Preheater inlet must be in liquid phase,
- Evaporator inlet must be in liquid phase,
- Turbine inlet must be in gas phase,
- Turbine outlet must be in gas phase,
- Condenser outlet must be in liquid phase,
- If system is with recuperator, hot side must be in gas phase, cold side must be in liquid phase,
- Condenser output temperature must be greater than pre-assumed condenser outlet temperature,
- If system is with recuperator, heat exchange in the recuperator must be greater than zero.

Loop firstly looks for the iteration steps for the above desired conditions. Then it looks for the highest gross efficiency from these iteration steps.

Outputs:

Code outputs an excel table at the end of run with the name of the working fluid and power generated. This excel table (as can be seen below) contains parameters of the working fluid at every point of cycle.

MATLAB flow chart is presented at Figure 6.2. ORC flow diagrams with and without recuperator is illustrated at Figure 6.3-6.4.

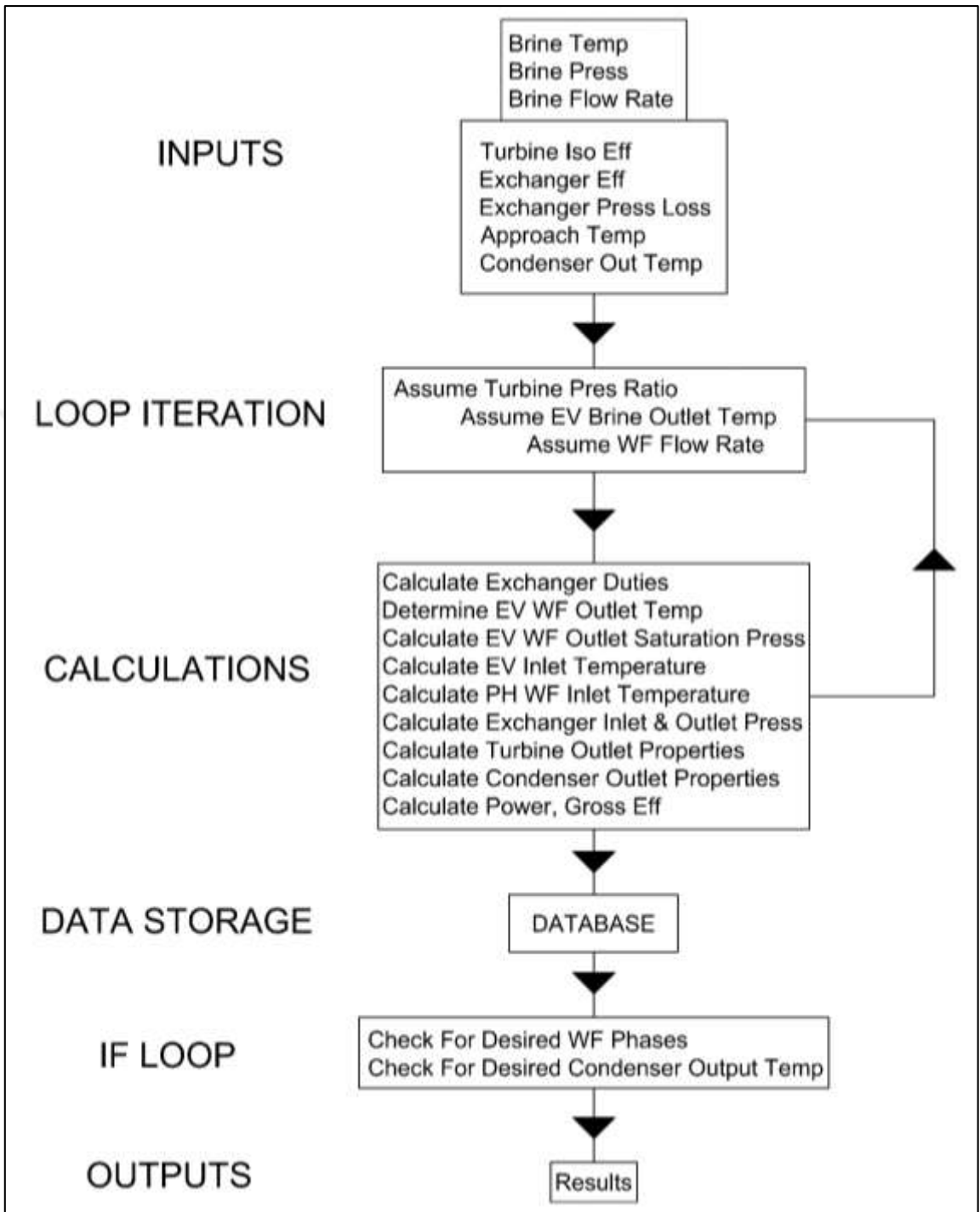


Figure 27 MATLAB flow chart for calculation of ORC

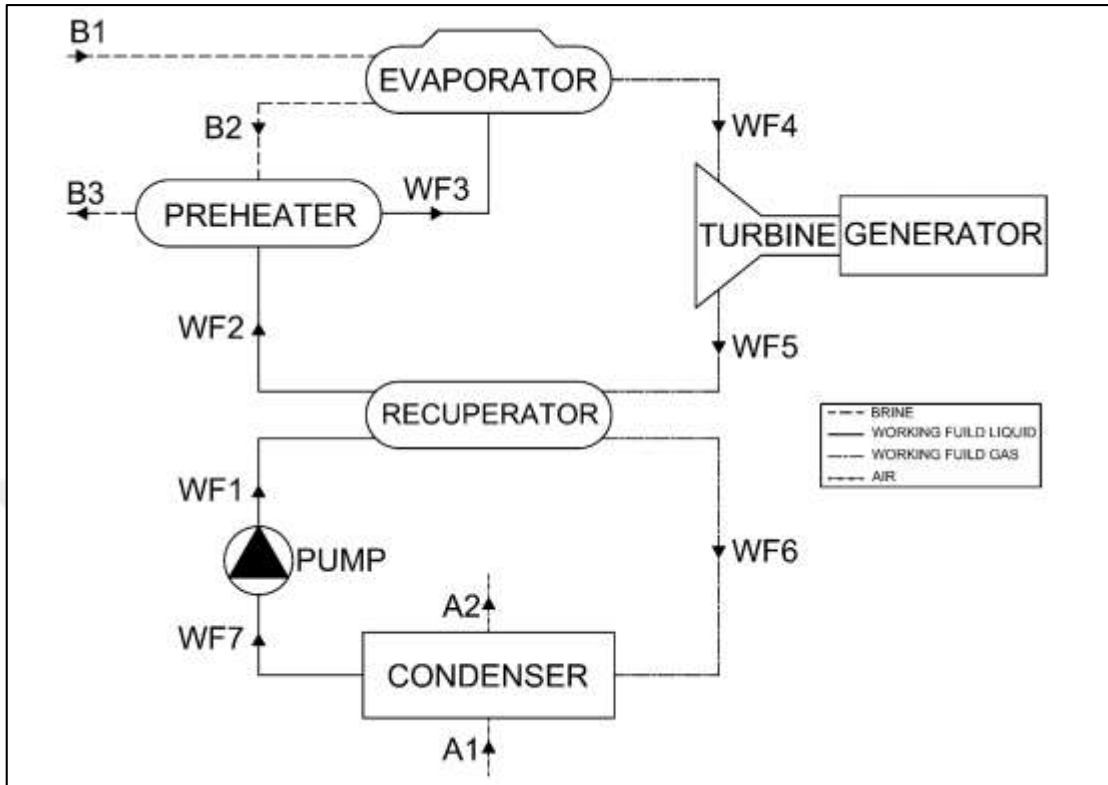


Figure 28 ORC with Recuperator

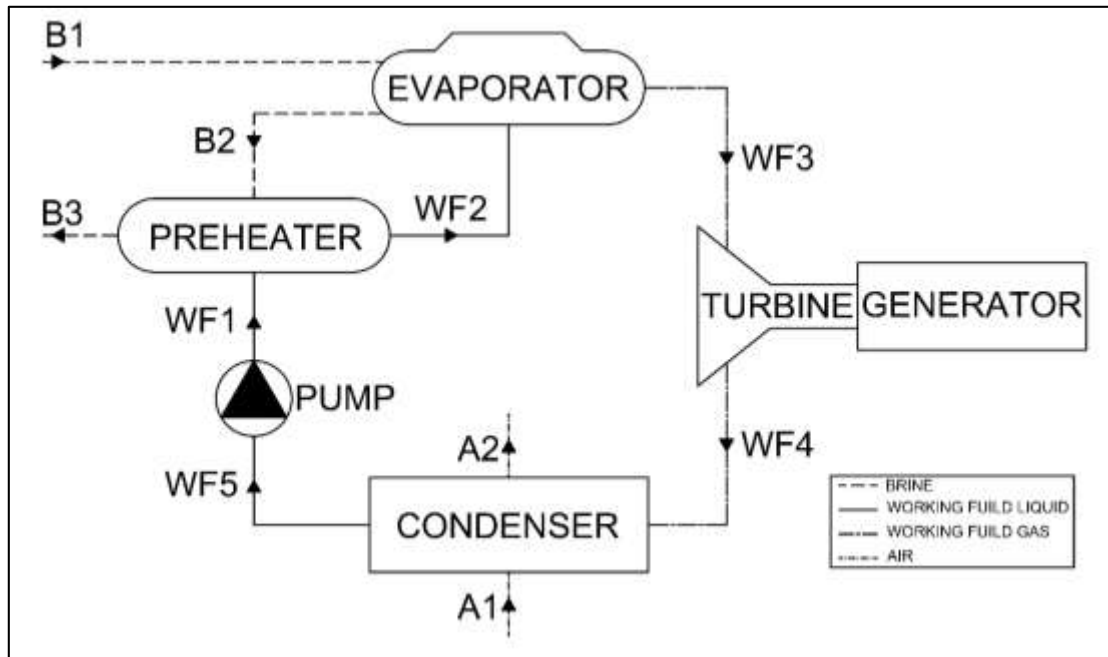


Figure 29 ORC without Recuperator

MATLAB GUI:

MATLAB GUI is created to ease the calculation steps and visualization of outputs. Most important parameters of the cycle are shown on the cycle flow diagram. Main inputs and outputs are shown on the panel at Figure 6.5.

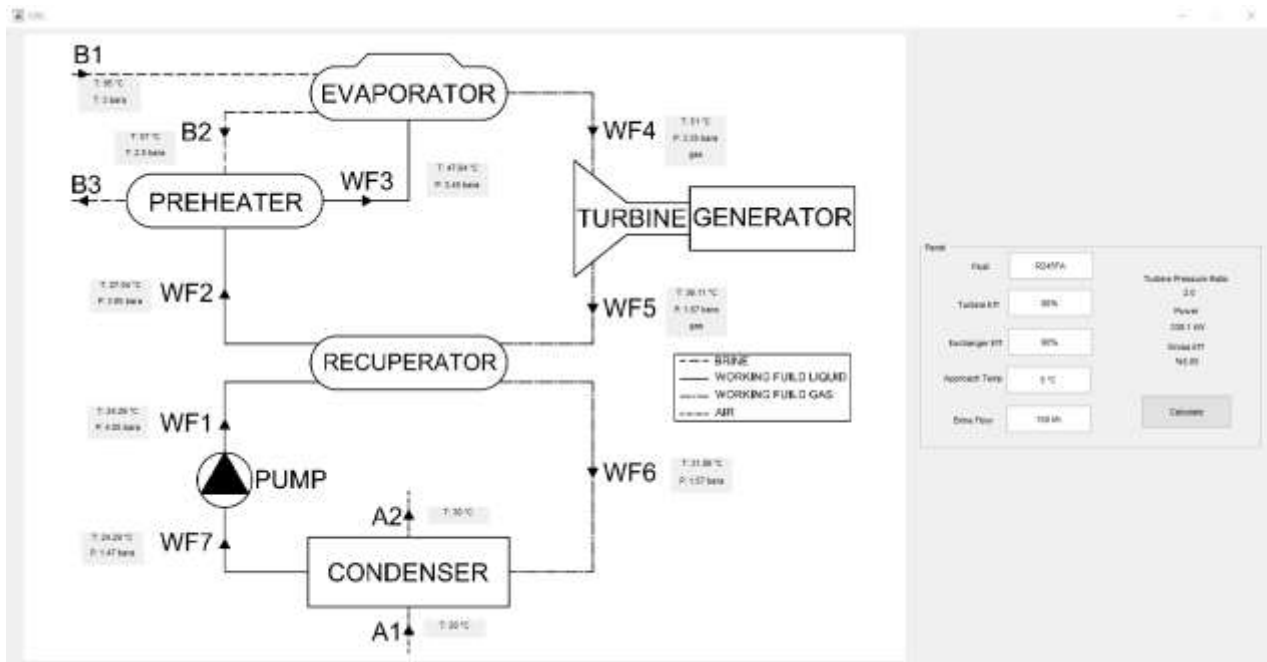


Figure 30 ORC Panel with inputs and outputs

Preliminary Results to Decide ORC Type

Results of the MATLAB calculations for both with recuperator are shown at Table 6.1. According to these calculations 338.1 kW gross power can be generated by R245FA at ORC with recuperator and thermal efficiency of the plant can found as 5.05%. The total pressure losses in condenser, recuperator, evaporator and preheater are calculated 0.9 bar.

Results of the MATLAB calculations for both without recuperator are shown at Table 6.2. According to these calculations 358 kW gross power can be generated by R245FA at ORC without recuperator and thermal efficiency of the plant can found as 5.35%. The total pressure losses in condenser, recuperator, evaporator and preheater are calculated 0.7 bar.

Table 6.1 ORC with recuperator

Gross Power: 338.1 kW		Gross Efficiency: 5.05%		Total Pressure Loss in HX: 0.9 bar			
Points	Flow Rate m³/h	Temperature °C	Pressure bar	Density kg/m³	Enthalpy kJ/kg	Entropy kJ/kgK	Phase
WF1	91.26	24.29	4.05	1341.20	232.12	1.11	liquid
WF2	91.78	27.04	3.95	1333.67	235.75	1.12	liquid
WF3	96.03	47.64	3.45	1274.62	263.49	1.21	liquid
WF4	6657.98	51.00	3.35	18.38	443.90	1.77	gas
WF5	13268.24	36.11	1.67	9.22	433.85	1.78	gas
WF6	13925.38	31.89	1.57	8.79	430.23	1.77	gas
WF7	91.32	24.29	1.47	1340.40	232.05	1.11	liquid

Table 6.2 ORC without recuperator

Gross Power: 358 kW		Gross Efficiency: 5.35%		Total Pressure Loss in HX: 0.7 bar			
Points	Flow Rate m³/h	Temperature °C	Pressure bar	Density kg/m³	Enthalpy kJ/kg	Entropy kJ/kgK	Phase
WF1	90.48	25.87	4.09	1336.91	234.21	1.12	liquid
WF2	95.69	51.15	3.59	1264.05	268.35	1.23	liquid
WF3	6317.29	52.30	3.49	19.15	444.84	1.77	gas
WF4	13223.47	36.32	1.66	9.15	434.07	1.78	gas
WF5	90.53	25.87	1.56	1336.12	234.13	1.12	liquid

The same calculations are repeated for R218, R134a, R245fa, R236fa, R123, iso-pentane, n-pentane, iso-butane, n-butane and then the gross energy production of ORC system without recuperator calculated higher than recuperator system. It is observed that for case temperatures, energy gain from the recuperator (by gaining temperature) is less than energy loss (by pressure losses) for cold and hot streams. It is noted that evaporator outlet point properties are the most crucial for the efficiency of the cycle. Preliminary chosen 5 °C approach temperature may change according to the evaporator design study. Another important point in terms of efficiency of the cycle is condenser outlet temperature. This value is assumed min 4 °C greater than the average air temperature. But air-cooled condenser design may change it in positive or negative way. Also, cycle must be studied for temperatures throughout a year. Cycle may work in winter, but it may not in summer.

After that, the detailed design studies for heat exchangers by using MATLAB program is performed. The flow chart of evaporator and preheater is shown at Figure 6.6 while flow chart for ACC is presented at Figure 6.7.

In this part, preheater and evaporator geometrical dimensions are evaluated for different type of working fluids. A MATLAB algorithm of each designed equipment will be implemented for all ORC for different working conditions. ORC Designer program is developed to make optimization for performance and geometrical conditions of the equipment's.

A model to evaluate the performance of an Organic Rankine cycle (ORC) at low temperature geothermal resources such as 150 tons/hour flow rate at 90 °C temperature. The system was evaluated nine dry organic working fluids, R218, R134a, R245fa, R236fa, R123, iso-pentane, n-pentane, iso-butane, and n-butane.

The important part of ORC Designer program is possibility to change all assumptions. The main inputs of the ORC Designer MATLAB Program are presented below:

- Evaporator approach temperature which is temperature difference between evaporator outlets for hot fluid and cold fluid is assumed 5 °C.
- Air cooled condenser approach temperature which is temperature difference between air inlet and working fluid outlet is assume 20 °C. It changes according to selected fluid and air temperature.
- Preheater saturation approach temperature which is temperature difference of Preheater working fluid side outlet temperature and working fluid saturation temperature at outlet pressure. The aim of this temperature difference is to prevent boiling in the preheater.
- Air cooled condenser (ACC) width is affects the tube length with increasing Gross Power and causes to increase the width. ACC width should be approximately 2-3 times of tube length.
- Evaporator and Preheater tube lengths which effect the diameter of exchanger.
- Amount of steam: Using steam in ORC will increase inlet total water flow rate but decrease the inlet temperature, check flow rate % and assumed ORC outlet temperature.
- Successful designs may not be realistic designs. Check outputs for negative enthalpy and phases. Theoretical GP should be approximately equal to Gross Power.
- For detail design, change Evaporator, Preheater and ACC default parameters.

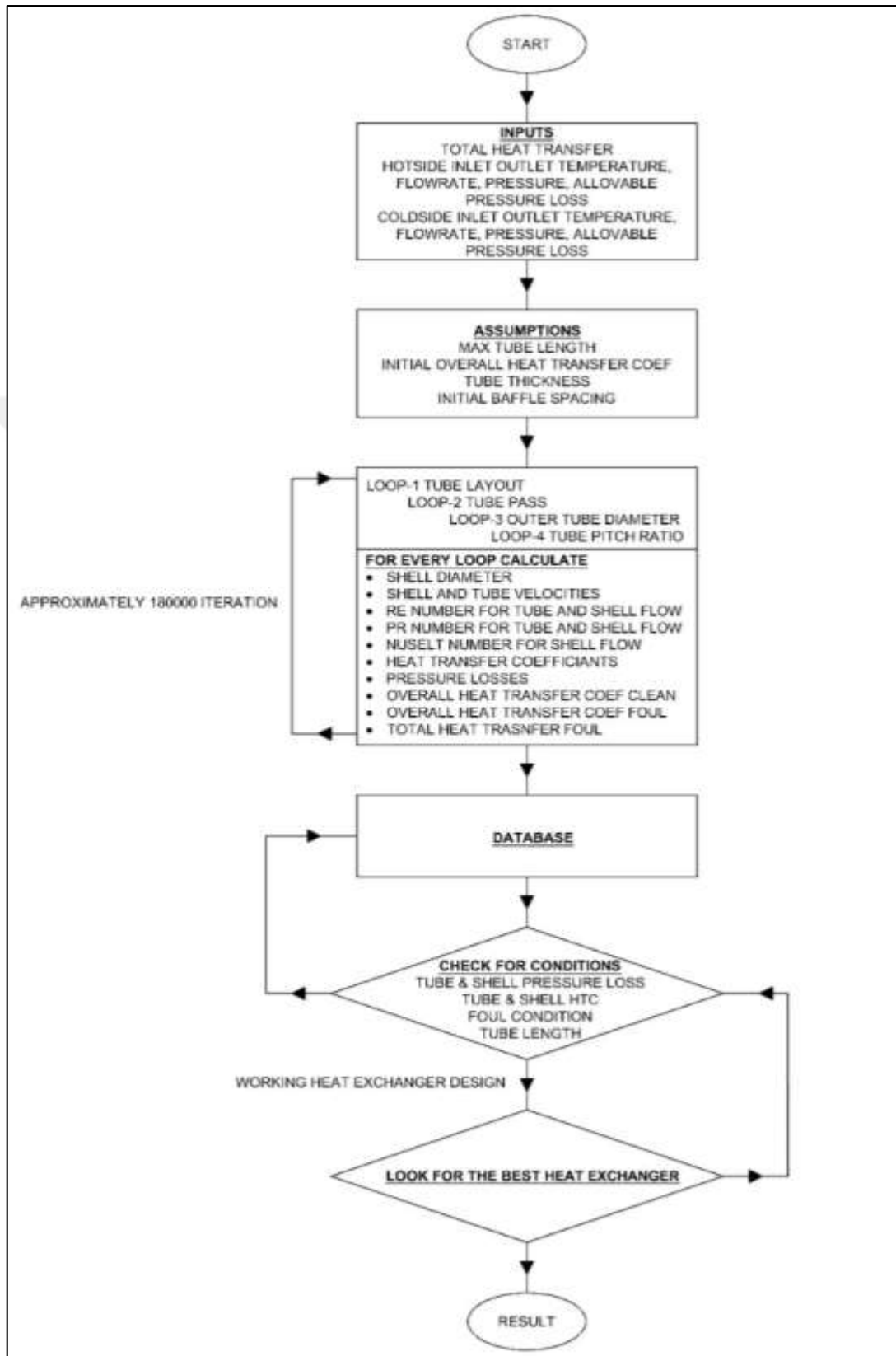


Figure 31 MATLAB flow chart for calculation of Preheater and Evaporator

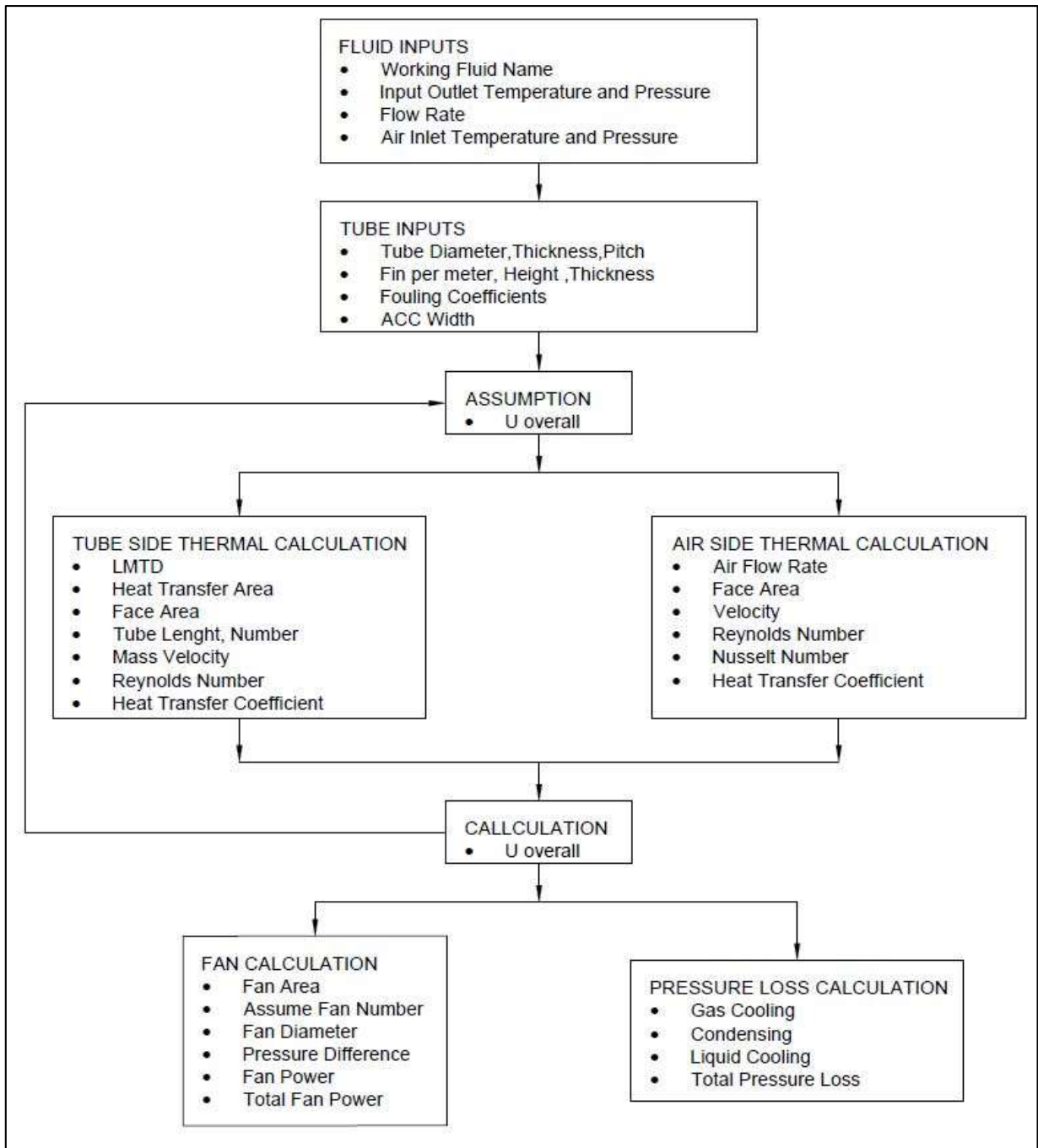


Figure 32 MATLAB flow chart of calculation for ACC

ORC Designer MATLAB algorithm is developed and after 180.000 iteration, main properties of heat exchangers which are shell diameters, tube diameters, number of tubes, tube count and layouts, hex length, shell side and tube side heat transfer coefficients, overall fouling heat transfer coefficient, pressure losses are determined.

The same algorithm was tried for the different heat exchanger design approaches and these approaches were compared with each other. Finally, the design approach method with the safest results was accepted during heat exchanger design. Preheater and evaporator geometrical dimensions are evaluated. Boiling in the evaporator was investigated.

According to these calculations, the comparison of all working fluids is presented Table-6.3. In this table, the turbine efficiency (TurbineEff) which is accepted as 85% means isentropic efficiency of turbine while heat exchanger efficiency (ExchangerEff) is defined as the ratio of the amount of heat transferred in the actual case to the amount of heat in the ideal (theoretical) case. Since the highest efficiency heat exchanger design has been studied in this thesis, the efficiency was assumed as 100% and the heat exchanger designs were performed. The gross power (kW) which is defined as the total electrical output of turbine while the net power (kW) is net electrical output after internal consumption of auxiliary equipment such as pump, air cooled condenser.

Theoretical GP (kW) is calculated gross power before detailed design and Pressure Ratio means working fluid's pressure ratio between turbine inlet and outlet. WF FlowRate(t/h) and B FlowRate(t/h) are the mass flow rates of working fluid and geothermal brine, respectively. GrossEff.(Gross Efficiency) and NetEff.(Net Efficiency) are calculated the ratio of gross and net power to the total heat transfer of the geothermal brine. H_Evaporator(kW) and H_Preheater(kW) are the total heat transfer between geothermal fluid and working fluid at each shell and tube heat exchangers while H_Condenser(kW) is the total heat transfer between air and working fluid at air cooled condenser.

Working fluid shall enter the turbine 1 °C superheat for proper functioning of the turbine. ACC Cons(kW) means electricity consumption of air-cooled condenser fans while ACC Length(m), and ACC Width is the length and width of air-cooled condenser. ACC Area(m²) can be calculated by multiplying of ACC Length and ACC Width. The number of tube rows means that how many rows of tubes passing through the condenser are on top of each other.

All these properties are calculated for 9 different working fluids consisting of isopentane, n-butane, n-pentane, iso-butane, R123, R245FA, R236 FA, R134A, and R218. The geothermal fluid conditions at ORC inlet are kept the same on all calculations as 90 °C temperature, 150 tons/hour flow rate, 3 bar pressure and it has been assumed that there is no steam. Annual average air temperature is selected 18 °C and altitude is defined as 100 m. The turbine efficiency is assumed as 85% and turbine inlet temperature is planned as 1 °C.

Figure 6.8 shows the comparison of gross and net efficiencies of each working fluid. The ranking of each working fluids from highest to lowest for gross power efficiency are R128, iso-butane, R123, R245FA, iso-pentane, n-butane, R236FA, n-pentane and R134A with 6.93%, 6.11%, 6.01%, 5.98%, 5.84%, 5.78%, 5.74%, 5.60%, 5.10% gross efficiencies while the ranking of each working fluids from highest to lowest for net power efficiency are R123, iso-pentane, R245FA, n-pentane, iso-butane, n-butane, R236FA, R218, R134A with 4.48%, 4.42%, 4.38%, 4.32%, 4.22%, 4.13%, 3.96%, 3.46%, 3.15% net efficiencies, respectively.

Figure 6.9 is illustrated the comparison of gross and net power generation of each working fluid. The ranking of each working fluids from highest to lowest gross power generation are R128, R134A, R236FA, iso-butane, n-butane, iso-pentane, n-butane, n-pentane and R123 with 394kWe, 268kWe, 261kWe, 257 kWe, 254 kWe, 245 kWe, 245 kWe and 243 kWe gross power generation while the ranking of each working fluids from highest to lowest net power generation are R218, n-pentane, iso-pentane, R245FA, R123, n-butane, R236FA, iso-butane, R134A with net power generation of 197kWe, 189 kWe, 186kWe, 182 kWe, 181 kWe, 180 kWe, 177 kWe and 166 kWe, respectively.

Table 6.3 ORC Designer MATLAB Program Results under the same conditions

COMPARISON OF THE DIFFERENT WORKING FLUIDS AT THE SAME CONDITIONS									
Fluid:	ISOPENTANE	NBUTANE	NPENTANE	ISOBUTANE	R123	R245FA	R236FA	R134A	R218
TurbineEff:	0,85	0,85	0,85	0,85	0,85	0,85	0,85	0,85	0,85
ExchangerEff:	1	1	1	1	1	1	1	1	1
Gross Power(kW):	245	254	245	257	243	249	261	268	394
Net Power(kW):	186	181	189	177	181	182	180	166	197
Theoretical GP (kW):	245	252	246	254	243	249	260	269	442
Press,R:	2.100	1.900	2.100	1.900	2.200	2.200	2.000	1.700	2.100
WF FlowRate(t/h):	40.177	41.175	39.791	43.279	80.022	73.676	106.326	108.663	276.774
B FlowRate(t/h):	150.000	150.000	150.000	150.000	150.000	150.000	150.000	150.000	150.000
GrossEff:	5,84%	5,78%	5,60%	6,11%	6,01%	5,98%	5,74%	5,10%	6,93%
NetEff:	4,42%	4,13%	4,32%	4,22%	4,48%	4,38%	3,96%	3,15%	3,46%
H_Evaporator(kW):	3.571.551	3.718.787	3.779.584	3.439.290	3.481.972	3.480.667	3.666.550	4.383.106	2.390.592
H_Preheater(kW):	633.204	672.239	601.511	761.534	562.326	680.648	881.971	874.966	3.298.069
H_Condenser(kW):	3.959.478	4.138.951	4.135.464	3.946.731	3.800.999	3.912.768	4.288.767	4.988.909	5.246.642
Superheat(°C):	1.000	1.000	1.000	1.000	1.000	1.000	1.000	1.000	1.000
Pump Cons,(kW):	4.952	10.188	3.917	15.267	4.643	7.019	14.108	25.892	119.049
ACC Cons,(kW):	54.559	62.374	52.096	64.332	57.396	59.855	66.883	76.787	78.320
ACC Length(m):	8.334	9.168	8.058	9.584	8.592	8.836	9.814	10.716	10.914
ACC Width(m):	20.000	20.000	20.000	20.000	20.000	20.000	20.000	20.000	20.000
ACC Area(m2):	166.679	183.356	161.164	191.684	171.839	176.716	196.276	214.312	218.288
Number of Tube Rows:	4.000	4.000	4.000	4.000	4.000	4.000	4.000	4.000	4.000

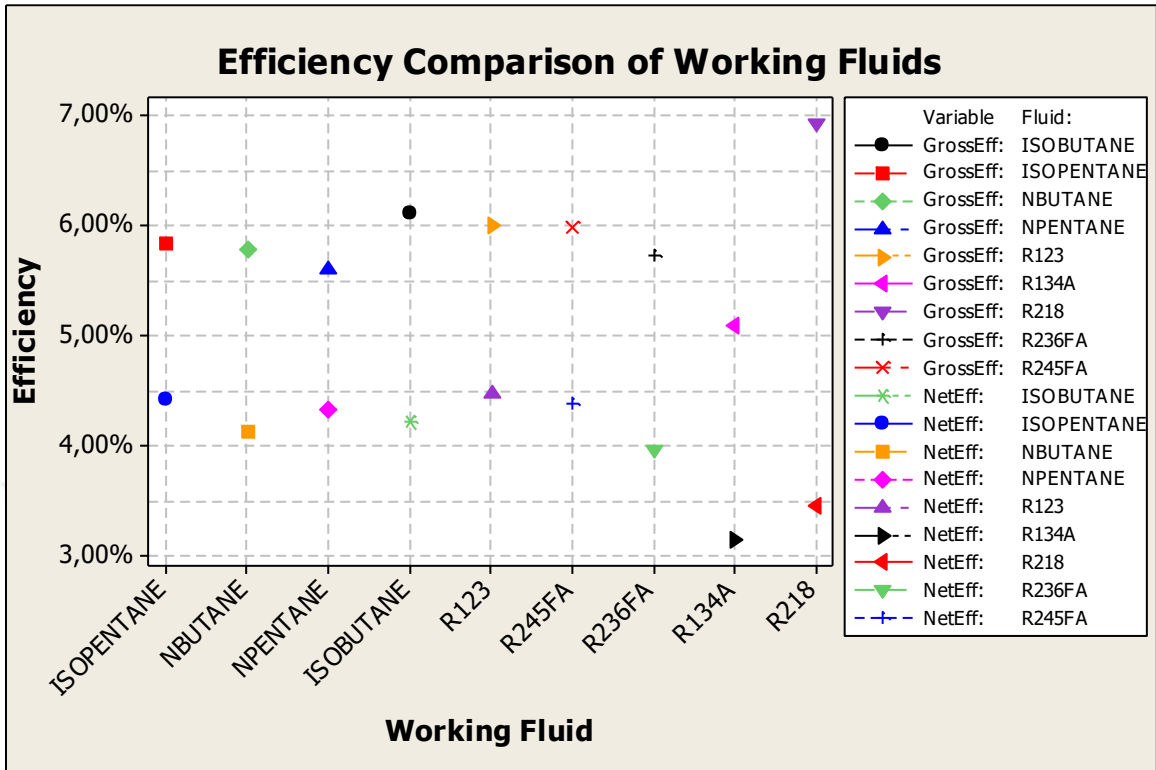


Figure 33 Comparison of efficiencies of the different working fluids

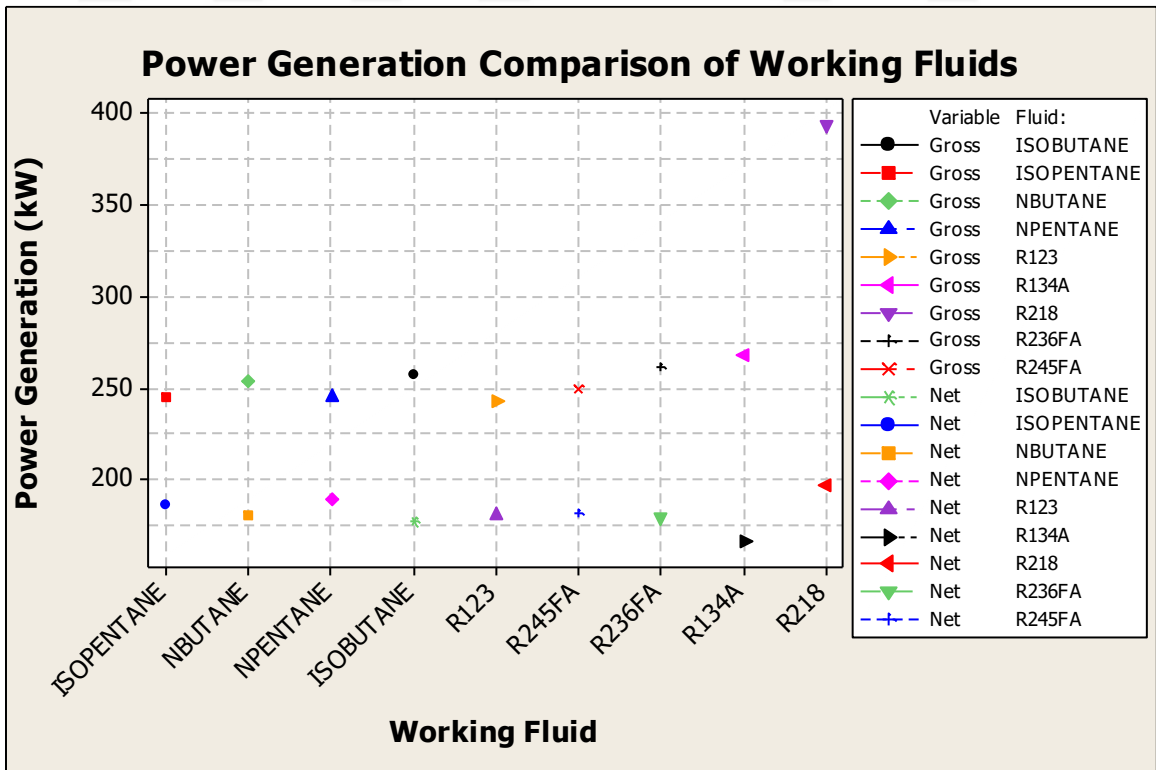


Figure 34 Comparison of power productions of the different working fluids

While the gross and net power production was maximum with 394 kW and 196 kW in case of R218, the working fluid flow rate was also maximum with the same fluid. Therefore, ORC with R218 working fluid has the highest the internal consumption of pump and ACC as 197 kW approximately. On the other hand, the net efficiency for the same fluid was the lowest one with 3.46%. The maximum net efficiency of 4.48% was achieved with R123.

In terms of the highest efficiency and net power generation, n-pentane is found as the optimum working fluid. Gross and net power generation with n-pentane are 245 kW_e and 189 kW_e electricity with 5.6% gross and 4.32% net efficiencies.

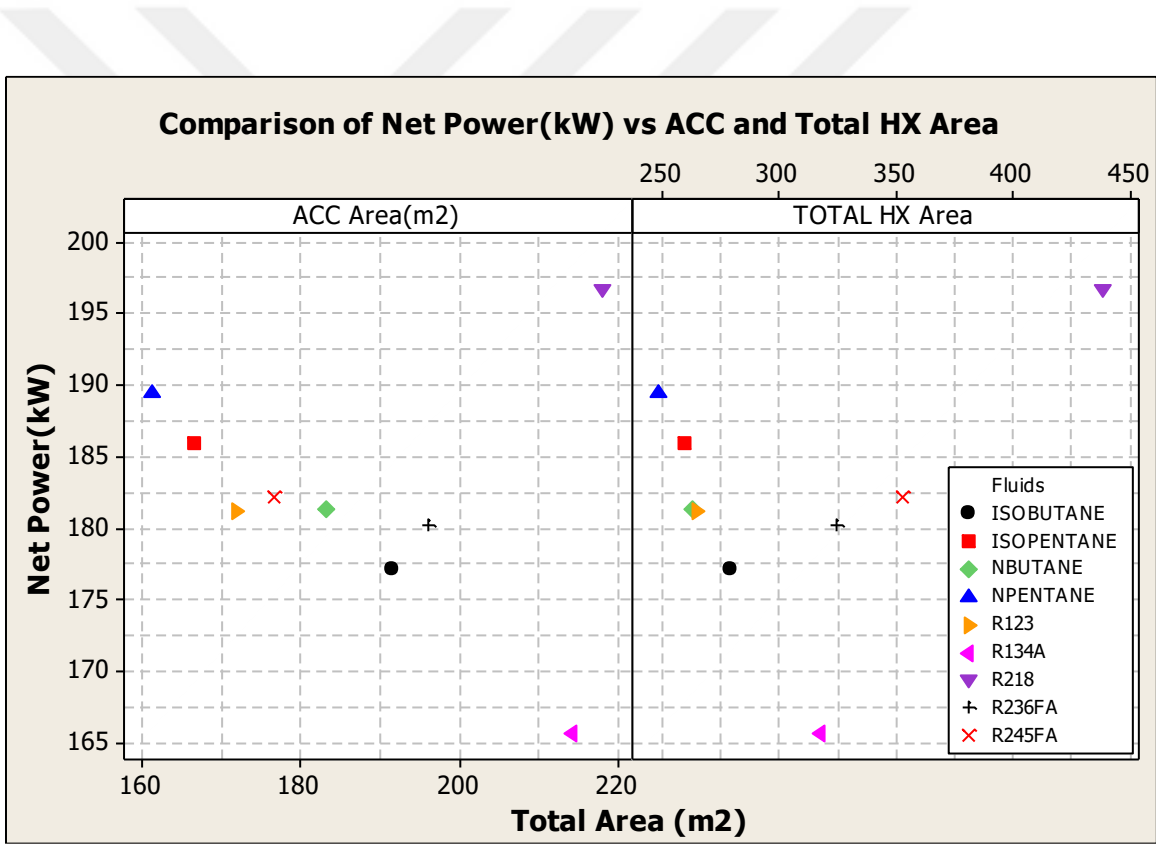


Figure 35 Comparison of net power vs ACC and total heat exchanger area for the different working fluids

Figure 6.10 shows the comparison of air-cooled condenser and heat exchangers (preheater+ evaporator) heat transfer surface area vs. net power generation for all working fluids. According to geometrical design, heat transfer and thermodynamics calculations of preheater, evaporator, and air-cooled condenser; n-pentane absorbs heat from geothermal water by using minimum area of

preheater and evaporator with 248.224 m² total area while it throws its heat into the air by using minimum air-cooled condenser area (161.164 m²) in all working fluids.

Therefore, n-pentane is also the most suitable fluid in terms of material cost.

Temperature-Heat transfer diagram is illustrated at Figure 6.11. Blue lines express the heat transfer at preheater while red lines express the heat transfer at evaporator. 13.72% of the total heat transfer takes place in the preheater for heating of n-pentane while 86,28% of the total heat transfer takes place in the evaporator for heating, boiling and 1°C superheating of n-pentane. The geothermal brine firstly enters the evaporator at 90 °C and leaves at 68.39 °C and then it enters to preheater. The temperature of brine decreases to 64.95 °C and geothermal fluid leaves from the cycle. The thermophysical properties of n-pentane, brine and air at each point of cycle is presented at Table 6.4.

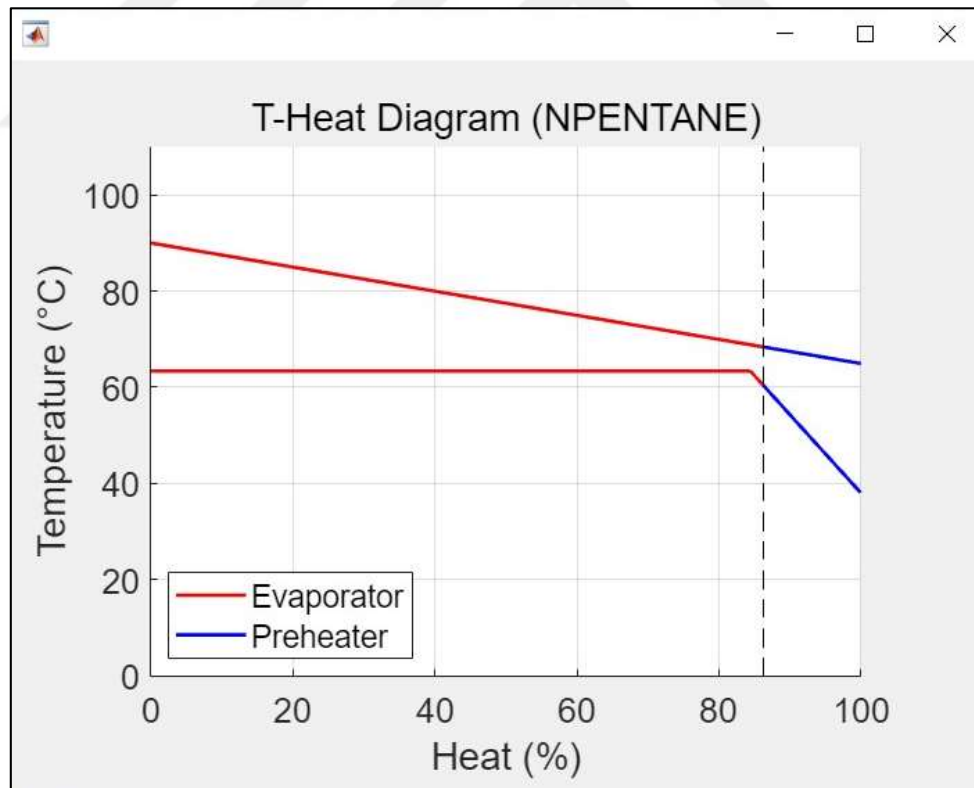


Figure 36 T-Q diagram output for n-pentane of ORC Designer Program

Table 6.4 Thermophysical properties of n-pentane, brine and air at each point of cycle

Points #	Flow Rate (m ³ /h)	Temperature (°C)	Pressure (bara)	Density (kg/m ³)	Enthalpy (kJ/kg)	Entropy (kJ/kgK)	Phase #
WF1	65,45	38,03	2,62	607,93	4,80	0,01	liquid
WF2	68,11	60,39	2,60	584,24	59,22	0,18	liquid
WF3	6.197,00	63,39	2,30	6,42	401,17	1,20	gas
WF4	12.906,43	48,15	1,09	3,08	378,75	1,22	gas
WF5	65,47	38,00	1,09	607,74	4,60	0,01	liquid
H1	155,39	90,00	3,00	965,30	377,04	1,19	liquid
H2	153,27	68,39	2,55	978,64	286,33	0,94	liquid
H3	152,98	64,95	2,42	980,55	271,89	0,89	liquid
A1	1.343.505	18,00	1,00	1,20	417,40	3,86	Air
A2	1.387.255	27,19	1,00	1,16	426,64	3,89	Air

N-pentane enters the preheater at 38.03 °C and the temperature of n-pentane increases to 60.30 °C at preheater. The temperature of n-pentane increases to 62.39 °C, boils and then superheats to 63.39 °C. Approximately, 85% of geothermal heat transfer is used for boiling and evaporating of n-pentane.

Pressure-Enthalpy (P-h) diagram and Temperature-Entropy (T-s) diagram are presented at Figure-6.12-6.13. According to these diagrams, the pump transfers to pentane into preheater at point 1 at 38.03 °C, 2.62 bar and 39.79 kg/s. The temperature of n-pentane increases to 60.39 °C and pressure of n-pentane decreases to 2.60 bar at point 2, then enters to evaporator. N-pentane heats up, boils and superheats up to 63.39 °C and its pressure decreases to 2.30 bara at point 3. N-pentane then passes through the turbine and expands. The temperature and pressure decrease to 48.15 °C and 1.09 bar at point 4. This pressure and temperature dropping process produce a rotational shaft power by transforming kinetic energy and then 245 kW gross energy obtained between point 3 and 4. After turbine, n-pentane enters the air-cooled condensers and then it cools down, becomes condensate and a little bit subcooled at constant pressure as 1.09 bar by using 447.8 kg/s mass flow rate of air at 18 °C. The temperature of air increases to 27.19 °C while the temperature of n-pentane decreases to 38 °C at point 5. Fans of air-cooled condenser use 52.096 kW electricity at this process. Finally, working fluid is pumped back into preheater by a pump from point 5 to 1 and then Rankine cycle is completed. Internal consumption of pump is calculated as 3.917 kW.

The total auxiliary consumption of ORC is calculated as 56 kW approximately and then net power generation is found as 189 kWe.

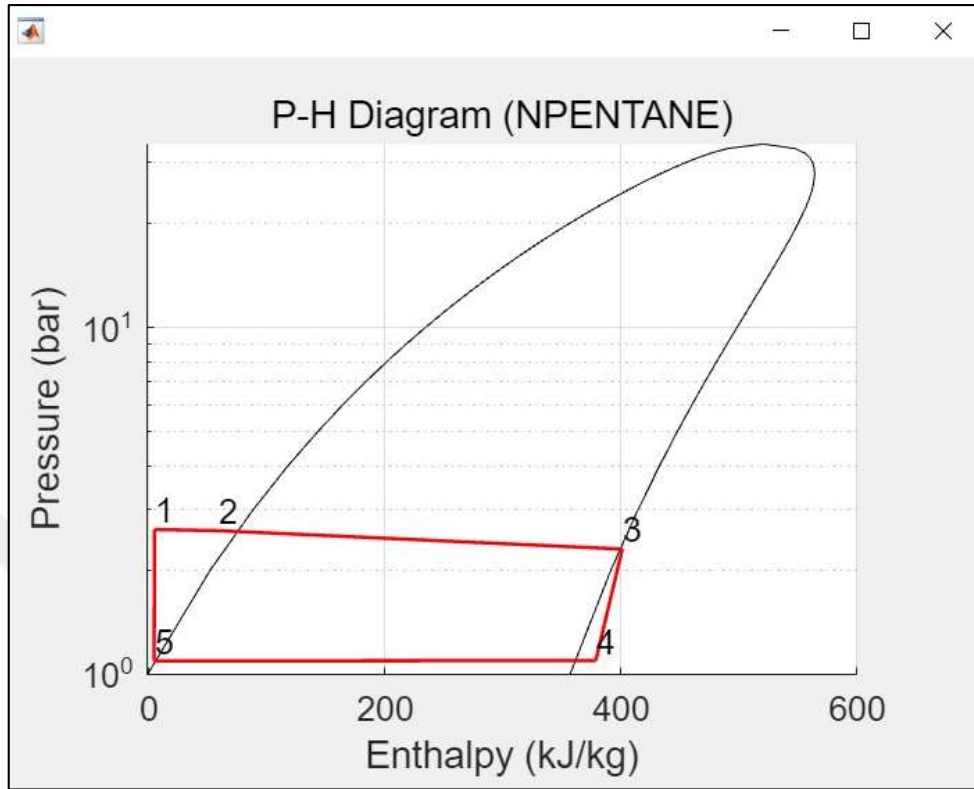


Figure 37 P-h diagram output for n-pentane of ORC Designer Program

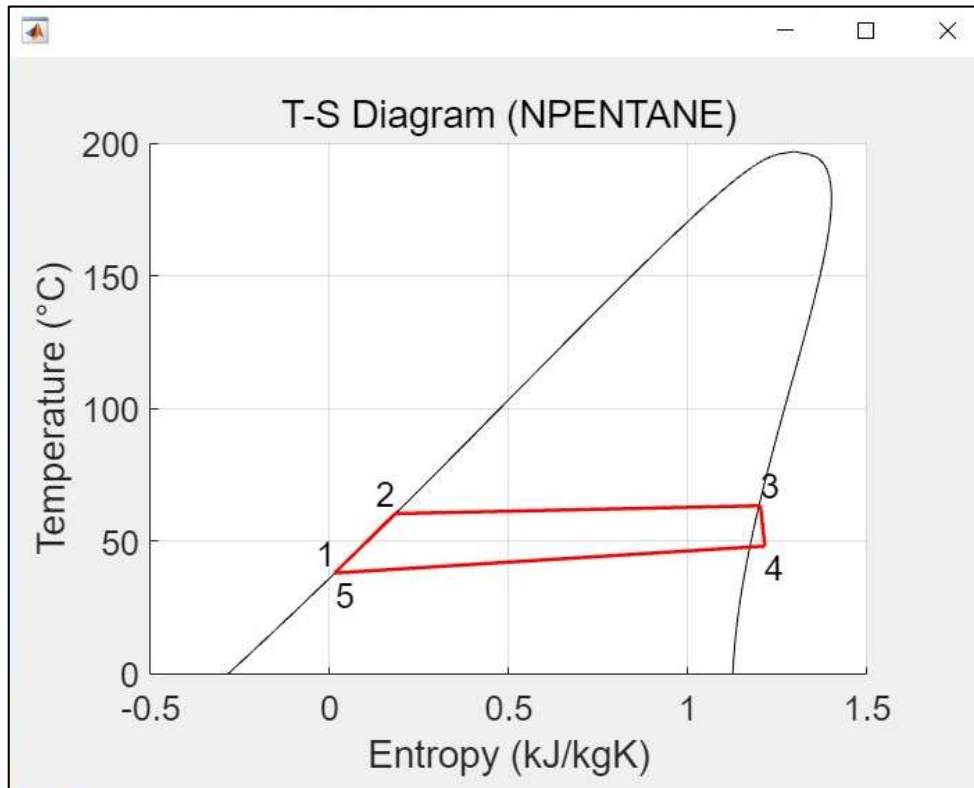


Figure 38 T-s diagram output for n-pentane of ORC Designer Program

The optimum geometrical results of preheater and evaporator is presented at Table 6.5. In the table, hot fluid means geothermal water while cold fluid is n-pentane. Evaporator uses Kettle Type Boiler (K-Shell) while preheater uses one pass Shell (E-Type). Duty means total heat transfer process in evaporator and preheater which are calculated 3965.084 kW and 609.808 kW, respectively.

Table 6.5 Data sheet of Evaporator and Preheater

PROPERTIES	EVAPORATOR	PREHEATER
Hot Fluid:	WATER	WATER
Working Fluid:	NPENTANE	NPENTANE
Shell Type:	K-Shell	E-Shell
Duty (kW):	3965,084	609,808
Heat Transfer Area (m2):	184,387	63,837
EMTD (°C):	13,44	14,656
Fouling OHTC (W/m2C):	1113,455	651,779
Clean OHTC (W/m2C):	1668,787	809,458
Pass Number:	1	2
Tube Number:	231	80
Tube Length (m):	10	10
Tube Diameter (mm):	25,4	25,4
Tube Thickness (mm):	2,1	2,1
Tube Layout (°):	45	45
Bundle Diameter (mm):	728	35
Shell Diameter (mm):	1456	463
COLD SIDE		
Flow Rate (kg/h):	39790,878	39790,88
Inlet Temperature (°C):	60,393	38,034
Outlet Temperature (°C):	63,393	60,393
Fouling Resistance (m2C/W):	11360	0,000088
Pressure Loss (bar):	0,3	0,036
HOT SIDE		
Flow Rate (kg/h):	150000	150000
Inlet Temp (°C):	90	68,393
Outlet Temperature (°C):	68,393	64,947
Density (kg/m3):	972,379	979,635
Specific Heat (j/kgC):	4195,719	4188,199
Dynamic Viscosity (Pa.s):	0,0003577	0,000423
Conductivity (W/mC):	0,667	0,657
Pr Number:	2,252	2,695
Fouling Resistance (m2C/W)	5682	0,000176
Pressure Loss (bar):	0,128	0,454

The total heat transfer area of evaporator and preheater are calculated 184.387 m² and 63.837 m², respectively. Pressure losses of working fluid side is obtained 0.3 bar and 0.036 bar at evaporator and preheater while pressure losses of geothermal brine is 0.128 bar and 0.454 bar at evaporator and preheater, respectively.

Air-cooled condenser design considerations and geometrical results are presented at Table 6.6. The total heat transfer from n-pentane to air is calculated 4135.462 kW. The total heat transfer area is obtained 19595.129 m² with 4 tube rows.

Table 6.6 Data sheet of ACC

PROPERTIES	VALUE
Cold Fluid:	AIR
Working Fluid:	NPENTANE
Fan Power (Kw):	52,096
Duty (kW):	4135,462
Air Inlet Temp (°C)	18
Air Outlet Temp (°C)	27,19
WF Inlet Temp (°C)	48,147
WF Outlet Temp (°C)	38
LMTD (°C)	14,219
Heat Transfer Area (m2):	19595,129
Air Flow Rate (kg/h):	1610057,376
Fouling OHTC (W/m2C):	14,842
Clean OHTC (W/m2C):	17,294
ACC Width (m):	20
Tube Number:	1362
Tube Length (m):	8,058
Tube Diameter (mm):	25,4
Tube Thickness (mm):	1,65
Number of Tube Rows:	4
Face Area (m2):	161,164
Fan Area (m2):	64,466
Tube Pressure Loss (Pa):	564,177
Air Pressure Loss (Pa):	88,466

1610057,376 kg/s air flows from bottom side to top side of ACC by fans which has 52.096 kW consumption. N-pentane loses very small amount pressure with 564.177 Pa (0.00564 bar) during condensing process.

7. DISCUSSION

This thesis aimed to develop an ORC system to utilize the low enthalpy and low flow rate geothermal resource which is unused in Turkey for power generation.

Generally, it is difficult to come across a detailed design of an ORC system's subcomponents directly. When examining the most ORC modelling studies in the literature, it is obvious that calculations are made with assumptions without considering the geometric properties of the internal components such as heat exchangers, ACC's, turbine, or pump.

In order to improve the thermal efficiency and power generation, different configurations of ORC system have been developed with recuperator and non-recuperator. The recuperator transfers some of the waste heat in the exhaust of turbine, thus preheating circulating working fluid before entering the preheater without external heat source. However, the recuperator also creates two times pressure drops at cold side and hot side.

According to preliminary ORC models, the efficiency and power output of ORC system without recuperator is calculated higher than ORC system with recuperator. The same calculations are performed for R218, R134a, R245fa, R236fa, R123, iso-pentane, n-pentane, iso-butane, n-butane and then the gross energy productions and efficiencies of ORC system without recuperator calculated higher than recuperator system. It means that energy gain from the recuperator due to heat transfer is less than energy loss due to pressure losses for cold and hot streams for low enthalpy geothermal resources. It also means that recuperator usage can be more effective for ORC at medium and high enthalpy geothermal resource. Therefore, the next models for the thesis are developed according to non-recuperator ORC system.

Air cooled condenser is used as condensing system of ORC at this thesis because its widespread use in the geothermal industry due to scarcity of water resources. However, the water-cooled condenser is used in general literature (Ata et al., 2019; Hu et al., 2021; Song et al., 2020; Shengjun et al., 2011) because it is more efficient and easier to calculate. Furthermore, the heat transfer coefficient evaluation in air-cooled condensers is difficult while the detailed design and geometrical scaling calculations are very complex.

In addition, the pressure drop calculations are performed in the ORC modelling for pre-heater, evaporator and air-cooled condenser, although it has been ignored in most other studies (Chacartegui et al., 2011; Wei et al., 2008; Karellas et al., 2012). Moreover, this thesis directly focuses on the detailed design and geometrical scaling calculations of heat exchangers for low heat geothermal resources while most of the literature only calculate the heat transfer surface area of heat exchangers (Hettiarachchi et al., 2007).

The most of the thermodynamical analysis or modelling studies are performed for higher temperature geothermal resources over 100 °C (Bahaa and Gerald, 2007; Yamada et al., 2012; Li et al., 2011) or lower capacity ORC applications for experimental purposes (Gang et al., 2011; Shengjun et al., 2011); while a model to evaluate the performance of an Organic Rankine cycle (ORC) at low temperature geothermal resources such as 150 tons/hour flow rate at 90 °C temperature for industrial applications in this study.

Under this thesis, an ORC Designer MATLAB algorithm and application is developed and after 180.000 iteration, main properties of heat exchangers which are shell diameters, tube diameters, number of tubes, tube count and layouts, hex length, shell side and tube side heat transfer coefficients, overall fouling heat transfer coefficient, pressure losses, etc. are determined. ORC Designer MATLAB application is user oriented, friendly application and the similar interfaces to heat exchanger design programs have been developed. It has an .exe file and it can even be installed on a computer without a MATLAB program. Every assumption is input, and the design can be changed according to the desired conditions.

During the ORC Designer MATLAB application calculations, some inputs are used directly industrial experiences such as preheater saturation approach temperature which is temperature difference working fluid side outlet temperature and working fluid saturation temperature at outlet pressure. The main purpose of this temperature difference is to prevent boiling in the preheater. We assumed it 2 °C although it can be variable in the program. Evaporator approach temperature which is temperature difference between evaporator outlets for hot fluid and cold fluid is assumed 5 °C. Air cooled condenser approach temperature which is temperature difference between air inlet and working fluid outlet is assume 20 °C. It changes according to selected fluid and air temperature in ORC designer program. Since turbine design is not the subject of this study, isentropic efficiency which is assumed 85% can be entered as input according to the turbine to be selected. According

to industrial standards, the working fluid shall enter minimum 1 °C superheat to protect turbine. When producing a heat exchanger, it should comply with industrial standards and materials that are easily available in the market should be used to keep the cost low, not be custom made. For this reason, it is necessary to enter the basic properties of the materials that can be used during manufacturing of system into the program. The length of the heat exchangers and the width of the ACC must be entered according to the maximum dimensions of the area where the ORC will be installed. If the length of the ACC or the diameters of the heat exchangers are high or low from expected value, the program should be run again with the new geometrical inputs.

ORC designer program was evaluated nine organic working fluids, R218, R134a, R245fa, R236fa, R123, iso-pentane, n-pentane, iso-butane, and n-butane under the same inputs. The best efficient and productive working fluid with 6.93% gross efficiency is selected R218 as 394 kWe gross power generation however it has the lowest net efficiency and highest power generation with 3.46% and 197 kWe, respectively. Only one preheater is used at all working fluids except R218. R218 uses two preheaters and drops re-injection temperature lower than 60 °C. Therefore, it gives the best gross and net power generation considering it has the lowest net efficiency. It means that manufacturing cost of ORC with R218 will be highest in the others working fluids. Therefore, R218 is eliminated because of low net efficiency and re-injection temperature and high manufacturing cost. The evaluation was continued by considering the remaining fluids.

The ranking of working fluids from highest to lowest net power efficiency are R123, iso-pentane, R245FA, n-pentane, iso-butane, n-butane, R236FA, R218, R134A with net efficiencies of 4.48%, 4.42%, 4.38%, 4.32%, 4.22%, 4.13%, 3.96%, 3.46%, 3.15%, respectively. The ranking of working fluids from highest to lowest net power generation are R218, n-pentane, iso-pentane, R245FA, R123, n-butane, R236FA, iso-butane, R134A with net efficiencies of 197kWe, 189 kWe, 186kWe, 182 kWe, 181 kWe, 180 kWe, 177 kWe and 166 kWe, respectively.

While the net efficiency of R123 is the highest one, the net power generation of it 182 kW and re-injection temperature at 66.88 °C. However, net power generation of n-pentane is 189 kW at 64.95 °C re-injection temperature although n-pentane is in the fourth place in efficiency ranking. ORC working with n-pentane as a working fluid makes the most use of geothermal fluid because n-pentane has a minimum re-injection temperature. N-pentane is found as the optimum working fluid in terms of the highest efficiency and net power generation. The total flow rate of n-pentane is

39.791 tons/hour at circulation. ORC with n-pentane generates 245 kWe gross and 189 kWe net electricity with 5.6% gross and 4.32% net efficiency by using 150 tons/hour geothermal brine at 90 °C while ambient air temperature is 18 °C. Also theoretical gross power is equals to ORC Designer program results. Internal consumptions of pump and ACC fans are calculated 3.917 kWe and 52.096 kWe, respectively. Additionally, ORC model with n-pentane has minimum heat transfer area at preheater, evaporator and air-cooled condenser which means that n-pentane is the most suitable fluid in terms of material cost.

Table 7.1 Geometrical comparison between the present results and Ref (Fu et al., 2015)

	PARAMETER	Ref. (Fu et al., 2015)	Present Study
PREHEATER	Tube inside/outside diameter	1.471/1.587 cm	2,12/2,54 cm
	Tube thickness	0.058 cm	0,21 cm
	Tube number	200	80
	Tube bundle	1 pass	2 passes
	Tube/Shell length	360 cm	1000 cm
	Shell diameter	32.45 cm	46,5 cm
	Baffle cut	30%	25%
	Baffle plate number	17	35
	Calculated heat transfer area	35,878 m ²	63,837 m ²
	EVAPORATOR	Tube inside/outside diameter	1.639/1.765 cm
Tube thickness		0.063 cm	0,21 cm
Tube number		300	231
Tube bundle		4 passes	1 pass
Tube/Shell length		360 cm	1000 cm
Number of tube rows		12	4
Free space above upper tube row		47%	-
Shell diameter		69,59 cm	145,6 cm
Heat transfer area		59,854 m ²	184,387 m ²
CONDENSER	Cooling Type	Water	Air
	Tube outside diameter	1.905 cm	2,54 cm
	Tube number	480	1362
	Tube bundle	2 passes	1 pass
	Width	-	20 m
	Tube/Shell length	360 cm	805,8 cm
	Distance upper row/centre	2.23 cm	-
	Number of tube rows	18	4
	Shell inside diameter	71.7 cm	-
	Heat transfer area	103,363776	19595,129 m ²

In terms of model validation, geometrical results of this study are compared with experimental results of another study (Fu et al., 2015) at Table 7.1. Fu et al. (2015) made a study on design, construction, and experimental testing of a 250 kWe ORC, consisting of a working fluid circulation pump, preheater, evaporator, turbine, generator, water cooled condenser and cooling tower. They had used a simple ORC with a preheater, an evaporator, a turbine, condenser, and pump which is only different from this study in terms of using of water-cooled condenser. In the study, hot water was supplied by a boiler as waste heat at 119.8 C.

The total heat transfer area of preheater and evaporator of existing study is 2.6 times higher than the total heat transfer area of reference study (Fu et al. (2015))’s preheater and evaporator. The main reason of the higher heat transfer area in preheater and evaporator at existing study is that geothermal water flow rate is 55.8% higher and temperature is 29.8 °C lower than reference study (Fu et al. (2015))’s working conditions. High flow rate and low temperature cause more heat transfer surface to occur. Since a water-cooled condenser is used in Fu et al. (2015), it will not be correct to compare the condensers.

Table 7.2 Thermodynamical and heat transfer comparison between the present results and Ref. Fu et al. (2015)

PARAMETER	Ref. Fu et al. (2015)	Present Study
Mass flow rate of hot water (kg/s)	26,7	41,6
Inlet temperature of hot water (°C)	119,8	90
Outlet temperature of hot water (°C)	94,7	68,393
Temperature difference of hot water (°C)	25,1	21,607
Working fluid	R245fa	n-pentane
Working fluid flow rate (kg/s)	11,85	11,05
Evaporation temperature (°C)	94,7	63.39
Superheat at evaporator outlet (°C)	1,7	1
Total heat transfer in preheater (kW)	1161	601,511
Total heat transfer in evaporator (kW)	1560	3779,584
Total heat transfer from hot water (kW)	2721	4381,095
Turbine design efficiency (%)	80	85
Pump design efficiency (%)	90	80
ORC gross efficiency (%)	-	5,60
ORC thermal efficiency (%)	7,94	4,32 (net)
Gross power output (kWe)	-	245
Net power output (kWe)	225	189

Although they designed the system for 15.39 kg/s hot water at 133.9 °C, they were able to use higher flow rate with 26.7 kg/s and lower inlet temperature with 119.8 °C during the experimental studies. The inputs, thermodynamic and heat transfer results comparison of reference study with present study are presented at Table 7.2.

The turbine design efficiency of existing study is 5% higher than Fu et al. (2015) while pump design efficiency is 10% lower than it. Working fluid at turbine inlet is 1.7 °C superheat at Fu et al. (2015) while it is 1 °C superheat in this study. In addition, the working fluid flow rates are very similar even if they are different. It cannot be said that there is a marginal difference in terms of these parameters. However, ORC in Fu et al. (2015) was designed 133.9 °C and tested 119.8 °C hot water inlet while ORC in this study is developed for low enthalpy geothermal resources lower than 90 °C. Their exit temperature is higher than existing study’s inlet conditions with 94.7 C temperature. Therefore Fu et al. (2015)’s ORC thermal efficiency is 3.62% higher than existing study. However, they preferred to use a water-cooled condenser, which is more efficient than an air-cooled condenser. According to industrial applications, the gross and net ORC efficiencies of water-cooled system is minimum 1% higher than air-cooled system.

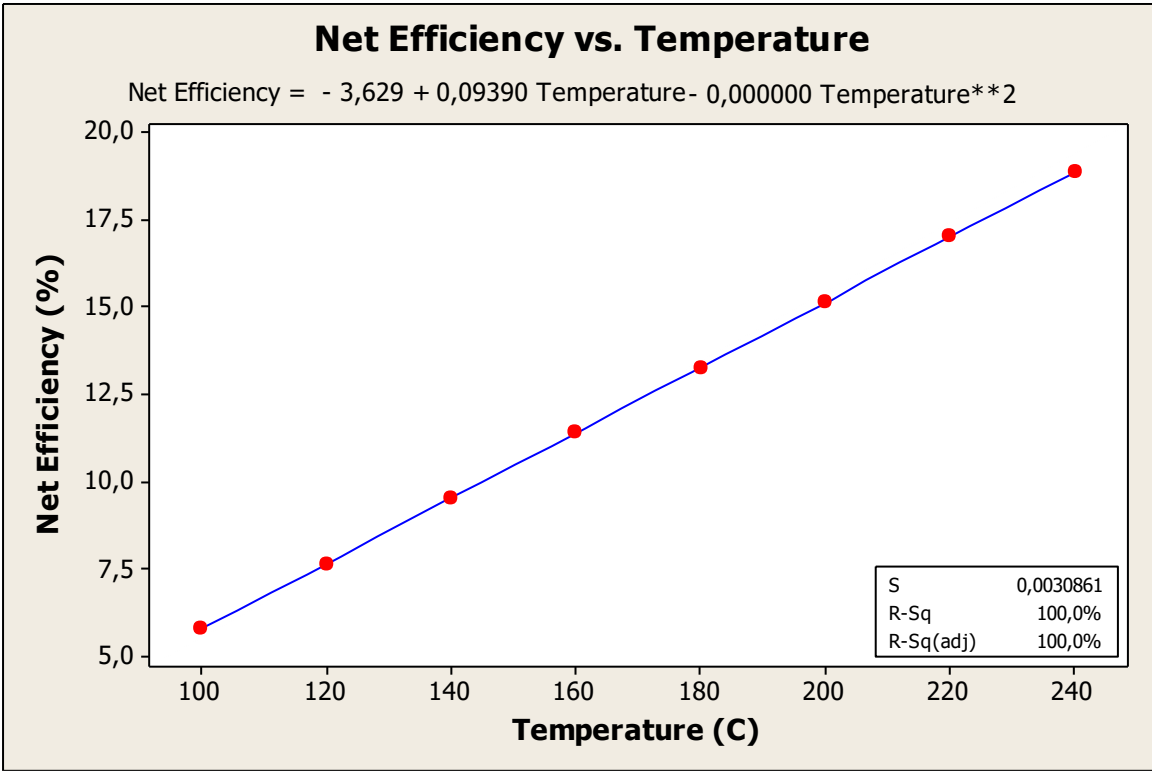


Figure 39 Net efficiency vs. Temperature Graph by using Geothermal Investment Tool (GMK Energy “Geothermal Investment Tool Application”, 2022)

When the study is examined in detail, the gross power of the ORC is not mentioned in the paper and the consumptions of the auxiliary equipment operating the system are not given. Considering that the total installed turbine power is 250 kWe at full capacity, they obtained 225 kWe net at off-design conditions. If the internal consumption of the working fluid circulation pump, cooling tower fans, cooling water circulating pumps and make-up water pump are not considered in the net power output calculation, ORC thermal efficiency can be less than 7.94%.

Geothermal investment tool (GMK Energy, 2022) is a geothermal power plant capacity calculator by using heating resource conditions which developed according to installed actual air-cooled geothermal power plants benchmarking. Figure 7.1 shows the effects of hot fluid inlet temperature on net efficiencies of air-cooled geothermal power plants. Industrial benchmarking study in Geothermal investment tool shows that each 1°C change in inlet temperature has a 0.094% effect on net efficiency.

If we want to compare Fu et al. (2015) with this study, 2.8% efficiency should be decreased in terms of inlet temperature difference while 1% efficiency should be decreased in terms of air-cooling effect. Therefore, ORC thermal efficiency of Fu et al. (2015) drops from 7.94% to 4.14% and then the efficiency of this study will be higher than Fu et al. (2015).

8. CONCLUSION AND RECOMMENDATION

The main purpose of this thesis is modelling an Organic Rankine Cycle and detailed design of its main equipment such as heat exchangers, preheaters and air-cooled condensers for low enthalpy geothermal resources. In Turkey, the total geothermal power plants are supplied with geothermal fluids from medium and high enthalpy geothermal reservoirs. Low enthalpy (≤ 100 °C) geothermal wells are not used for power generation unless their geothermal fluid flow rate is sufficiently high.

This thesis will guide the domestic production, development and prototyping of the power generation unit (micro-ORC) operating according to the Organic Rankine Cycle to generate electricity from low enthalpy geothermal resources.

In geothermal fields with temperature higher than 100 °C in Turkey and worldwide, geothermal resources are usually used for electricity generation. Low enthalpy fields below this temperature are used in other areas where high temperatures are not needed, such as district heating, greenhouse heating, etc. Companies conducting geothermal exploration and drilling activities with the intention of building a geothermal power plant either abandon their projects or leave their sites dormant if they find resources with a temperature of 100 °C and below. In addition, companies whose only reservoir temperatures are above 100 °C are not satisfied with geothermal exploration work. They are looking to use artesian or artificial production methods (pumping) to reach a temperature of 100 °C and above at the wellhead.

There are companies around the world producing low-capacity ORC and combined heat and power (CHP) systems. However, their low temperature operating systems limit capacity (200 kW max) or require temperatures above 200 °C as waste heat power recovery units. There are many companies that commercially produce low-capacity ORCs (Exergy, Turboden, Electrathern, Rank, Orcan etc.) at temperatures over 100 °C for small scale plants.

This thesis aimed to develop an ORC system to utilize the low enthalpy, low flow rate geothermal fluid, which is unused in Turkey, for power generation. A detailed MATLAB model is developed to evaluate the performance of an Organic Rankine Cycle (ORC) and detailed sub-component (preheater, evaporator and air-cooled condenser) design on low-temperature geothermal resources

such as 150 tonnes/hour flow at 90 °C temperature. The system was evaluated with nine dry organic working fluids: R218, R134a, R245fa, R236fa, R123, iso-pentane, n-pentane, iso-butane, and n-butane. In this study, the following conclusions were reached:

- Results of the preliminary calculations for recuperator and non-recuperator system shows that thermal efficiency and power output of non-recuperator system is higher than recuperator system. Therefore, non-recuperator ORC system is selected for detailed design calculations.
- The best efficient and productive working fluid is selected R218 as gross power generation while the best one is R123 as net power generation.
- Only one preheater is used at all working fluids except R218. R218 uses two working fluids and drops re-injection temperature lower than 60 °C. Therefore, it gives the best net power generation considering it has the lowest net efficiency.
- N-pentane and iso-butane give the maximum net power generation as 189 kWe and 177 kWe respectively while R218 net power output as 197 kWe.
- When net efficiency and power generation are considered together, the suitable working fluids are n-pentane, iso-butane, n-butane, R245fa, respectively.
- The ranking of working fluids from highest to lowest net power efficiency are R123, iso-pentane, R245FA, n-pentane, iso-butane, n-butane, R236FA, R218, R134A with net efficiencies of 4.48%, 4.42%, 4.38%, 4.32%, 4.22%, 4.13%, 3.96%, 3.46%, 3.15%, respectively.
- The ranking of working fluids from highest to lowest net power generation are R218, n-pentane, iso-pentane, R245FA, R123, n-butane, R236FA, iso-butane, R134A with net efficiencies of 197kWe, 189 kWe, 186kWe, 182 kWe, 181 kWe, 180 kWe, 177 kWe and 166 kWe, respectively.
- N-pentane is found as the optimum working fluid in terms of the highest efficiency and net power generation. The total flow rate of n-pentane is 39.791 tons/hour at circulation. ORC with n-pentane generates 245 kWe gross and 189 kWe net electricity with 5.6% gross and 4.32% net efficiency by using 150 tons/hour geothermal brine at 90 °C while ambient air temperature is 18 °C.
- Internal consumptions of pump and ACC fans are calculated 3.917 kWe and 52.096 kWe, respectively.

- ORC model with n-pentane has minimum heat transfer area at preheater, evaporator and air-cooled condenser which means that n-pentane is the most suitable fluid in terms of material cost.
- The optimum geometrical results of preheater, evaporator and air-cooled condenser are obtained for n-pentane as working fluid.
- In terms of model validation, geometrical results of this study are compared with experimental results of another study (Fu et al., 2015)
- Since a high-temperature source and water-cooled condenser are used in the compared study, its efficiency has been reduced compared to 90 °C heat source and air-cooled condenser usage by using benchmarking approach. Thus, the efficiency of our system is calculated higher than Fu et al., 2015.
- With the studies to be done after this thesis, the turbine and pump detail designs can be made, and the datasheet documents of the whole ORC system can be obtained.

REFERENCES

- Admiraal, D.M., Bullard, C.W. (1993). *Heat Transfer in Refrigerator Condensers and Evaporators* (pp 3-26), Urbana, USA.
- American Petroleum Institute (1997). *Air-Cooled Heat Exchangers for General Refinery Services, API STANDARD 661* FOURTH EDITION, NOVEMBER 1997.
- Ata, S., Kahraman, S., Sahin, R. (2019). Thermal efficiency evaluation of an organic Rankine cycle with n-pentane as working fluid. *International Journal of Energy Applications and Technologies* 6(2), 31-38.
- Bahaa, S., Gerald, K. (2007). “Working fluids for low temperature organic rankine cycles, *Energy*, 32, 1210–1221.
- Baral S, Kim D, Yun E, Kim K.C. (2015). Energy, Exergy and Performance Analysis of Small-Scale Organic Rankine Cycle Systems for Electrical Power Generation Applicable in Rural Areas of Developing Countries. *Energies*, 8(2):684-713.
- Braimakis, K. and Karellas, S. (2018). Exergetic optimization of double stage Organic Rankine Cycle (ORC). *Energy*, No:149, pp 296-313.
- Bronicki, L., (2013). *Short review of the long history of ORC power systems*. In: ASME ORC13.
- Capata, R., Hernandez, G. (2014). “Preliminary design and simulation of a turbo expander for small rated power organic rankine cycle (ORC)”, *Energies*, 7, 7067–7093.
- Chacartegui, R., Munoz Escalona, J., Sanchez, D., Monje, B., Sanchez, T. (2011). “Alternative cycles based on carbon dioxide for central receiver solar power plants”, *Applied Thermal Engineering*, 31, 872–879.
- Cho, S.Y. and Cho, C.H. (2015). An experimental study on the organic Rankine cycle to determine as to how efficiently utilize fluctuating thermal energy. *Renewable Energy*, No. 80, pp. 73-79.

- Coker, A.K. (2015). *Ludwig's Applied Process Design for Chemical and Petrochemical Plants*. Gulf Professional Publishing, Elsevier Books. ISBN: 978-0-7506-8524-5.
- Dong, S., Zhang, Y., He, Z., Yu, Z., Zhang, Y., Kong, X. (2015). Optimum design method of Organic Rankine Cycle system based on semi-empirical model and experimental validation. *Energy Conversion and Management*, No. 108, pp. 85-95.
- Du, Y., Yang, Y., Hu, D., Hao, M., Wang, J., Dai, Y. (2018). Off-design performance comparative analysis between basic and parallel dual-pressure organic Rankine cycles using radial inflow turbines. *Applied Thermal Engineering*, No. 138, pp. 18-34.
- Erdeweghe, S.,V., Bael, J.,V., Laenen, B., D'haeseleer, W. (2019). Design and off-design optimization procedure for low-temperature geothermal organic Rankine cycles. *Applied Energy*, No: 242, 716–731.
- Erdogan, A., Colpan, C.O., Cakici, D.M. (2017). Thermal design and analysis of a shell and tube heat exchanger integrating a geothermal based organic Rankine cycle and parabolic trough solar collectors, *Renewable Energy*. Volume 109, Pages 372-391.
- Eyerer, S., Wieland, C., Vandersickel, A., Spliethoff, H. (2016). Experimental study of an ORC (Organic Rankine Cycle) and analysis of R1233zd-E as a drop-in replacement for R245fa for low temperature heat utilization. *Energy*, No. 103, pp. 660-671.
- Fu, B.R., Lee, Y.R. Hsieh, J.C. (2015). Design, construction, and preliminary results of a 250-kW organic Rankine cycle system. *Applied Thermal Engineering*, No. 80, pp. 339-346.
- Galanis N., Cayer E., Roy P., Denis E.S., Desilets M. (2009). "Electricity generation from low temperature sources", *J Applied Fluid Mechanics*, 2, pp. 55–67.
- Gang, P., Li, J., Li, Y., Wang, D., Ji, J. (2011). "Construction and dynamic test of a small-scale organic rankine cycle", *Energy*, 36, 3215–3223.
- GMK Energy (2022). "Geothermal Investment Tool Application" (20.08.2022, 15:10), https://play.google.com/store/apps/details?id=com.gmkenerji&hl=en_US&gl=US
- Gonzalez H.A., Newton, P.J., Costall A.W. (2015). "Design methodology for radial turbo expanders in mobile organic Rankine cycle applications", *Applied Energy*, 157, 729–743.

Guo, T., Wang, H., Zhang, S. (2011). “Comparative analysis of natural and conventional working fluids for use in transcritical Rankine cycle using low-temperature geothermal source”, *International Journal of Energy Research*, 35, 5049–5062.

Han, S., Seo J.B., Choi, B.S. (2014). Development of a 200 kW ORC radial turbine for waste heat recovery. *Journal of Mechanical Science and Technology*, No. 28(12), pp. 5231-5241.

Hettiarachchi, H., Golubovic, M., Worek, M., Ikegami, Y. (2007). “Optimum design criteria for an organic Rankine cycle using low-temperature geothermal heat source”, *Energy*, 32, 1698–1706.

https://www.wermac.org/equipment/heatexchanger_part5.html (20.08.2022, 20:01)

Hu, B., Guo, J., Yang, Y., Shao, Y. (2021). *Optimization of low temperature geothermal organic Rankine power generation system*. The 8th International Conference on Energy and Environment Research ICEER.

Hu, D., Li, S., Zheng, Y., Wang, J., Dai, Y. (2015). Preliminary design and off-design performance analysis of an Organic Rankine Cycle for geothermal sources. *Energy Conversion and Management*, No. 96, pp. 175-187.

Kakac, S. (1992). *Boilers, Evaporators, and Condensers*, Published: 1991 by John Wiley & Sons., ISBN 13: 9780471621706.

Kakaç, S., Paykoç, E. (1988). Chapter 2- Basic Relationships for Heat Exchangers, Springer Science and Business Media LLC.

Kang, S.H. (2016). “Design and preliminary tests of ORC (organic Rankine cycle) with two-stage radial turbine”, *Energy*, 96, 142–154.

Karellas, S., Schuster, A., Leontaritis, A. (2012). “Influence of supercritical ORC parameters on plate heat exchanger design”, *Applied Thermal Engineering*, 33–34, 70–76.

Kazi, S.N (2011). Jovan Mitrovic (Ed.), *Fouling and Fouling Mitigation on Heat Exchanger Surfaces*, Published: March 9th, 2012, DOI: 10.5772/32990

Khaliq, A., Basant, K., Kumar R., (2012). “First and second law investigation of waste heat based combined power and ejector-absorption refrigeration cycle”, *Int. J. Refrig*, 35, 88–97.

- Landelle, A., Tauveron, N., Haberschill, P., Revellin, R., Colasson, S. (2017). Organic Rankine cycle design and performance comparison based on experimental database. *Applied Energy*, No. 204, pp. 1172-1187.
- Lee, H.S (2010). Thermal design heat sinks thermoelectrics heat pipes compact heat exchangers and solar cells (pp. 274-279). New Jersey: Published by John Wiley & Sons, Inc.
- Lee, D.H., Yang, Y.M., Park, C.D., Lee, S.W., Park, B.S. (2015). *Development and Test of a 100kW Class ORC Power-Generator for Low Temperature Geothermal Applications*. ASME ORC 2015.
- Lee Y.R, Kuo C.R, Liu C.H, Fu B.R, Hsieh J.C, Wang C.C. (2014). Dynamic Response of a 50 kW Organic Rankine Cycle System in Association with Evaporators. *Energies* 7(4):2436-2448.
- Lemort, V., Quoilin, S., Cuevas, C., Lebrun, J. (2009). “Testing and modeling a scroll expander integrated into an organic Rankine Cycle”, *Applied Thermal Engineering*, 29, 3094–3102.
- Li, H., Hu, D., Wang, M., Dai, Y. (2016). Off-design performance analysis of Kalina cycle for low temperature geothermal source. *Applied Thermal Engineering*, No: 107, 728–737.
- Li, J., Ge, Z., Duan, Y., Yang, Z., Liu, Q. (2018). Parametric optimization and thermodynamic performance comparison of single-pressure and dual-pressure evaporation organic Rankine cycles. *Applied Energy*, No. 217, pp. 409-421.
- Li, W., Feng, X., Yu, L., Xu, J. (2011). “Effects of evaporating temperature and internal heat exchanger on organic rankine cycle”, *Applied Thermal Engineering*, 31, 4014–4023.
- Li, X., Zhang, Q. 2012. “The first and second law analysis on an organic rankine cycle with ejector”, *Solar Energy*, 93, 100–108.
- Li, X., Zhao, C., Hu, X. (2012). “Thermodynamic analysis of Organic Rankine Cycle with Ejector”, *Energy*, 42, 342–349.
- Li, X., Zhao, C., Jia, Y. (2011). “Increased low-grade heat source power generation capacity with ejector”, International Conference on Measuring Technology and Mechatronics Automation.
- Michael, E., Kazimierz, G., Reza, G.K., Joseph, V.L. (1996). *Production Engineering*, Elsevier BV.

- Molés, F., Navarro-Esbri, J., Peris, B., Mota-Babiloni, A. (2016). Experimental evaluation of HCFO-1233zd-E as HFC-245fa replacement in an Organic Rankine Cycle system for low temperature heat sources. *Applied Thermal Engineering*, No.98, pp. 954-961.
- Mondejar, M.E., Andreasena, J.G., Regidora, M., Rivaa, S., Kontogeorgisb, G., Persicoc, G.,Haglinda, F. (2018). Prospects of the use of nanofluids as working fluids for organic Rankine cycle power systems. *Energy Procedia*, No. 129, pp. 160-167.
- NPTEL (2015) *Process Design of Heat Exchanger: Types of Heat Exchanger, Process Design of Shell and Tube Heat Exchanger, Condenser and Reboilers*, “Chemical Engineering Design – II”, 1-41.
- Pei G., Li Jing, Li Yunzhu, Wang Dongyue, Ji Jie. (2011). “Construction and dynamic test of a small-scale organic rankine cycle”. *Energy*, 36,32, 15-23.
- Quoilin, S., Lemort, V., Lebrun, J. (2010). “Experimental study and modeling of an Organic Rankine Cycle using scroll expander”, *Applied Energy*, 87, 1260–1268.
- Ranjeet, H., Umesh, P., Ajinkya, J. (2020). Thermal Design of Tube and Shell Heat Exchanger and Verification by HTRI Software. *International Journal of Engineering Research & Technology*, 9(12), 525-530.
- Reza, K., Hadi, G., Mohammad, E., Hadi, R. (2017). Thermodynamic modeling and performance analysis of four new integrated organic Rankine cycles (A comparative study), *Applied Thermal Engineering*.
- Russel, T.W.F., Anne, S.R., Norman, J.W. (2008). Cambridge Series in Chemical Engineering. A.Varma (Ed.), *Mass and Heat Transfer* (pp 55-109), Cambridge University Press.
- Schuster, A., Karellas, S., Aumann, R. (2010). “Efficiency optimization potential in supercritical organic rankine cycles”, *Energy*, 35, 1033–1039.
- Shengjun, Z., Huaixin, W., Tao, G. (2011). Performance comparison and parametric optimization of subcritical Organic Rankine Cycle (ORC) and transcritical power cycle system for low-temperature geothermal power generation, *Applied Energy*, No.88, 2740–2754.

- Shao, L., Ma, X., Wei, X., Hou, Z., Meng, X. (2017). Design and experimental study of a small-sized organic Rankine cycle system under various cooling conditions, *Energy*. Volume 130, Pages 236-245.
- Shao, L., Zhu, J., Meng, X., Wei, X., Ma, X. (2017). Experimental study of an organic Rankine cycle system with radial inflow turbine and R123. *Applied Thermal Engineering*, No. 124, pp. 940-947.
- Singh, B.R., Singh, O.A. (2012). “Study of performance output of a multivane air engine applying optimal injection and vane angles”, *International Journal Rotating Machinery*, 2012, 1–10.
- Song, J., Loo, P., Teo, J., Markides, C.N. (2020). Thermo-Economic Optimization of Organic Rankine Cycle (ORC) Systems for Geothermal Power Generation: A Comparative Study of System Configurations, *Process and Energy Systems Engineering*, 1(14).
- Sun, J., Li, W. (2011). “Operation optimization of an organic rankine cycle (ORC) heat recovery power plant”, *Applied Thermal Engineering*, 31, 2032–2041.
- Tahir, M., Yamada, N., Hoshino, T. (2010). “Efficiency of compact organic rankine cycle system with rotary-vane-type expander for low-temperature waste heat recovery”, *International Journal of Civil and Environmental Engineering*, 4, 11–16.
- Tarrad, A.H (2011). A Correlation for the Prediction of Nucleate Pool Boiling Performance of Pure Liquids from Enhanced Tubes, *Jordan Journal of Mechanical and Industrial Engineering*, 5(2), 139-144.
- Tulsa, Okla. (1998). *Gas Processors Suppliers Association*. Air-Cooled Exchangers, “Engineering Data Book”, 10.1-10.18.
- Wang, Y., Liu, X., Ding, X., Weng, Y. (2016). Experimental investigation on the performance of ORC power system using zeotropic mixture R601a/R600a. *International Journal of Energy Research* 2016.
- Wang, Y., Zhao, J., Chen, G., Deng, S., An, Q., Luo, C., Alvi, J. (2018). A new understanding on thermal efficiency of organic Rankine cycle: Cycle separation based on working fluids properties. *Energy Conversion and Management*, No. 157, pp. 169-175.

Wei, D., Lu, X., Lu, Z., Gu, J. (2008). “Dynamic modeling and simulation of an Organic Rankine Cycle (ORC) system for waste heat recovery”, *Applied Thermal Engineering*, 28, 1216–1224.

Wolverine Tube Inc. (2006) “Condensation Inside Tubes”, “Engineering Data Book III”, 8.1- 8.27.

Wolverine Tube Inc. (2006) “Boiling Heat Transfer on External Surfaces”, “Engineering Data Book III”, 9.1- 9.38.

Wu, C., Wang, S., Li, J. (2018). Parametric study on the effects of a recuperator on the design and off-design performances for a CO₂ transcritical power cycle for low temperature geothermal plants. *Applied Thermal Engineering* No: 137, 644–658.

Xu, R., Hem, Y. (2011). “A vapor injector-based novel regenerative organic rankine cycle, *Applied Thermal Engineering*, 31, 1238–1243.

Yamada, N., Anuar, M., Trung, K. (2012). “Study on thermal efficiency of low-to medium-temperature organic rankine cycles using HFO-123yf, *Energy*, 41, 789–800.

APPENDIX

ORC Designer MATLAB Program Notepad Contents

NPENTANE-189 - Not Defteri

Dosya Düzenle Görünüm

14-Aug-2022
20:10:48

Points #	Flow Rate (m3/h)	Temperature (°C)	Pressure (bara)	Density (kg/m3)	Enthalpy (kJ/kg)	Entropy (kJ/kgK)	Phase #
WF1	65.45	38.03	2.62	607.93	4.80	0.01	liquid
WF2	68.11	60.39	2.60	584.24	59.22	0.18	liquid
WF3	6197.00	63.39	2.30	6.42	401.17	1.20	gas
WF4	12906.43	48.15	1.09	3.08	378.75	1.22	gas
WF5	65.47	38.00	1.09	607.74	4.60	0.01	liquid
H1	155.39	90.00	3.00	965.30	377.04	1.19	liquid
H2	153.27	68.39	2.55	978.64	286.33	0.94	liquid
H3	152.98	64.95	2.42	980.55	271.89	0.89	liquid
A1	1343505.06	18.00	1.00	1.20	417.40	3.86	Air
A2	1387255.07	27.19	1.00	1.16	426.64	3.89	Air

Fluid: NPENTANE

TurbineEff: 0.850

ExchangerEff: 1.000

Gross Power(kw): 245.370

Net Power(kw): 189.358

Theoretical GP (kw): 245.631

Press.R: 2.100

WF FlowRate(t/h): 39.791

B FlowRate(t/h): 150.000

GrossEff: 0.0560

NetEff: 0.0432

H_Evaporator(kw): 3779.584

H_Preheater(kw): 601.511

H_Condenser(kw): 4135.464

Superheat(°C): 1.000

Pump Cons.(kw): 3.917

ACC Cons.(kw): 52.096

ACC Length(m): 8.058

ACC Width(m): 20.000

ACC Area(m2): 161.164

Number of Tube Rows: 4.000

NPENTANE-189-Evaporator - Not Deferi		
Dosya	Düzenle	Görünüm
Hot Fluid:	WATER	
Working Fluid:	NPENTANE	
Shell Type:	K-Shell	
Duty (kw):	3965.084	
Heat Transfer Area (m2):	184.387	
EMTD (°C):	13.440	
Dirty OHTC (W/m2C):	1113.455	
Clean OHTC (W/m2C):	1668.787	
Tube Number :	231.000	
Tube Length (m):	10.000	
Tube Diameter (mm):	25.400	
Tube Thickness (mm):	2.100	
Tube Layout (°):	45.000	
Bundle_Diameter (mm):	728.000	
Shell_Diameter (mm):	1456.000	
COLD SIDE		
Flow Rate (kg/h):	39790.878	
Inlet Temperature (°C):	60.393	
Outlet Temperature (°C):	63.393	
Fouling Resistance (m2C/W)	1.136e+04	
Pressure Loss (bar):	0.300	
HOT SIDE		
Flow Rate (kg/h):	150000.000	
Inlet Temp (°C):	90.000	
Outlet Temperature (°C):	68.393	
Density (kg/m3):	972.379	
Specific Heat (j/kgC):	4195.719	
Dynamic Viscosity (Pa.s):	3.577e-04	
Conductivity (W/mC):	0.667	
Pr Number:	2.252	
Fouling Resistance (m2C/W)	5.682e+03	
Pressure Loss (bar):	0.128	

NPENTANE-189-ACC - Not Defteri

Dosya Düzenle Görünüm

Hot Fluid:	WATER
Working Fluid:	NPENTANE
Power (kW):	52.096
Duty (kW):	4135.462
Air Inlet T (°C):	18.000
Air Outlet T (°C):	27.190
WF Inlet T (°C):	48.147
WF Outlet T (°C):	38.000
LMTD (°C):	14.219
Dirty OHTC (W/m2C):	14.842
Clean OHTC (W/m2C):	17.294
Heat Transfer Area (m2):	19595.129
Air Flow Rate (kg/h):	1610057.376
ACC Width (m):	20.000
Tube Length (m):	8.058
Tube Diameter (mm):	25.400
Tube Thickness (mm):	1.650
Number of Tubes:	1362.000
Face Area (m2):	161.164
Fan Area (m2):	64.466
Tube Pressure Loss (Pa):	564.177
Air Pressure Drop (Pa):	88.466

NPENTANE-189-Preheater - Not Deferi		
Dosya	Düzenle	Görünüm
Hot Fluid:	WATER	
Working Fluid:	NPENTANE	
Shell Type:	E-Shell	
Duty (kW):	609.808	
Heat Transfer Area (m ²):	63.837	
EMTD (°C):	14.656	
Dirty OHTC (W/m ² C):	651.779	
Clean OHTC (W/m ² C):	809.458	
Pass Number:	2.000	
Tube Number:	80.000	
Tube Length (m):	10.000	
Tube Diameter (mm):	25.400	
Tube Thickness (mm):	2.100	
Tube Layout (°):	45.000	
Baffle_Number:	35.000	
Shell_Diameter (mm):	463.000	
COLD SIDE		
Flow Rate (kg/h):	39790.878	
Inlet Temp (°C):	38.034	
Outlet Temp (°C):	60.393	
Density (kg/m ³):	596.308	
Specific Heat (j/kgC):	2433.392	
Dynamic Viscosity (Pa.s):	1.442e-04	
Conductivity (W/mC):	0.103	
Pr Number:	3.396	
Fouling Resistance:	8.800e-05	
Pressure Loss:	0.036	
HOT SIDE		
Flow Rate (kg/h):	150000.000	
Inlet Temperature (°C):	68.393	
Outlet Temperature (°C):	64.947	
Density (kg/m ³):	979.635	
Specific Heat (j/kgC):	4188.199	
Dynamic Viscosity (Pa.s):	4.227e-04	
Conductivity (W/mC):	0.657	
Pr Number:	2.695	
Fouling Resistance:	1.760e-04	
Pressure Loss:	0.454	

SCIENTIFIC ETHICAL STATEMENT

T.C.

AYDIN ADNAN MENDERES UNIVERSITY

GRADUATE SCHOOL OF NATURAL AND APPLIED SCIENCES

SCIENTIFIC ETHICAL STATEMENT

I hereby declare that I composed all the information in my doctoral thesis entitled “DESIGNING OF AN ORGANIC RANKINE CYCLE POWER PLANT BY USING LOW ENTHALPY GEOTHERMAL RESOURCES” within the framework of ethical behaviour and academic rules, and that due references were provided and for all kinds of statements and information that do not belong to me in this study in accordance with the guide for writing the thesis. I declare that I accept all kinds of legal consequences when the opposite of what I have stated is revealed.

MURAT KARADAŞ

28/07/2022

CIRRICULUM VITAE

Last name, First name: Karadaş, Murat

Nationality: Turkey

Foreign language: English

EDUCATION

Level	Institute	Date of graduation
Ph.D. - Mechanical Engineering	Adnan Menderes University	Cont.
M.Sc. - Energy Engineering	Izmir Institute of Technology	June-2013
B.Sc. - Mechanical Engineering	University of Gaziantep	June-2010
B.B.A. - Business	Anadolu University	June-2012

WORK EXPERIENCE

Year	Place/ Institute	Title
2015-cont.	GMK Renewable Energy Engineering Company	General Manager
2013-2015	Greeneco Energy Electricity Generation Company	Project Manager
2010-2013	Menderes Geothermal Power Generation Company	R&D Engineer
2009-2010	Mercedes-Benz Turk Truck Company	Project Engineer

ACADEMIC PUBLICATIONS

1. DISSERTATIONS

KARADAS, M., “Performance assessment of a binary cycle geothermal power plant”, Izmir Institute of Technology, The Graduate School of Engineering& Sciences, Energy Engineering Programme. Advisor: Prof. Dr. H. Murat Çelik, Co-advisors: Prof.Dr. Gülden Gökçen Akkurt and Prof.Dr. Macit Toksoy, September, 2013.

2. INTERNATIONAL BOOKS AND BOOK CHAPTERS

KARADAS, M., GOKCEN AKKURT, G., 2014., “Rapid development of geothermal power generation in Turkey”, In Geothermal Systems & Energy Resources: Turkey and Greece (edit by Jochen Bundschuh). CRC Press, Taylor & Francis Group, 7 March 2014.

3. SCI JOURNALS

KARADAS, M., CELIK, M., TOKSOY, M., SERPEN, U., “Multiple linear regression analysis of performance parameters of a binary cycle geothermal power plant”, Geothermics. March 2015, Vol.54: pp 68-75.

4. INTERNATIONAL AND NATIONAL CONFERENCE PROCEEDINGS

KARADAS, M., 2022., “Utilizing Heat With Closed-Loop Systems - EGS Investigation of Heat And Electric Recovery Opportunities of Non-Productive Deep Geothermal Wells”, Proceedings, 5th International Geothermal Energy Congress and Exhibition IGC Turkey 2022, Kaya Thermal Hotel & Convention Center, İzmir, Turkey, Sept. 19-21, 2022.

KARADAS, M., 2021., “Production Increasing Methods In Geothermal Plants Under Variable Reservoir Conditions”, Proceedings, GT’2021 5th Geothermal Turkey Workshop and Conference, Geothermal Power Plant Investors Association, Grand Ankara Hotel & Convention Center, Ankara, Turkey, Nov. 17-18, 2021.

KARADAS, M., 2019., “Process Design in Geothermal Energy Applications”, Oral Presentation, 4th International Process Summit and Exhibition, WOW Congress Center, Yesilkoy, Istanbul, Turkey, Oct. 22-24, 2019.

KARADAS, M., 2019., “Non-Condensable Gases in Geothermal Power Plants with Microalgae”, Proceedings, 4th International Geothermal Energy Congress and Exhibition IGC

Turkey 2019 and World Bank Workshop, Kaya Thermal Hotel & Convention Center, İzmir, Turkey, Nov. 6-8, 2019.

KARADAS, M., 2019., “An Organic Rankine Cycle Geothermal Power Plant Design by Using Low Enthalpy Geothermal Resources”, Proceedings, GT’2019 Geothermal Turkey Workshop and Conference, Geothermal Power Plant Investors Association, Bilkent Hotel & Convention Center, Ankara, Turkey, Feb. 6-7, 2019.

KARADAS, M., 2018., “Performance, Maintenance, Operation and Process Control Software for Geothermal Power Plants: Thermosoft”, Oral Presentation, 3rd International Process Safety Symposium and Exhibition, WOW Congress Center, Yesilkoy, İstanbul, Turkey, Sep. 18-20, 2018.

KARADAS, M., 2018., “Direct Contact Steam Condenser Design”, Proceedings, GT’2018 Geothermal Turkey Workshop and Conference, Geothermal Power Plant Investors Association, Bilkent Hotel & Convention Center, Ankara, Turkey, Apr. 11-12, 2018.

KARADAS, M., 2018., “The use of low pressure waste steam which is released to atmosphere in power generation: Direct Contact Steam Condenser Project”, Proceedings, 3rd International Geothermal Energy Congress and Exhibition IGC Turkey 2019 and World Bank Workshop, Sheraton Ankara Hotel & Convention Center, Ankara, Turkey, Marc. 14-15, 2018.

KARADAS, M., AKKURT, G.G., 2014., “Rapid development of geothermal power generation in Turkey”, Oral Presentation, International Geothermal Conference, Freiburg – Germany, May. 14-16, 2015.

KARADAS, M., SERPEN, U., AKSOY, N., 2014., “Some investigations on decline in Dora-1 brine flow rate, Case Study: AS-1 production well”, Proceedings, Thirty-Ninth Workshop on Geothermal Reservoir Engineering, Stanford University, Stanford, California, USA, Feb. 24-26, 2014.

KARADAS, M., CELIK, M., TOKSOY, M., GOKCEN AKKURT, G., 2013., “Performance modeling of a geothermal power plant by regression analysis” (in Turkish), TESKON 2013, XI. National Installation Engineering Congress, Geothermal Energy Seminar, Izmir, Turkey, Apr. 17-20, 2013.

5. SOME TRAININGS AND SEMINARS ATTENDED

Sept. 19-21, 2022. 5th International Geothermal Energy Congress and Exhibition IGC Turkey 2022, Kaya Thermal Hotel & Convention Center, Izmir, Turkey.

Nov. 17-18, 2021. GT'2021 Geothermal Turkey Workshop and Conference, Geothermal Power Plant Investors Association, Grand Ankara Hotel & Convention Center, Ankara, Turkey

Nov. 6-8, 2019 4th International Geothermal Energy Congress and Exhibition IGC Turkey 2019, Kaya Thermal Hotel & Convention Center, İzmir, Turkey.

Sep. 23, 2019 EGEN Innovation Fund Workshop on Geothermal Energy & ETIP-DG Stakeholders Meeting, European Geothermal Energy Council, Brussel, Belgium.

Feb. 6-7, 2019 GT'2019 Geothermal Turkey Workshop and Conference, Geothermal Power Plant Investors Association, Bilkent Hotel & Convention Center, Ankara, Turkey.

Marc. 14-15, 2018 3rd International Geothermal Energy Congress and Exhibition IGC Turkey 2018, Sheraton Ankara Hotel & Convention Center, Ankara, Turkey.

Apr. 11-12, 2018 GT'2018 Geothermal Turkey Workshop and Conference, Geothermal Power Plant Investors Association, Bilkent Hotel & Convention Center, Ankara, Turkey.

May. 22-23, 2017 2nd International Geothermal Energy Congress and Exhibition IGC Turkey 2017, Swissôtel Büyük Efes Hotel & Convention Center, İzmir, Turkey.

Feb. 8-9, 2017 GT'2017 Geothermal Turkey Workshop and Conference, Geothermal Power Plant Investors Association, Bilkent Hotel & Convention Center, Ankara, Turkey.

Oct. 23-27, 2016 40th GRC Annual Meeting & GEA Expo, Geothermal Resource Council, Sacramento, California, USA.

Jul. 14-17, 2016 Turboden Factory and Reference Geothermal Power Plants Trip, Mitsubishi Turboden SRL, Milan, Italy and Munich, Germany.

Dec. 8 - 10, 2015 Power-Gen International Conference 2015, Las Vegas Convention Center, Las Vegas, Nevada, USA.

May. 4 - 7, 2015 Offshore Technology Conference (OTC), NRG Park, Houston Texas, USA.

Nov. 19 - 22, 2014 Design Review Meetings of Greeneco Project in Exergy, Exergy SPA, Milano, Italy.

Apr. 26 – May 7, 2014 Seventeen Geothermal Fields Trip for Different Type of ORC, ESP and LSP Pumps Applications Investigation, Salt Lake City, Utah and Reno, Nevada, USA.

Apr. 3-5, 2014 İstanbul Carbon Submit: Carbon Management, Technologies & Trade, İTÜ Süleyman Demirel Kültür Merkezi, İstanbul.

Sept. 29 - Oct. 2, 2013 37th GRC Annual Meeting & GEA Expo, Geothermal Resource Council, Las Vegas, Nevada, USA.

Oct. 4, 2013 Technical Training in the Geysers Geothermal Field and Power Plants, Calpine Corporations, Geysers, California, USA.

Oct. 5, 2013 Technical Training in Steamboat Springs Geothermal Field and Power Plants, Ormat Technologies Inc., Nevada, USA.

Mar. 29-31, 2012 Seminar of Feasibility Report Preparation on Energy Investments, World Energy Council Turkish National Committee, Ankara Turkey

Feb. 01, 2010 KAIZEN, Mercedes-Benz Turk Company, Aksaray Turkey.